RESEARCH ON
THERMIONIC ELECTRON EMITTING SYSTEMS

Final Report

This report covers the period from 16 June 1965 through 15 September 1966

Varian Associates
611 Hansen Way
Palo Alto, California

Navy Department Bureau of Ships
Contract No. NObs-92494 Project Serial No. SR007-12-01, Task 807

Varian Engineering
Report No. 338-1F

Copy No. 14

RESEARCH ON THERMIONIC ELECTRON EMITTING SYSTEMS

Final Report

This report covers the period from
16 June 1965 to 15 September 1966

Navy Department Bureau of Ships

Contract No. NObs-92494 Project Serial No. SR007-12-01, Task 807

Prepared by: I. Weissman

Varian Associates
611 Hansen Way
Palo Alto, California

TABLE OF CONTENTS

LIST OF ILLUSTRATIONS

LIST OF ILLUSTRATIONS (Cont'd)

LIST OF ILLUSTRATIONS (Cont'd)

LIST OF ILLUSTRATIONS (Cont'd)

ABSTRACT

This report deals with the synthesis and evaluation of a unique type of thorium, thin-film, thermionic electron emitter. The synthesis procedure involves chemical vapor deposition of a surface layer of a refractory metal onto a thorium dispensing substrate. The unique features of the process are a high degree of preferred uniaxial crystal orientation which can be obtained in the deposited layer, and a measure of control over the particular direction in the layer that is preferentially oriented. By virtue of this orientation, surfaces can be fabricated consisting predominantly of one of the better emitting crystal planes of the particular combination of substrate and adsorbate and enhanced emission thus realized.

In the majority of this year's work the grain-oriented surface layers investigated were tungsten. Three different types of dispensers were evaluated, each utilizing a different thermochemical reaction for production of the free thorium necessary to sustain the surface coverage at emitting temperatures. Both thermal stability of preferred orientation and thermionic emission capabilities were evaluated. Methods were evolved for fabricating the emitting structures so as to enhance thermal stability.

The emitters tested exhibited a spread of over 15% in their measured values of vacuum work function (3.0 to 3.55 eV). With a single exception they exhibited high thermionic constants (70-120). Thermal stability was good for one type of dispenser evaluated, and relatively poor for the other two.

A deposition system was built for fabricating dispenser emitters with niobium surface layers, and experiments were done which show that a measure of selectivity over preferred orientation can be achieved for niobium just as it can for tungsten.

INTRODUCTION AND SUMMARY

This report describes a one-year investigation dealing with a unique class of thermionic electron emitter. The work is a continuation of a research project which was initiated at Varian Associates in 1962, and was company funded previous to this reporting period. (Work done prior to this contract period is described in References 1 and 2.) It involves a study of the metallurgical and thermionic properties of grain-oriented dispenser type emitters, particularly emitters consisting of thorium dispensing substrates onto which highly grain-oriented outer layers of a suitable refractory metal are deposited by the process of chemical vapor deposition (CVD). In operation these emitters perform as conventional thin film type cathodes with thorium atoms being supplied by diffusion from the substrate through the grain-oriented outer layer to the surface. Early in the project it was demonstrated that under appropriate conditions emitters synthesized in this way, by virtue of the unique surface characteristics of the oriented layers, can be better electron emitters than their randomly oriented counterparts.

During this reporting period several embodiments of the above type emitters, all with tungsten oriented surface layers, were fabricated and extensively investigated. Three different types of thorium dispensing substrates were studied, each involving a different thermochemical reaction for the continuous production of the free thorium necessary to maintain the emitter active at thermionic temperature.

From the point of view of practical utility, the most vital question considered during this year's work was that involving the degree of thermal stability (i.e. the extent to which the deposit retains its preferred orientation when subjected to high temperatures) of the grain-oriented emitting structure. The oriented surface layer must be well bonded to the underlying substrate and in addition must be very thin (e.g. of the order of 0.001" to 0.002") in order to enable easy diffusion of thorium from the underlying substrate reservoir to the surface. It was found that ordinarily such

surface layers, though highly preferentially oriented "as-deposited," randomized in a short time when heated to thermionic temperatures. The cause of this rapid degradation of preferred orientation was determined, and methods were evolved for fabricating each of the three basic types of emitter structures so that they retained their "as-deposited" preferred orientation through extended periods of operation at thermionic temperatures. (Measurements on some emitters tested have extended over periods greater than 100 hours.)

With regard to the CVD process for plating tungsten by hydrogen reduction of the hexafluoride, additional control of orientation was achieved during this year and it is now a routine matter to produce any one of three different preferred orientations in either the planar or the cylindrical geometry. In addition, a considerable degree of reproducible control over deposit microstructure has also been achieved which makes possible the deposition of oriented surface layers with different degrees of porosity. This control of porosity is believed to be critically important both with respect to initial activation and to the maintenance of an active monolayer surface at the higher emitter temperatures.

Richardson constants and work functions have been determined for each of the three thorium on tungsten emitter types. Work functions are found to vary over a range of 3.0 to 3.55 eV, the value being dependent on both the orientation of the surface layer and on the type of substrate. The measured "A" values with one exception were uniformly high, varying from a maximum value of 120 ± 40 down to 70 ± 40. (Error tolerances are established by drawing extreme lines through the experimental points.)

Experiments have been done to establish the feasibility of depositing preferentially oriented niobium by hydrogen reduction of the tetrachloride. Preliminary results indicate that control of the preferred crystal direction can be obtained and that this method will be suitable for fabricating dispenser emitter structures with oriented niobium surface layers.

TUNGSTEN VAPOR DEPOSITION

A. GENERAL

Grain-oriented tungsten deposits are formed on heated substrates by hydrogen reduction of tungsten hexafluoride in accordance with the reaction,

$$WF_6 + 3H_2 \rightarrow W + 6HF \ .$$

A schematic diagram and a photograph of the apparatus used are shown in Figures 1 and 2. Except for the reaction chambers, the same apparatus is used for both planar and cylindrical deposits. Precise control over several important parameters has been found to be essential to the reproducible control of the properties of large area deposits. To achieve a uniform planar deposit, an appropriate nozzle configuration must impinge the reactants uniformly on all areas of the surface and the flow pattern in the deposition chamber must be such that reaction products are uniformly removed from the entire surface. For planar deposits a large-area, water-cooled, shower-head type nozzle, with an appropriate baffle between it and the incoming gas stream, to break up streaming onto the heated substrate, has proven satisfactory. By trial and error an optimum spacing between nozzle and substrate has been obtained which results in a proper flow pattern for uniform deposition. In the cylindrical case, a co-linear multiple inlet nozzle with baffling between it and the incoming gas stream impinges the reactants onto a rotating cylindrical heated substrate. For either geometry control of substrate temperature to within a tolerance of $\pm$ 5°C and control of flow rates of reactants to within 5% is also required for good reproducibility. Also it is imperative that the deposition chambers be let down to an inert atmosphere for loading and unloading and maintained free of moisture. Continuous flushing of the deposition apparatus with purified dry hydrogen when not in use and hydrogen firing of each substrate after loading it into the deposition chamber has been made standard practice and along with the other controls described above, yields almost perfect reproducibility of deposits.

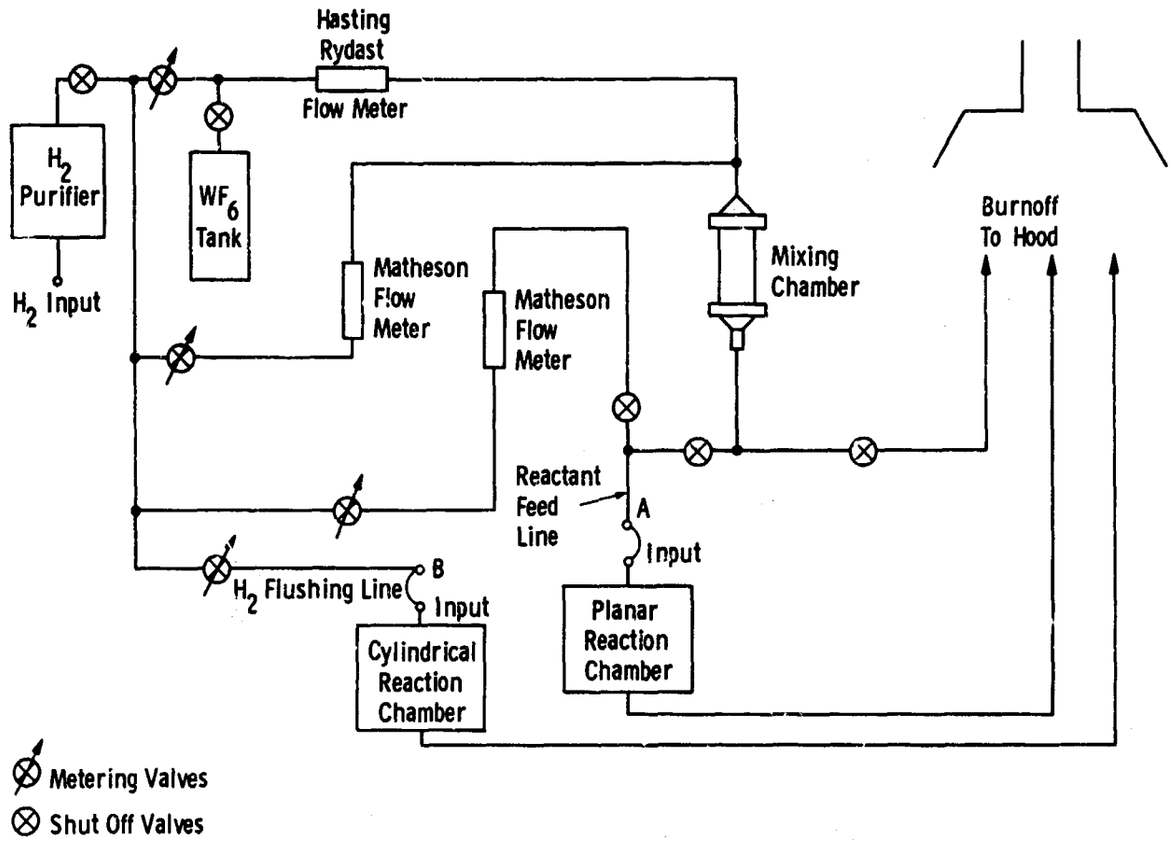

Figure 1. Schematic Diagram of Apparatus for Vapor Depositing Planar and Cylindrical Tungsten Emitter Surfaces. Hydrogen Flushing Line and Reactant Feed Line are Interchanged from Position Shown to use Cylindrical Reaction Chamber

Figure 2. Apparatus for Vapor Plating of Planar and Cylindrical Tungsten Emitter Surfaces. Cylindrical Reaction Chamber Shown at Right in Open Position

B. PREFERRED ORIENTATION

Accurate reproducible control of the properties of the grain-oriented outer layer of the emitters is of prime importance to the success of this approach. The proper crystal direction must be preferentially oriented normal to the surface so that the surface is constituted predominantly of a crystal plane that yields desirable emission characteristics. In work done on this project prior to this contract period it was established that by modifying deposition parameters, planar tungsten deposits having any one of several different crystal directions preferentially oriented normal to the surface could be obtained. Two of these orientations, namely the [100] and [111] directions were obtained relatively easily over wide ranges of variation of thermodynamic parameters. The others occurred in a very limited transition range of the parameters between those values that yielded the (100) and (111) orientations, and were difficult to control and reproduce. Within the ranges of the parameters that yielded either (100) or (111) oriented tungsten, significant differences in deposit properties such as half-width of distribution about surface normal, grain size, deposit uniformity, etc., were obtained.

As a result of further improvements in deposition techniques developed during this past year a third preferred orientation (210) for polycrystalline tungsten is now reproducibly available and all three orientations are readily obtained in both planar and cylindrical geometries. The conditions that yield the various orientations are shown in Figure 3. It should be emphasized that while the exact locations of the lines representing transitions from one orientation to another will vary with changes in detailed flow conditions such as might result from a change in nozzle-substrate spacing, the relative positions for obtaining various orientations in the two-dimensional space illustrated will remain as shown, i.e. at a given substrate temperature, the (111) orientation is obtained with low WF_6 flow rates, the (210) orientation with intermediate WF_6 flow rates, and the (100) orientation with high WF_6 flow rates. The (210) region is less extensive in the cylindrical geometry than in the planar geometry

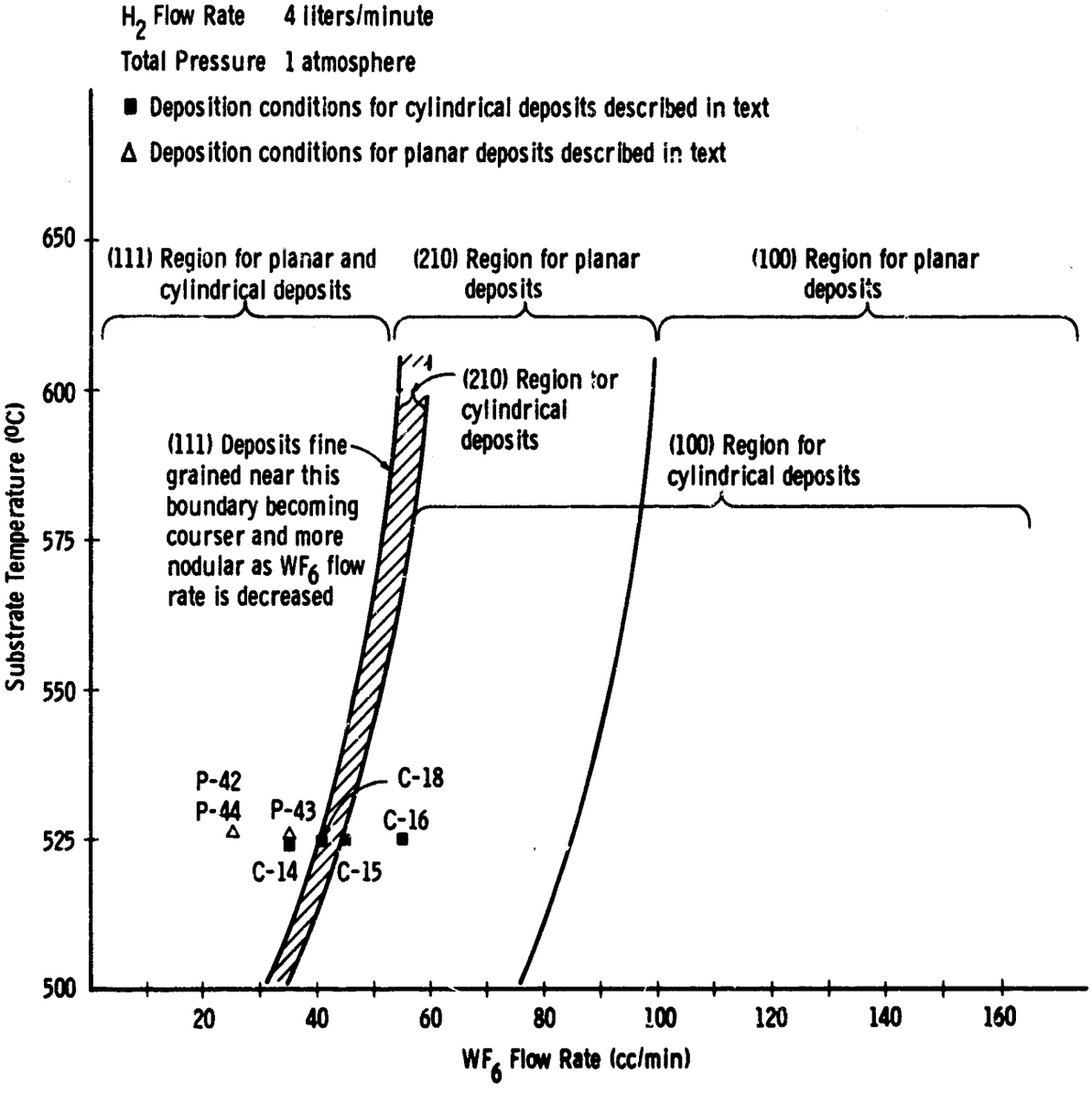

Figure 3. Deposition Parameters for Grain Oriented Tungsten Deposits

but is adequate in either case for reproducible control of orientation. The triangles and squares in Figure 3 indicate the values of parameters used for some of the deposits described in the text.

Characterization of preferred crystal orientation of a polycrystalline material is normally done by X-ray pole-figure analysis.[3] Complete pole figures describe the distribution of a given crystal direction in a full hemisphere about the surface normal as a function of polar and azimuthal angles. For chemically vapor deposited tungsten the preferred crystal direction is generally found to be symmetrically peaked about the direction of the surface normal.* Therefore, a section taken through the polar plot is sufficient to describe the entire pole figure. In this report a section through a pole-figure plot will be termed a "pole-figure scan." In practice, the pole figure is plotted by mounting the sample in a standard diffractometer, with a special pole-figure adapter which rotates it independently about two orthogonal axis. The X-ray source and geiger counter are set at the appropriate angle to detect Bragg reflections from the crystal plane whose distribution is being measured. For a cylindrically symmetric distribution, only the polar angle need be varied to generate a pole-figure scan. The angular displacement of the peak of the distribution from the normal uniquely identifies the crystal direction which is preferentially oriented normal to the surface. X-ray pole-figure scans of cylindrical tungsten deposits C-14, C-15, C-16, and C-18, all done on 0.3" diameter cylindrical copper substrates, are shown in Figure 4. They illustrate the transition from one orientation to another. Deposit number C-15 is a mixture of (100) and (210) oriented crystallites as evidenced by the peak at 0° and the pair of peaks at approximately 26° each side of the surface normal. ((200) diffraction peaks at an angle of inclination of 26° from the surface normal indicate a concentration of (210) crystal planes in the plane of the surface.)

- - - - - - -

* If the crystallites are sufficiently large, the diffracted energy from individual ones will be resolved in a pole-figure scan. In that case the scan should be considered as a random sampling of uniformly distributed crystallites with the location of the group of peaks characterizing the orientation of the deposit (see Appendix A).

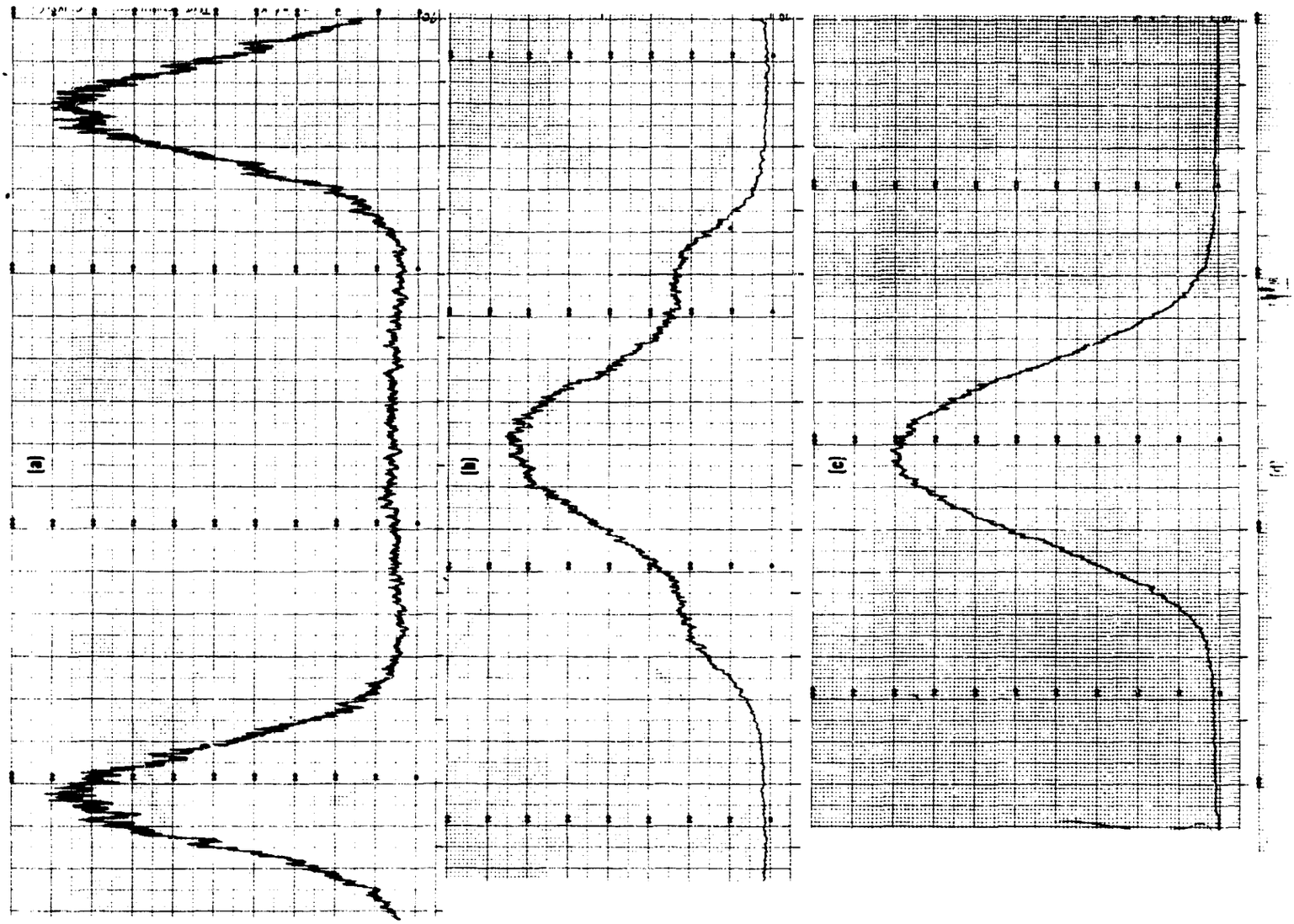

Figure 4. Plots of the Integrated Intensity of C
of Cylindrical Deposits Indicated in F
Inclination of the Planes to the Surf
(b) Deposit C-15; Mixed (210) (100) Or
Orientation (d) Deposit C-18; (210) Or

A.

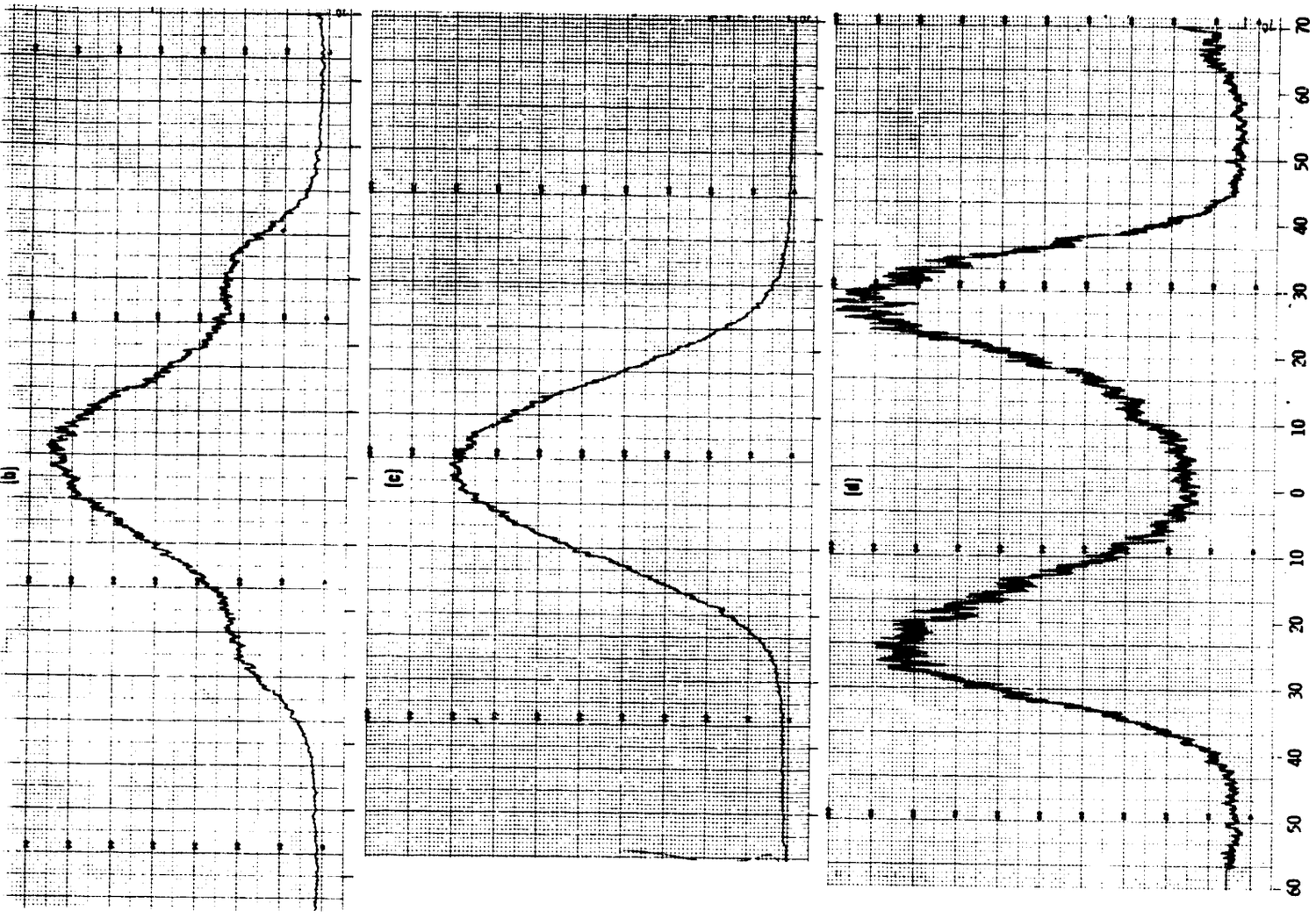

Figure 4. Plots of the Integrated Intensity of Cu Kα X-Radiation from the [200] Planes of Cylindrical Deposits Indicated in Figure 3, as a Function of the Angle of Inclination of the Planes to the Surface (a) Deposit C-14; (111) Orientation (b) Deposit C-15; Mixed (210) (100) Orientation (c) Deposit C-16; (100) Orientation (d) Deposit C-18; (210) Orientation

B.

C. OPTIMIZATION OF DEPOSIT CHARACTERISTICS

Electron emission data for the individual crystal planes of tungsten with adsorbed thorium films have been described in References 4 and 5. Reference 4 deals with field emission measurements on small single crystal points and Reference 5 with thermionic emission from single crystal filaments. In both cases maximum emission was obtained from regions of the surface concentrated about the [111] crystal direction. Coincidentally, as described in the previous section, preferential orientation of the [111] crystal direction perpendicular to the surface is readily obtained for polycrystalline tungsten prepared by chemical vapor deposition from the hexafluoride. Therefore, optimization and evaluation of thorium-coated tungsten emitters with (111) preferentially oriented surface layers has been the primary initial objective in this work.

The sharpness of the distribution of the [111] crystal direction about the surface normal was initially adopted as a criterion for optimization of (111) oriented tungsten. 0.0025" thick deposits were prepared having measured full half widths as small as 5.3° (Figure 5) and true full half widths after correcting for X-ray optics* of 4.2°. After some investigation it became evident, however, that such sharply peaked concentrations of [111] crystal directions about the normal were obtained for thin deposits, only if the substrate surface itself had (111) preferred orientation. As described in detail in Appendix B it is found that micropolishing of a tungsten substrate surface produces a <111> <100> double fiber texture in the substrate surface layer. (111) deposits done directly onto such micropolished substrates exhibit sharply peaked "as-deposited" distributions of (111) preferentially oriented cyrstallites about the surface normal. Such deposits, however, are found to be highly unstable and their

---

* For the full half width corrections the pole-figure line shapes are assumed to be Gaussian. The line obtained by scanning a perfect tungsten single crystal has a full half width of 3.3° due to X-ray optics. It can be readily shown that for these conditions

$$(\text{full half width})^2_{\text{TRUE}} = (\text{full half width})^2_{\text{MEASURED}} - (3.3)^2 .$$

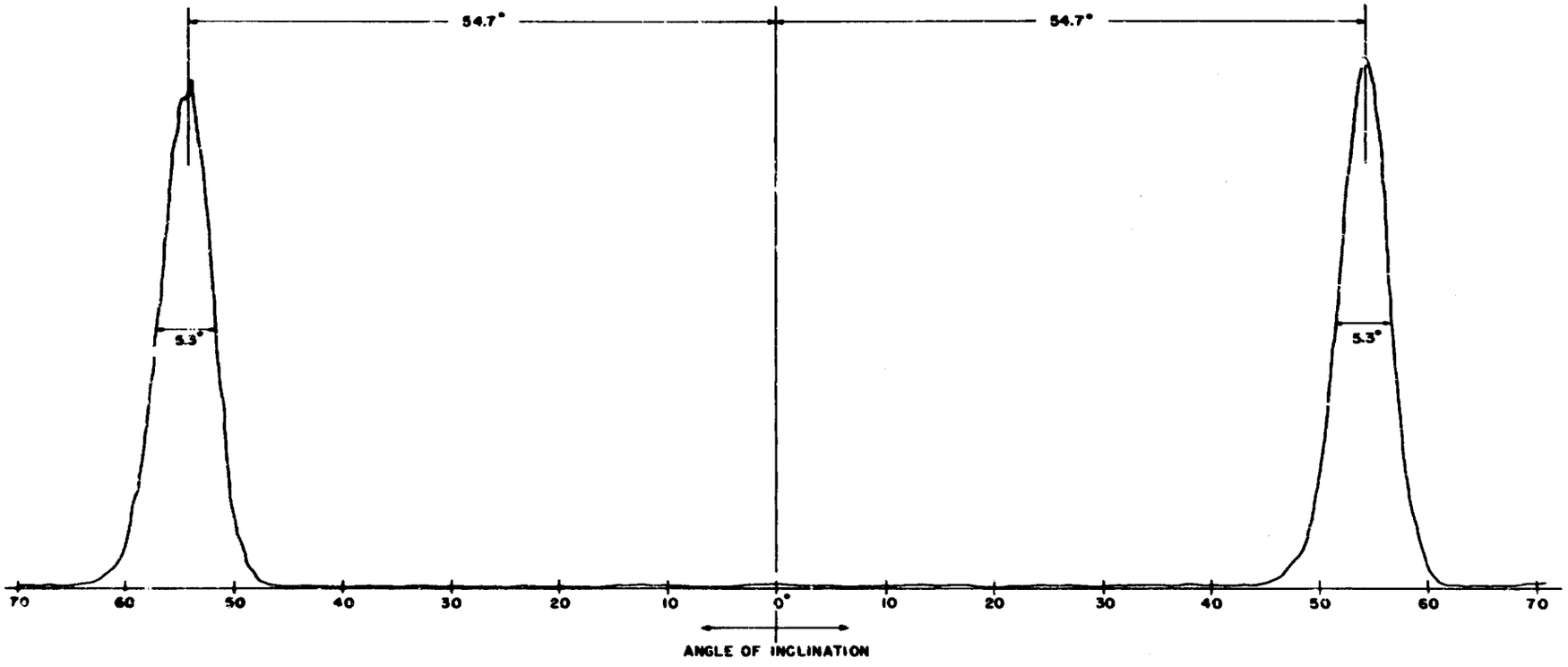

Figure 5. A Plot of the Integrated Intensity of Cu Kα X-Radiation Diffracted from the [200] Planes of P-2-W as a Function of the Angle of Inclination of the Planes to the Surface. Substrate Micro-Polished to 1 Micron Diamond Finish Prior to Deposition

preferred orientation rapidly degrades when they are heated to thermionic emission temperatures. If, prior to depositing, the double fiber textured surface layer is removed, either by heat treating or etching the surface, the resulting deposit done under identical conditions has a broader distribution of preferentially oriented planes and the pole figure tends to be multiply peaked, indicating larger crystallites (Figure 6).

Thus for high temperature applications, the sharpness of the "as-deposited" distribution of preferentially oriented planes is an inadequate criterion of optimization. For large crystallites (either as deposited or as a consequence of subsequent crystal growth) the pole-figure scan is multiply peaked (Appendix A) and the concept of distribution half width becomes entirely meaningless.

Minimum requirement on substrate-deposit bond strength is another factor which might have restricted the useful range of deposition parameters. Bond strength tests were made on a number of samples to determine the importance of this factor. Results of these tests, described fully in Appendix C, indicate that substrate-deposit bonding imposes no restriction on the choice of deposition parameters over the entire range of interest.

A meaningful criterion which does define optimum deposition parameters for (111) oriented deposits in this application is based on the empirical observation that the density of nucleation sites is larger, and thus the deposits finer grained as the transition line between the (111) and (210) regions is approached (Figure 3). Thus, in the (111) region at fixed temperature a larger WF_6 flow rate yields a finer grained and less nodular deposit. At a fixed WF_6 flow rate a lower substrate temperature yields the same result. Figures 7 and 8 illustrate two (111) oriented deposits grown at the same substrate temperature onto identically prepared substrates. P-44-ThW (Figure 7) was grown at a WF_6 flow rate of 25 cc/min (see triangles in Figure 3) and the deposit is nodular and quite porous, whereas P-43-ThW (Figure 8) grown at a WF_6 flow rate of 35 cc/min (see triangles in Figure 3) is a less nodular and denser deposit.

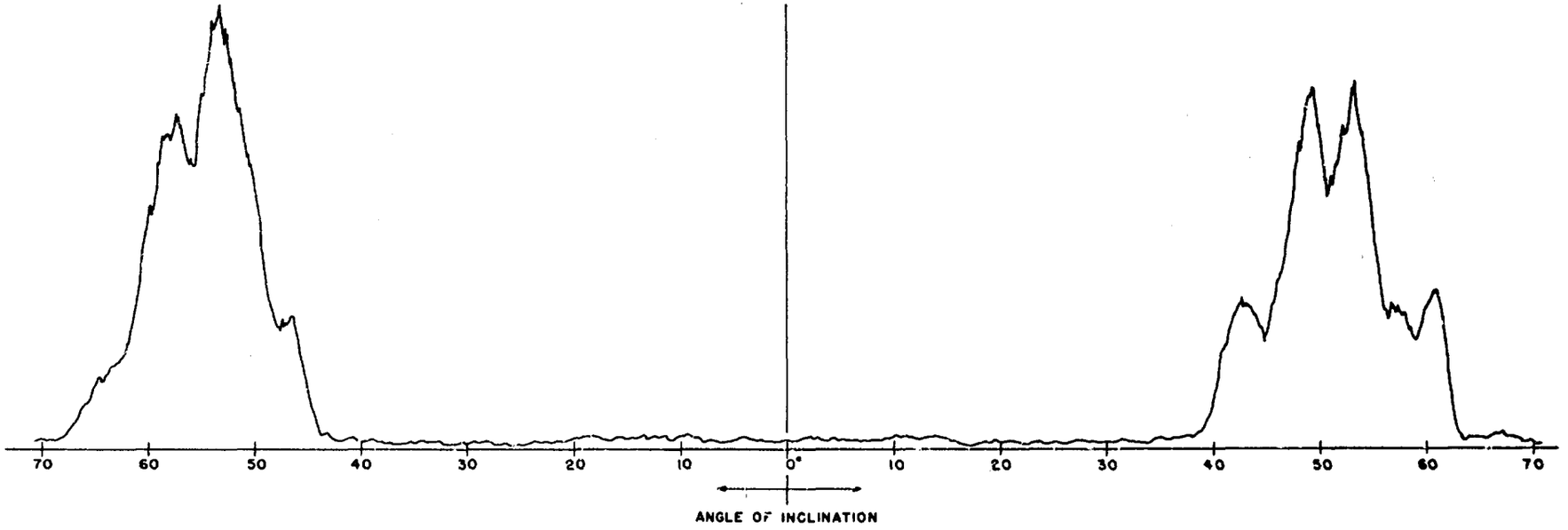

Figure 6. A Plot of the Integrated Intensity of Cu Kα X-Radiation Diffracted from the [200] Planes of P-28-W as a Function of the Angle of Inclination of the Planes to the Surface. Same Deposition Conditions as P-2-W Except Substrate Heated at 1700°C for 40 Minutes After Polishing

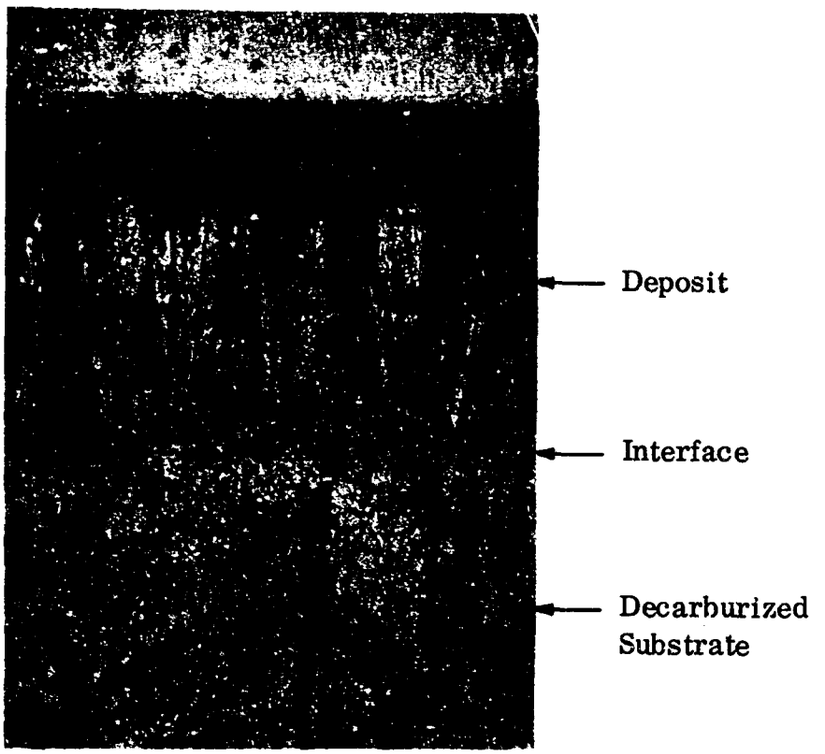

(111) Oriented deposit on a type 1 emitter substrate with a strain free, microscopically smooth, single-phase surface. WF_6 flow rate-25cc/min.

Figure 7. Section of P-44-ThW (Scale, X589)

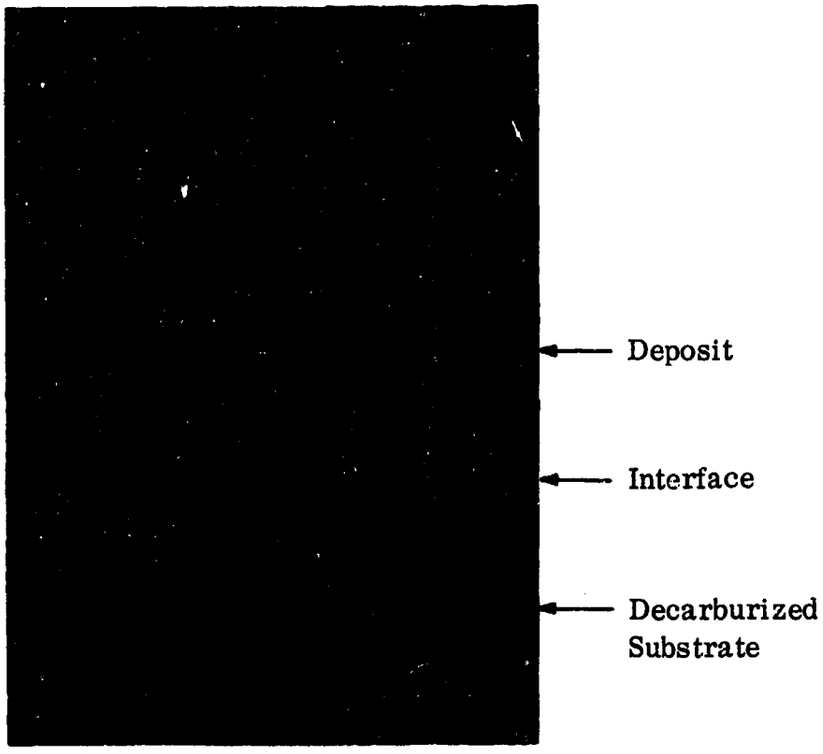

(111) Oriented deposit on a type 1 emitter substrate with a strain free, microscopically smooth, single phase surface. WF_6 flow rate-35cc/min.

Figure 8. Section of P-43-ThW (Scale, X589)

Substrate characteristics can also influence the degree of nodularity and density of the deposit. However, proper substrate preparation (described in detail in the section on emitter fabrication) minimizes this effect and renders it negligible.

In the operation of an emitter it is desirable that the oriented surface layer present low impedance to the flow of thorium from the dispenser substrate to the emitting surface. The maximum operating temperature is limited to that at which the rate of supply of thorium atoms via diffusion from the dispenser becomes insufficient to maintain optimum surface coverage. In addition to reducing this maximum emitter temperature, any impedance to the flow of thorium to the surface will also increase the time required for activation and make the emitter more subject to poisoning. Some degree of porosity in the grain-oriented surface layer is therefore desirable. Utilization of the inherent nodular growth tendency of the (111) oriented deposit to obtain this porosity is a natural solution since it can be achieved in a controllable and reproducible way by merely selecting the proper deposition parameters that will yield a deposit with the desired porosity. Optimum porosity must be determined by extensive measurements of both emitter activation times and high temperature emitter performance.

D. THERMAL STABILITY OF ORIENTATION

For the reasons cited in the previous section plus a vast amount of corroborating experimental data, thermal stability rather than being dependent upon deposition parameters appears to be principally a function of substrate preparation and deposit-substrate compatability. Generally, it is found for a variety of substrate types that thermal stability of the emitter surface is enhanced if the substrate is fully annealed prior to deposition. In particular, work damage and strain in the most superficial surface layers due to polishing the surface of the substrate must be completely eliminated before depositing. It has been shown in Reference 6, as well as in this present work, that vapor deposited tungsten cathodes do experience grain growth during operation at high temperatures. This growth is not detrimental to the present application as long as the initial preferred orientation is preserved. In the planar geometry there is no limit to

the allowable grain size. In the cylindrical geometry, however, the final grain size must be small compared to the radius of curvature of the surface.

Deposits such as P-24-W (Figure B-4, Appendix B) grown on appropriately oriented but strained substrates exhibit an extremely sharp "as-deposited" orientation of their preferred crystal direction. However, as shown in the figure the orientation is not preserved during heating. Without the benefit of preferred orientation in the substrate, (111) deposits, 0.0025" thick, tend to have their crystallite directions oriented in a cone of half angle approximately 10° about the surface normal and the crystallites tend to be larger in the "as-deposited" condition (Figure 6). For a thermally stable deposit, additional crystal growth as a result of subsequent heating may occur and the diffraction peaks from individual crystallites may be further resolved in the pole figure, but by and large they will remain concentrated in the same cone of half angle 10°.

EMITTER FABRICATION

A. SUBSTRATES - THERMOCHEMICAL CONSIDERATIONS

The following listed types of planar thorium dispensing substrates were evaluated during this reporting period:

Type 1: 2% thoriated tungsten; carburized (emitter designation* P-n-ThW).

Type 2: Tungsten, tungsten carbide, thorium hydride; cermet (emitter designation P-n-C).

Type 3: "L" type; thorium hydride and/or thorium metal behind a high porosity (71.8% dense) sintered tungsten substrate with a CVD oriented surface coating (emitter designation P-n-SW).

Each of the substrates listed above involves a different thermal or thermochemical reaction as its mode of producing free thorium. The reactions believed to be most important in each case are listed below:

Type 1: $$\underset{(c)}{ThO_2} + \underset{(c)}{2W_2C} \rightleftarrows \underset{(c)}{4W} + \underset{(g)}{2CO} + \underset{(g)}{Th}$$

Type 2: $$\underset{(c)}{ThC_2} + \underset{(c)}{4W} \rightleftarrows \underset{(c)}{2W_2C} + \underset{(g)}{Th}$$

Type 3: $$\underset{(c)}{Th} \rightleftarrows \underset{(g)}{Th}$$

The equilibrium partial pressures of free thorium over each of these reactions is the driving force for the diffusion of thorium from the reservoir through the oriented

---

* The first index (P) specifies geometry (planar); the second index (n) specifies the number of the particular emitter (n = 1, 2, 3...); the third index (ThW, C, or SW) identifies the type of substrate.

layer to the surface. These partial pressures can be determined from the best available thermodynamic data using the Gibbs-Helmholtz free energy equation which for a reaction with up to two gaseous reaction products can be written in the form:

$$\log_{10}\left(p_1\right) = \frac{.2185}{n}\left(-\frac{\Delta H^\circ}{T} + \Delta S^\circ\right) - \frac{\beta}{n}\log_{10}\frac{\beta}{\alpha} + 2.88$$

where

n = total number of moles of gaseous reaction products

p_1 = partial pressure of gaseous reaction product 1 in Torr

α = number of moles of gaseous reaction product 1

β = number of moles of gaseous reaction product 2

ΔH° = change in enthalpy

ΔS° = change in entropy

T = temperature in °K

Using the data in Table I, obtained from the sources indicated in the last column of that table, the following expressions are obtained for partial pressures of thorium for each of the reactions.

$$\text{Type 1:} \quad \log_{10} p = 10.75 - \frac{2.77 \times 10^4}{T}$$

$$\text{Type 2:} \quad \log_{10} p = 8.84 - \frac{3.26 \times 10^4}{T}$$

$$\text{Type 3:} \quad \log_{10} p = 8.872 - \frac{2.878 \times 10^4}{T}$$

Thus the greatest driving force for diffusion is provided by the type 1 thoriated tungsten substrate. Other factors, however, may favor the use of type 2 and type 3 substrates, for example neither of them involve the evolution of a second gaseous

TABLE I

Substance	Phase	H_{1800} (K Cal/mole)	S_{1800} Cal/mole-°K	How Obtained
Th	(g)	145.9	56.46	$S_{1800}^{(c)}$ and $(H_{1800}^{(c)} - H_{298})$ from Ref. 7, p.115. . . . . ΔS°_{1800} and ΔH°_{1800} calculated from thorium vapor pressure equation of Darnell. (Private correspondence with I. Brodie.)
W	(c)	9.84	19.47	Ref. 7, p. 124.
C	(c)	7.19	9.02	Ref. 7, p. 28.
CO	(g)	-14.7	60.92	Ref. 7, p. 29.
W_2C	(c)	20.47	49.0	For reaction $2W + C \rightarrow W_2C$; $\Delta F^\circ_{298} = -6.4 - 1.0\,T$, Ref. 8 . . . . . $\Delta F_T = \left[\Delta H_{298} + \int_{298}^{T} \Delta C_p dT\right] - T\left[\Delta S_{298} + \int_{298}^{T} \frac{\Delta C_p}{T} dT\right]$ By Neuman and Kopp rule $\Delta C_p \approx 0$; Ref. 9. $\therefore \Delta F_T \approx \Delta H_{298} - T\Delta S_{298}$.
ThC_2	(c)	-1.88	49.3	S_{298} and dependence of C_P on T. Ref. 10, p. 1521. S_{1800} calculation from these data. . . . . For reaction $Th + 2C \rightarrow ThC_2$; $\Delta H^\circ_{298} = -30.7$ K Cal/mole, Ref. 10, p. 1516.

TABLE I (Cont'd.)

Substance	Phase	H_{1800} (K Cal/mole)	S_{1800} Cal/mole-°K	How Obtained
ThC_2				H_{1800} from Ref. 7, p. 28, 115 and from above value of ΔH_{298} using Neuman and Kopp rule, Ref. 9.
ThO_2	(c)	-265	47.46	Ref. 7, p. 115.

product as is the case for the type 1 substrate. Also, factors related to compatability of substrate and deposit may favor any of the three types over any of the others.

B. FABRICATION PROCEDURES - GENERAL

Types 1 and 2 planar emitters (overall dimensions shown in Figure 9) were fabricated to fit into an existing demountable test stand. Type 3 planar emitters were designed to fit into the same test diode but are necessarily more complex in structure (Figure 18).

In accordance with considerations discussed in previous sections fabrication procedures were evolved for each of the three types to satisfy the following two basic conditions.

1. Substrate must be entirely strain-free both throughout its volume and at the substrate-deposit interface, prior to deposition of the grain-oriented surface layer.

2. Substrate surface must be sufficiently smooth and uniform to have a negligible effect on the microstructure of the deposit.

Condition 1 is required to maximize the probability of achieving adequate thermal stability of the overall structure. Condition 2 is necessary to insure reproducible control of both deposit orientation and microstructure. Fiber texture and strain induced in pure tungsten substrates as discussed in previous sections also appear in each of the three types of dispenser substrates due to cold working (polishing, etc.) and other required steps such as carburizing. These effects as they apply to each type emitter will be discussed in the following sections.

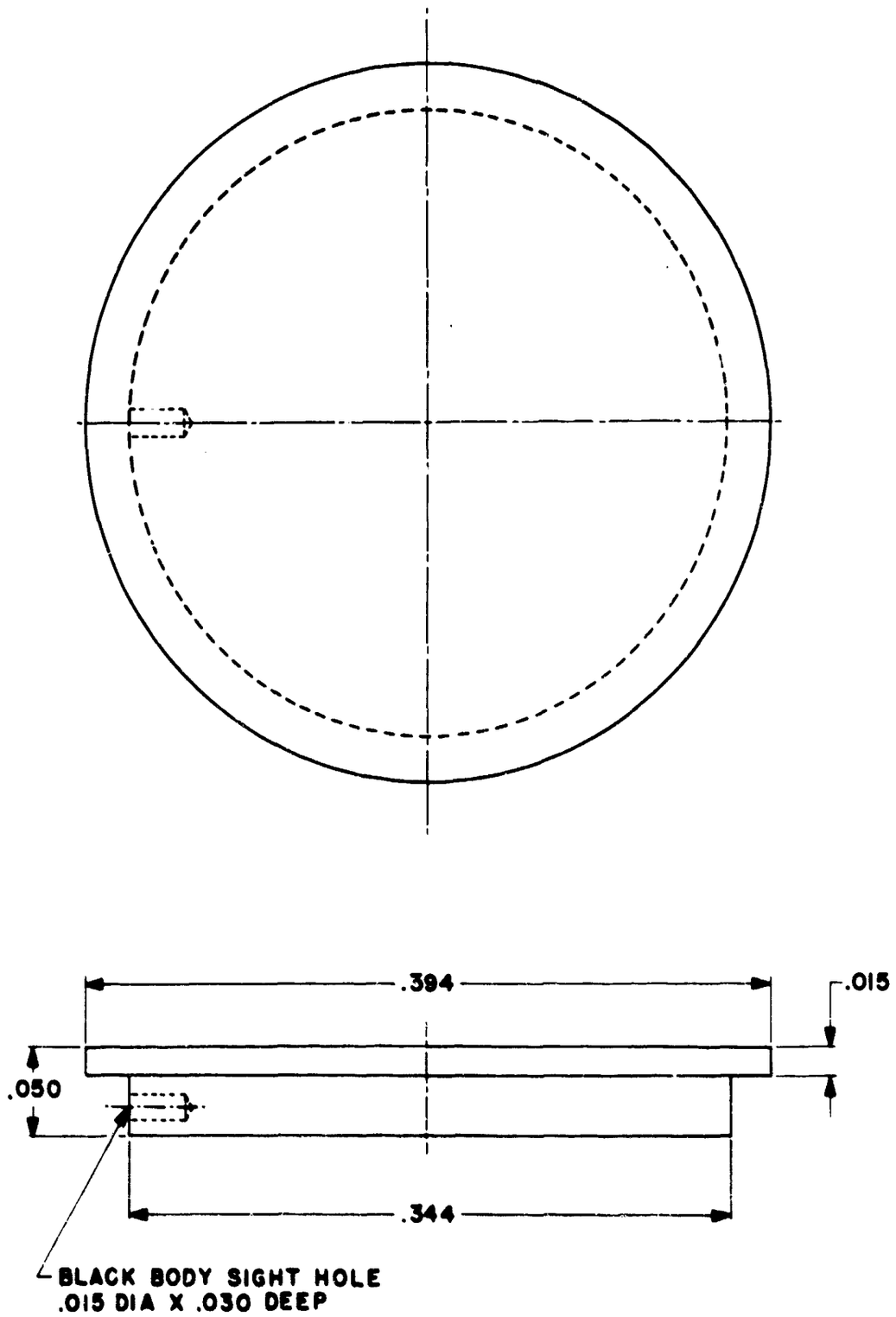

Figure 9. Planar Thermionic Emitter for Demountable Test Diode

C. TYPE 1 EMITTERS

Type 1 dispenser substrates are machined from high purity 2% thoriated tungsten drawn rod. Their surfaces are carburized to a depth of 0.006" to 0.008" by coating them uniformly with fine carbon powder suspended in a suitable binder, and then vacuum firing to approximately 2000°C. This entire process is repeated several times in order to obtain a sufficiently deep carbide. After carburization* the carbide in the surface layer exhibits a pronounced fiber texture with its c-axis preferentially oriented normal to the surface. The fiber texture in the carbide develops during the carburization and is largely unaffected by subsequent micropolishing. An α-W_2C, (00·2) pole-figure scan ($2\theta = 38.1°$) of the carburized surface layer of one such carburized substrate (Figure 11) illustrates the extent to which the c-axis is oriented normal to the surface. For comparison, a curve for a random powder sample is included on the figure. The fall-off of intensity of the random sample response with angle is not inherent to the analytical technique, but is a consequence of the X-ray optics used in this particular case.

Figure 12 is an ordinary diffractometer scan of the same substrate surface. The magnitudes of the (00·2) and (00·4) α-W_2C lines again attest to the preferred orientation of the carbide. In addition, however, this scan shows that there is tungsten still present in the carburized surface layer (see footnote below). The magnitudes of the (110) and (220) tungsten lines relative to the other tungsten lines indicate that it is highly oriented with the [110] crystal direction normal to the surface. Since these substrate disks were sections machined from a drawn thoriated tungsten rod, this orientation of the tungsten is undoubtedly the result of the residual fiber texture induced by the drawing process. Micropolishing of these substrates tends to slightly randomize the orientation of the tungsten, but if there is any tendency to affect the orientation of

---

* After carburization the surface is predominantly α-W_2C, which has a hexagonal crystal structure. Some uncarburized tungsten islands are still present throughout the layer, however (Figure 10).

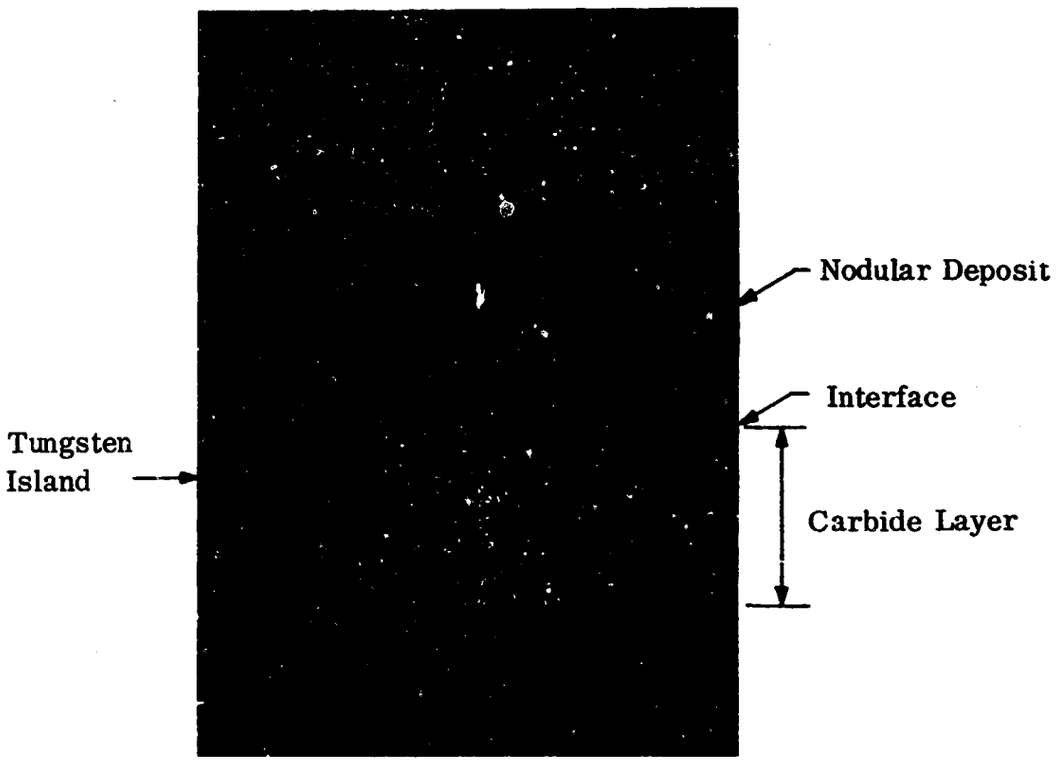

(111) Oriented deposit on an "as carburized" type 1 emitter substrate surface. Note the islands of tungsten scattered throughout the carbide layer.

Figure 10. Section of P-42-ThW (Scale, X306)

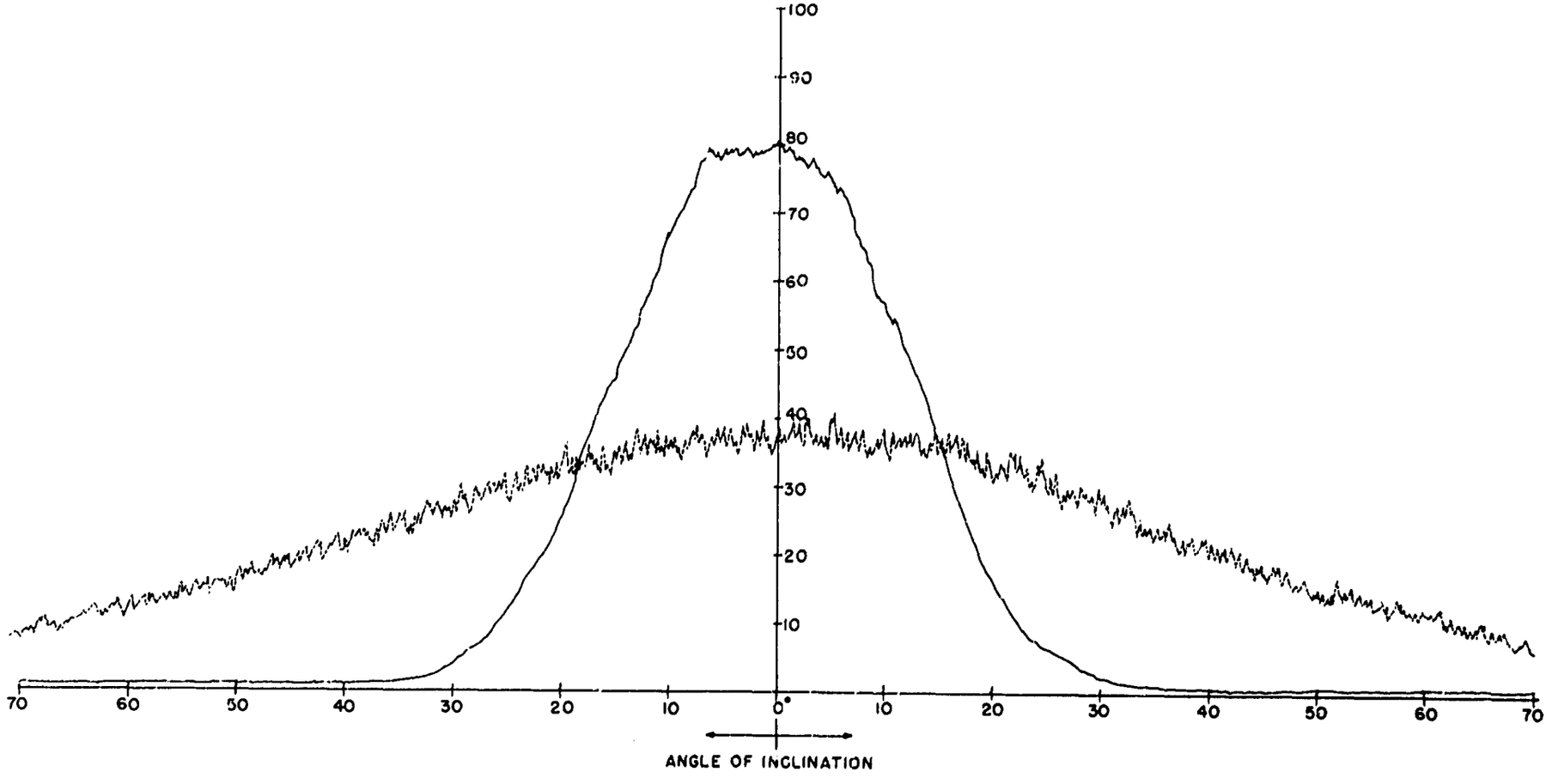

Figure 11. Plots of the Integrated Intensity of Cu Kα X-Radiation Diffracted from the (00·2) Planes of a Type 1 Substrate (P-44-ThW) as a Function of the Angle of Inclination of the Planes to the Surface. (Solid Curve, Substrate; Dotted Curve, a Random Powder Sample)

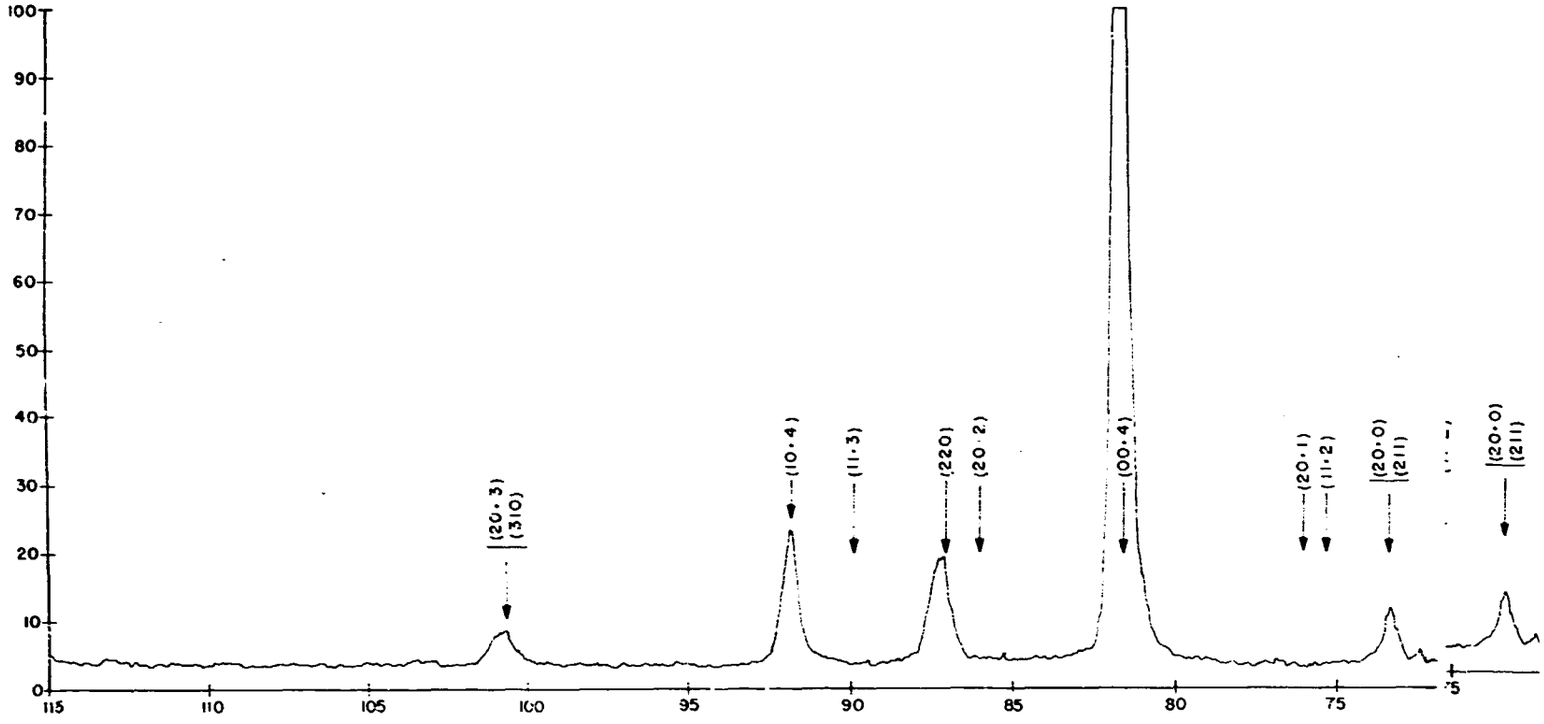
100
90
80
70
60
50
40
30
20
10
0
115
110
105
100
95
90
85
80
75
(20·3)
(310)
(10·4)
(11·3)
(220)
(20·2)
(00·4)
(20·1)
(11·2)
(20·0)
(211)
(20·0)
(211)

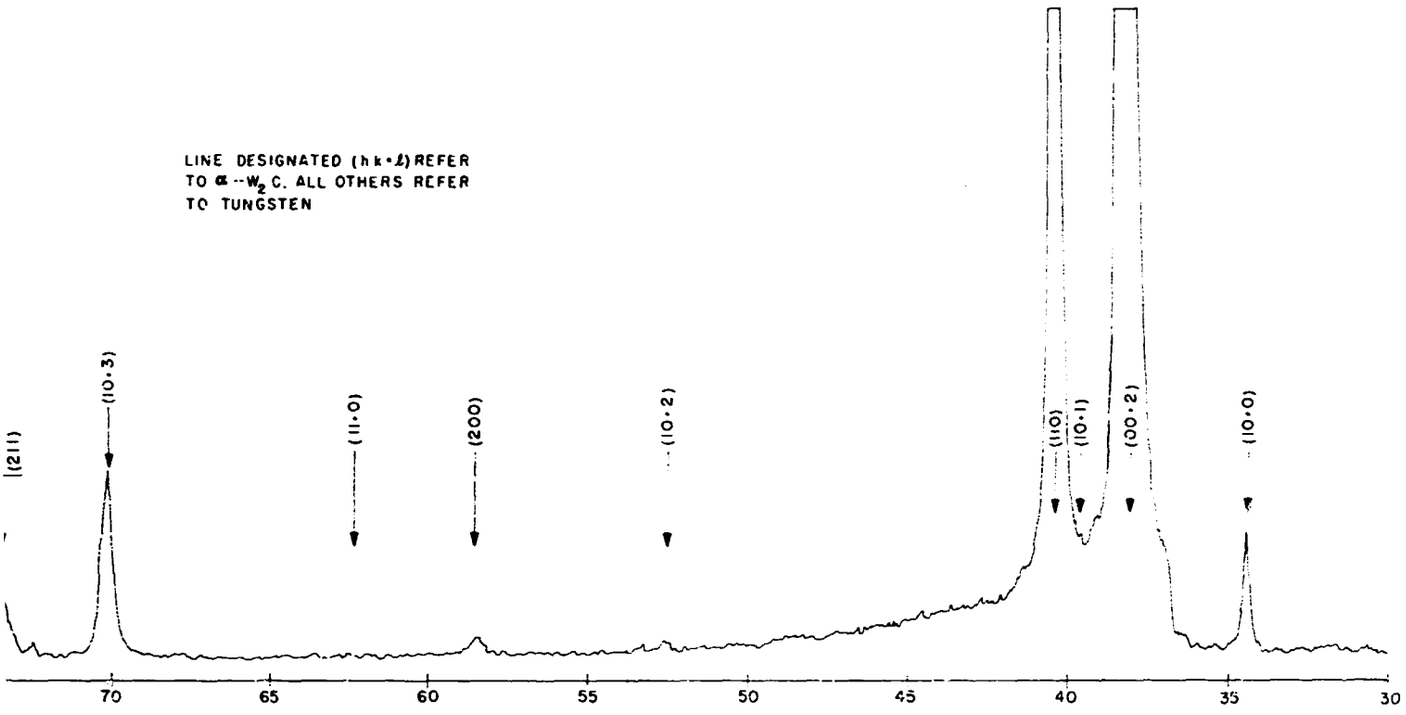

Figure 12. Diffractometer Scan of a Type 1 Dispenser Substrate Surface After Carburization (Cu Kα X-Radiation)

B.1

the carbide, it is so slight as to be undetectable by ordinary X-ray techniques. Thus in all probability, the carburized surface of a type 1 substrate suffers less plastic deformation than a plain tungsten surface due to micropolishing. Despite this fact the "as-carburized" surface is not suitable as a substrate for deposition because small regions of the surface that are not carburized act as preferred sites for rapid growth of the oriented crystallites (Figure 10). To circumvent this undesirable effect, the carbide layer is decarburized to a depth of approximately 0.001". This is followed by additional micropolishing and annealing of the resulting single phase tungsten surface which removes surface roughness due to the phase transition and yields finally a uniform single phase, strain-free surface onto which the deposit can be made.* The carbide, essential for good emission in this type cathode,[11] is still present but not in the uppermost layer of the substrate. After decarburization, X-ray diffraction shows the surface to be entirely free of any carbide.

A decarburized surface of a type 1 substrate is shown in Figure 13a. The final micropolishing after decarburization leaves the surface smooth but superficially strained. As shown in Figure 14a, the final anneal to remove this strain produces some surface roughness, but much less than that which results from the phase transition.

The complete procedure for preparing type 1 emitters can be summarized as follows:

1. Micropolish emitting surface to 6 μ diamond finish.

2. Carburize emitting surface to a depth >0.006 inch.

3. Micropolish carburized emitting surface to 6 μ diamond finish.

---

*The substrates for P-43-ThW and P-44-ThW (Figures 7 and 8) were both processed as indicated here. P-42-ThW and P-44-ThW were both deposited with WF_6 flow rates of 25 cc/min. Their preparation differed only in substrate pre-treatment.

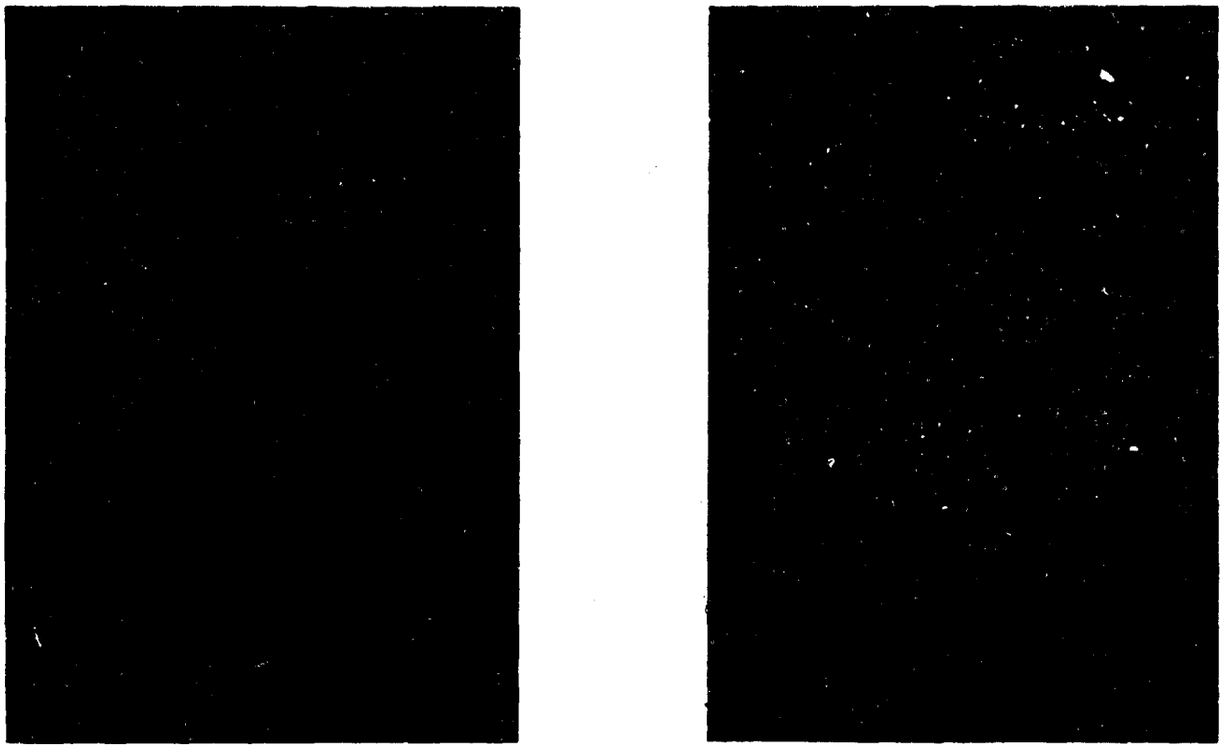

(a) P-44-ThW; Type 1

(b) P-53-C; Type 2

Figure 13. Surfaces of Type 1 and Type 2 Emitter Substrates After Decarburizing. Note Roughness Resulting from the Phase Transition. (Scale, X589)

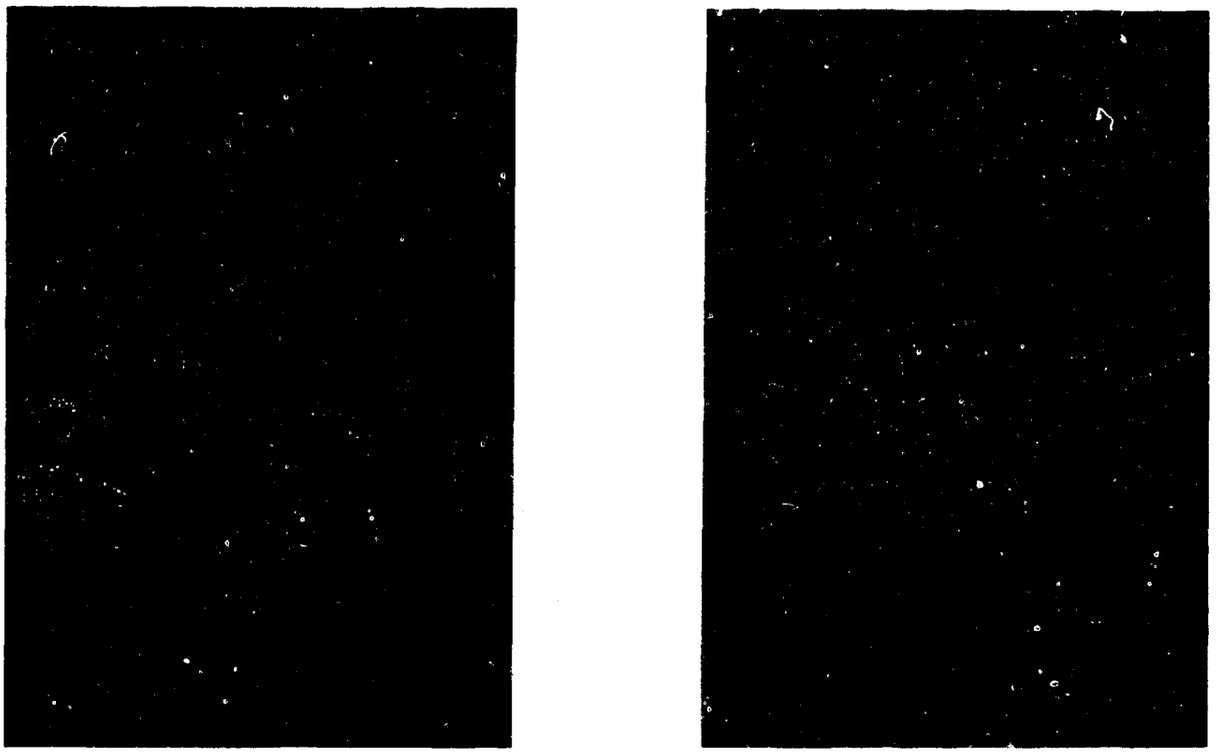

(a) P-44-ThW; Type 1

(b) P-53-C; Type 2

Figure 14. Surfaces of Type 1 and Type 2 Emitter Substrates After Decarburizing, Polishing and Annealing. (Scale, X589)

4. Decarburize surface to a depth of 0.001 inch (dry hydrogen fire 1 hour at 1620°C).

5. Micropolish decarburized emitting surface to 1 μ diamond finish.

6. Anneal (vacuum fire 20 minutes at approximately 1900°C).

7. Clean and load into deposition chamber.

8. H_2 fire in situ prior to deposition for 1 hour at 700°C.

9. Deposit (111) grain-oriented surface layer.

10. Micropolish deposited surface layer to develop surface perpendicular to the [111] crystal direction.

D. TYPE 2 EMITTERS

Billets from which type 2 dispenser substrates are machined were prepared by mixing tungsten, tungsten carbide, and thorium hydride powders in proportions 89.5%, 10%, and 0.5% respectively, pressing the mixed powders, and then sintering at 2400°C. (This process for preparing thorium tungsten cermet cathodes was first described in detail in the literature in Reference 12.) The surfaces of substrates machined from these billets are predominantly tungsten. Grinding produces a layer of depth greater than one micron in which both the tungsten and carbide X-ray diffracted line intensities correspond closely to the ASTM reported values for a random sample (Figure 15a). Micropolishing of the surface produces no significant preferred orientation in the carbide surface layer. However, it does produce a significant preferred orientation of the tungsten. A comparison of Figures 15a and 15b shows that micropolishing enhances diffraction from the $\{111\}$ crystal planes of tungsten predominantly at the expense of $\{100\}$ planes.

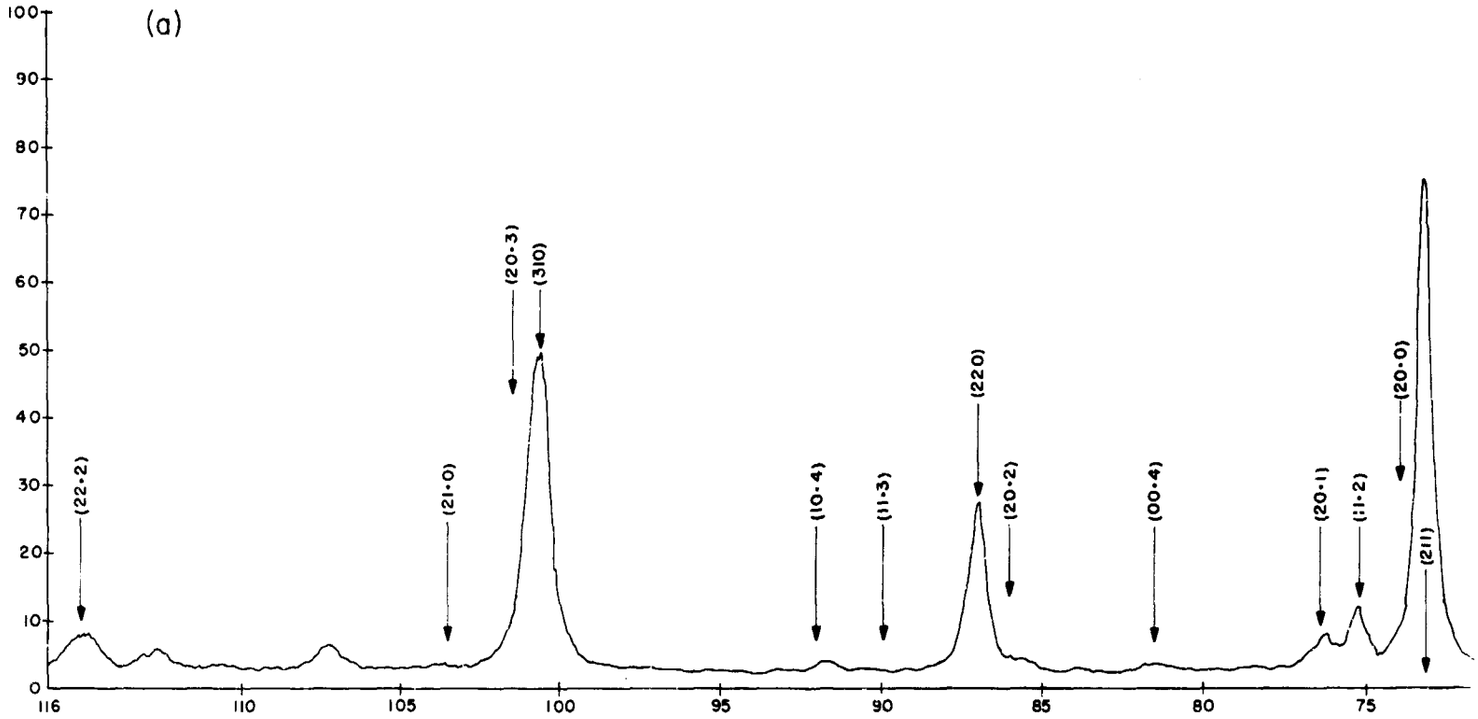
(a)
(22·2)
(21·0)
(20·3)
(310)
(10·4)
(11·3)
(220)
(20·2)
(00·4)
(20·1)
(11·2)
(20·0)
(211)
100
90
80
70
60
50
40
30
20
10
0
116
110
105
100
95
90
85
80
75

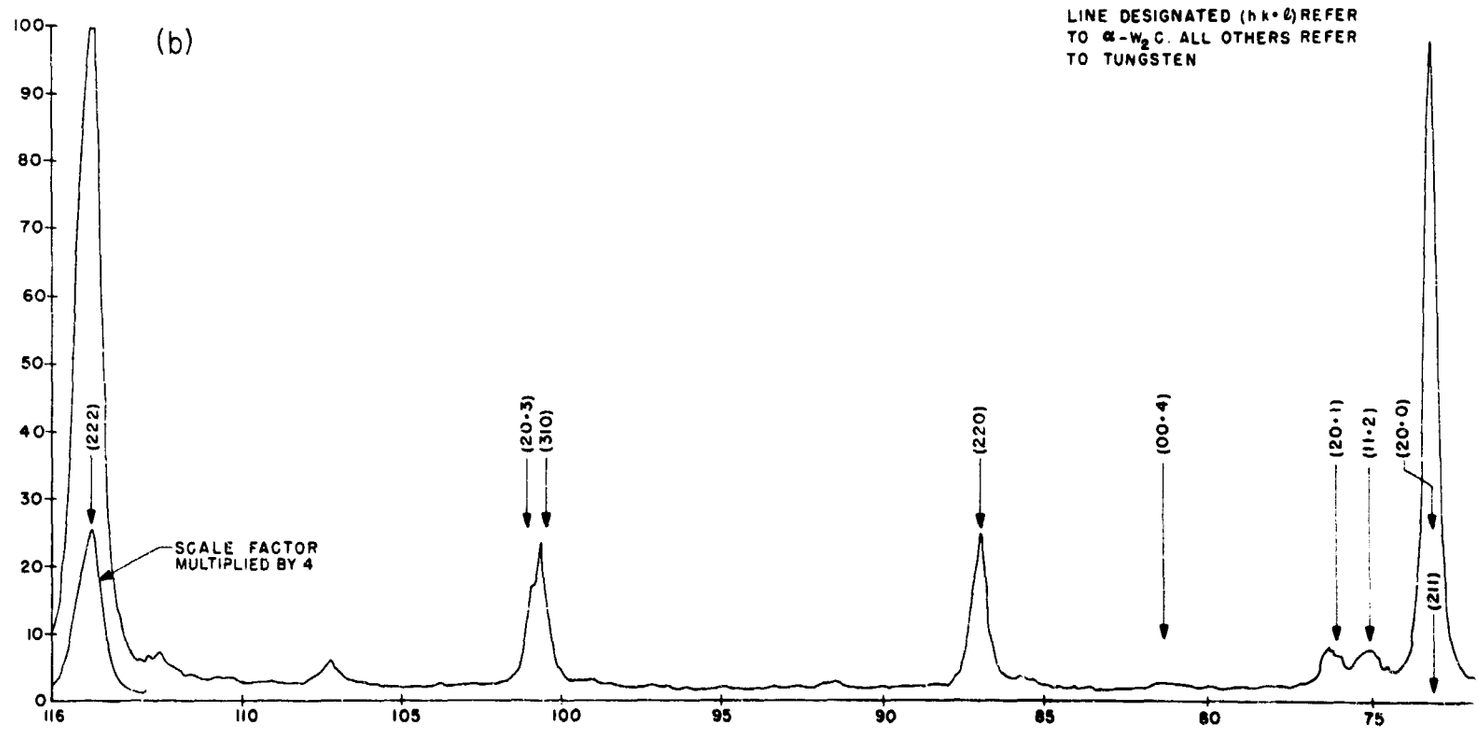
(b)
LINE DESIGNATED (h k • ℓ) REFER TO α-W2C. ALL OTHERS REFER TO TUNGSTEN
(222)
SCALE FACTOR MULTIPLIED BY 4
(20·3)
(310)
(220)
(00·4)
(20·1)
(11·2)
(20·0)
(211)
100
90
80
70
60
50
40
30
20
10
0
116
110
105
100
95
90
85
80
75

A.

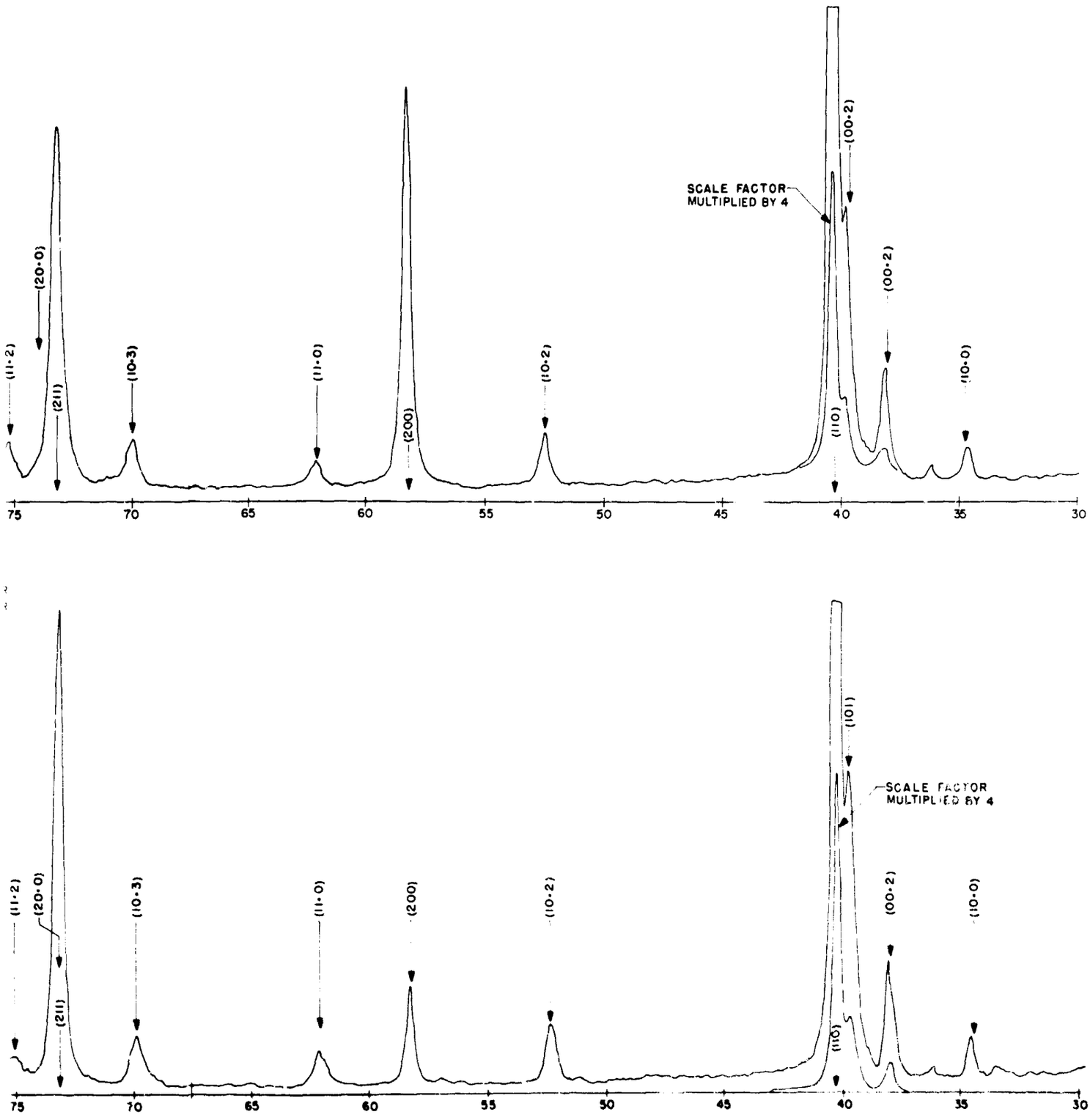

Figure 15. Diffractometer Scan of a Type 2 Dispenser Substrate Surface. (Cu Kα X-Radiation) (a) Ground Surface, (b) Micropolished Surface)

B.

Figure 16a is a (200) X-ray pole-figure scan for tungsten of a typical micropolished type 2 substrate (P-47-C). The peaking at approximately 54° off normal clearly indicates (111) preferred orientation due to the polishing. The dotted curve is a random sample response included for comparison. Figures 16b and 16c respectively show the effect on the substrate orientation of vacuum firing for 30 minute periods, first at 1700°C (Figure 16b) and then at 2000°C (Figure 16c). Another type 2 substrate (P-39-C) was micropolished and tungsten deposited onto it under conditions identical to P-2-W (Figure 5). A (200) X-ray pole-figure scan of the deposit surface layer is shown in Figure 17a. Figures 17b and 17c show the deterioration of the deposit orientation after vacuum firing for 30 minute periods, first at 1700°C (Figure 17b) and then at 2000°C (Figure 17c). Comparing Figures 16 and 17 it is evident that the deterioration of the deposit orientation is closely associated with the recrystallization and growth of the plastically deformed substrate surface layer. After the 2000°C heat treatment, the (111) orientation is almost gone and the crystallites in the deposit have grown to a size such that only a few contribute to produce diffraction peaks in an individual pole-figure scan. A complete pole figure would be required to fully characterize the orientation of the specimen in this state.

For the same reason as for type 1 emitters, i.e. to achieve a uniform single phase strain-free substrate surface, decarburization, micropolishing and annealing was done on type 2 substrates prior to deposition. A decarburized surface of a type 2 substrate is shown in Figure 13b. After micropolishing, the surface is smooth but superficially strained. As shown in Figure 14b the final anneal to remove this strain produces some surface roughness but, again, much less than that which results from the phase transition.

The complete procedure for preparing type 2 emitters from their sintered billets is summarized below.

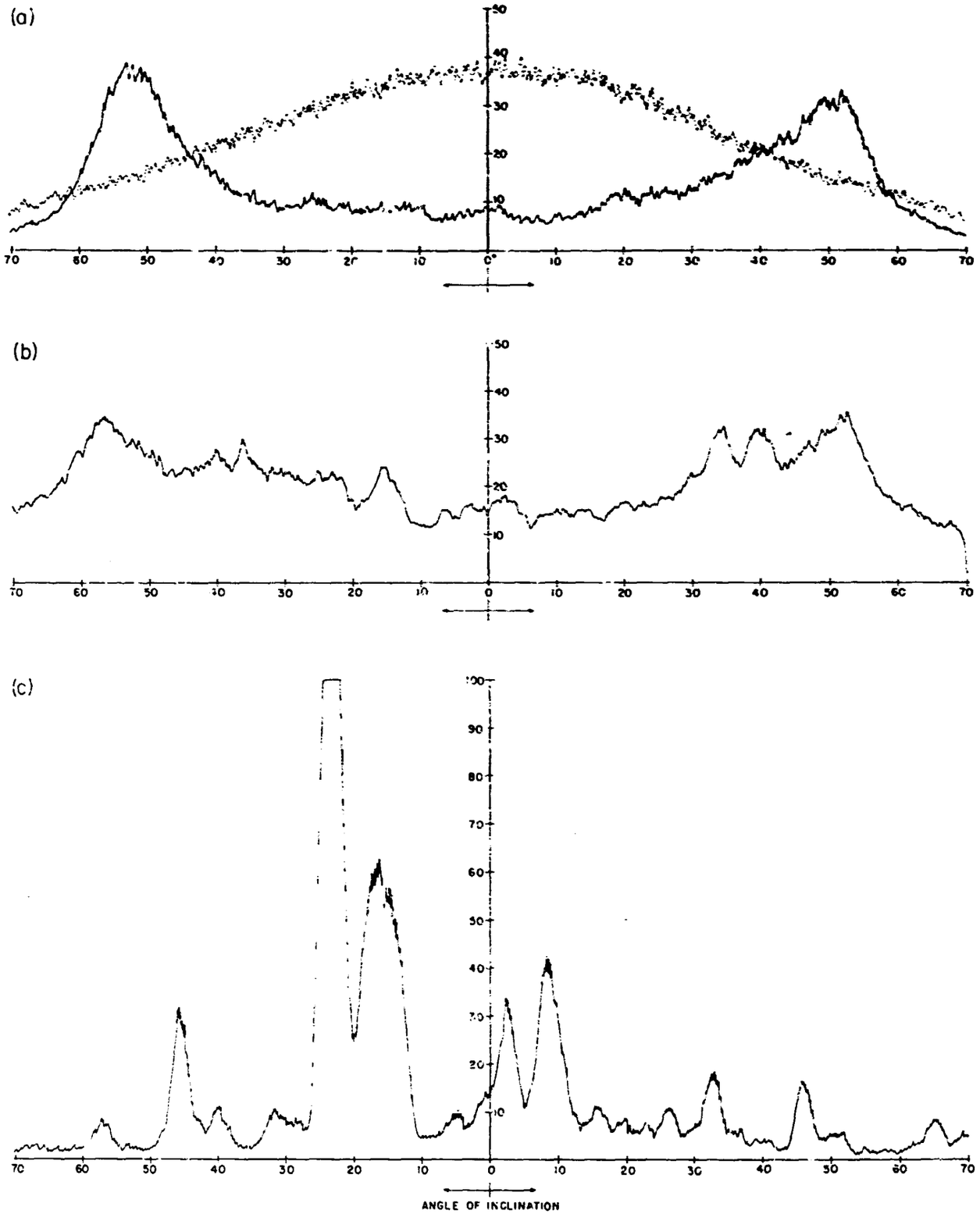

Figure 16. Plots of the Integrated Intensity of Cu Kα X-Radiation Diffracted from the [200] Planes of a Type 2 Substrate (P-47-C) as a Function of the Angle of Inclination of the Planes to the Surface. (a) Solid Curve, Micropolish Substrate; Dotted Curve, a Random Powder Sample (b) After Vacuum Firing for 30 Minutes at 1700°C (c) After Vacuum Firing for 30 Minutes at 2000°C

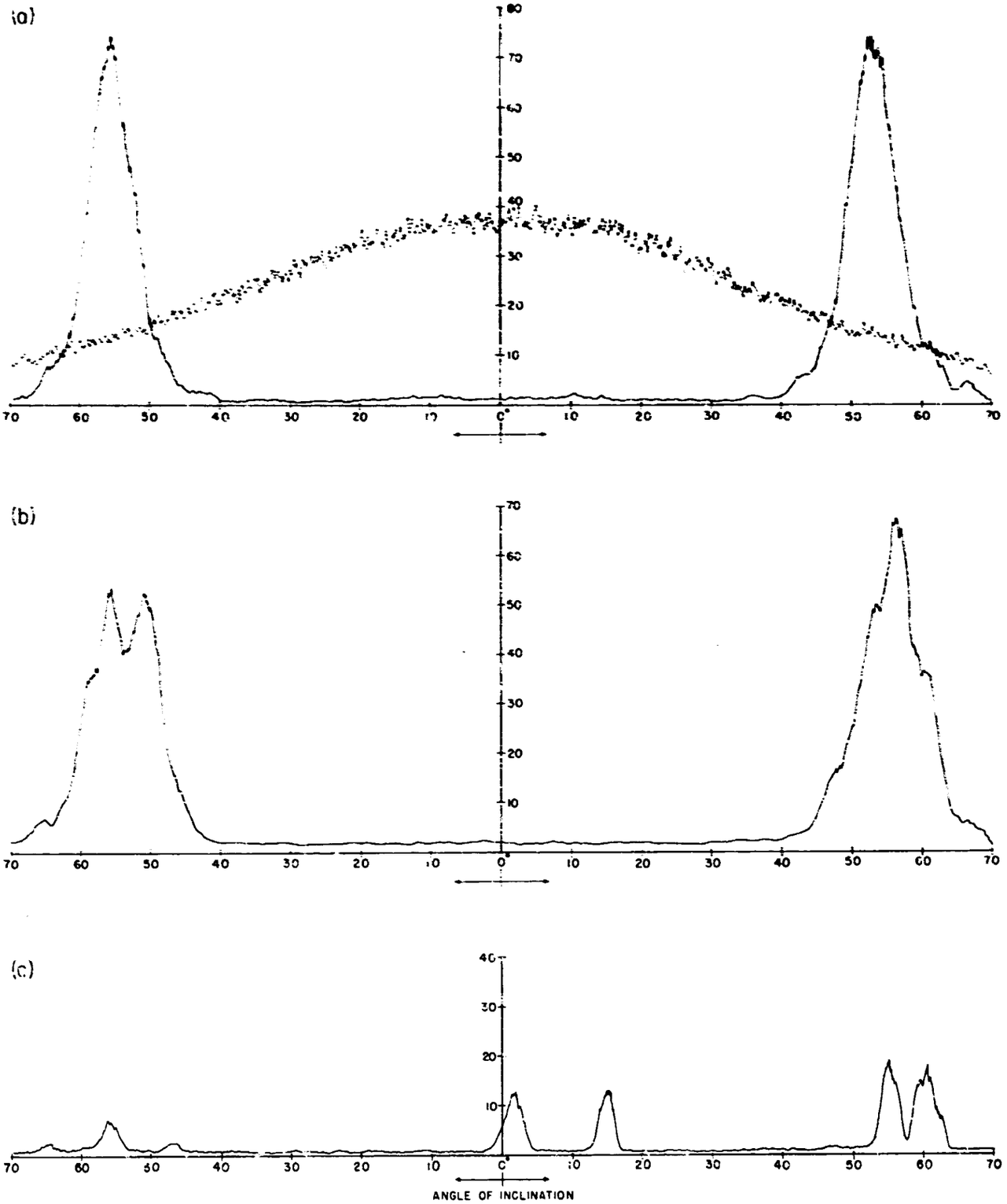

Figure 17. Plots of the Integrated Intensity of Cu Kα X-Radiation Diffracted from the [200] Planes of P-39-C as a Function of the Angle of Inclination of the Planes to the Surface. (a) Solid Curve; Deposit as Deposited on Micro-polished Substrate; Dotted Curve, a Random Powder Sample (b) Deposit, After Vacuum Firing for 30 Minutes at 1700°C (c) Deposit, After Vacuum Firing for 30 Minutes at 2000°C

1. **Micropolish emitting surface to 6 μ diamond finish.**

2. **Decarburize surface to a depth of 0.001" (dry hydrogen fire 1 hour at 1620°C).**

3. **Micropolish decarburized emitting surface to 1 μ diamond finish.**

4. **Anneal (vacuum fire 20 minutes at approximately 1900°C).**

5. **Clean and load into deposition chamber.**

6. **H_2 fire in situ prior to deposition for 1 hour at 700°C.**

7. **Deposit (111) grain-oriented surface layer.**

8. **Micropolish deposited surface layer to develop surface perpendicular to the [111] crystal direction.**

E. TYPE 3 EMITTERS

The type 3 emitter is by far the most difficult to fabricate. However, since in the case of both type 1 and type 2 substrates the thorium is tied up in a stable compound: thoria in the former and thorium dicarbide in the latter, while in the type 3 substrate the thorium is free, and its rate of arrival at the surface is limited only by its rate of diffusion through the grain-oriented surface layer, the effort was considered worthwhile. Billets from which type 3 substrates are machined are 71.8% dense sintered tungsten. The pores of the billet are copper-loaded during the initial machining operations and throughout most of fabrication of the emitter structure. Figure 18 shows the construction of a completed type 3 emitter; the entire procedure for fabricating it follows.

1. Machine copper-loaded tungsten blank for main body, leaving thorium reservoir and back plug spaces solid.

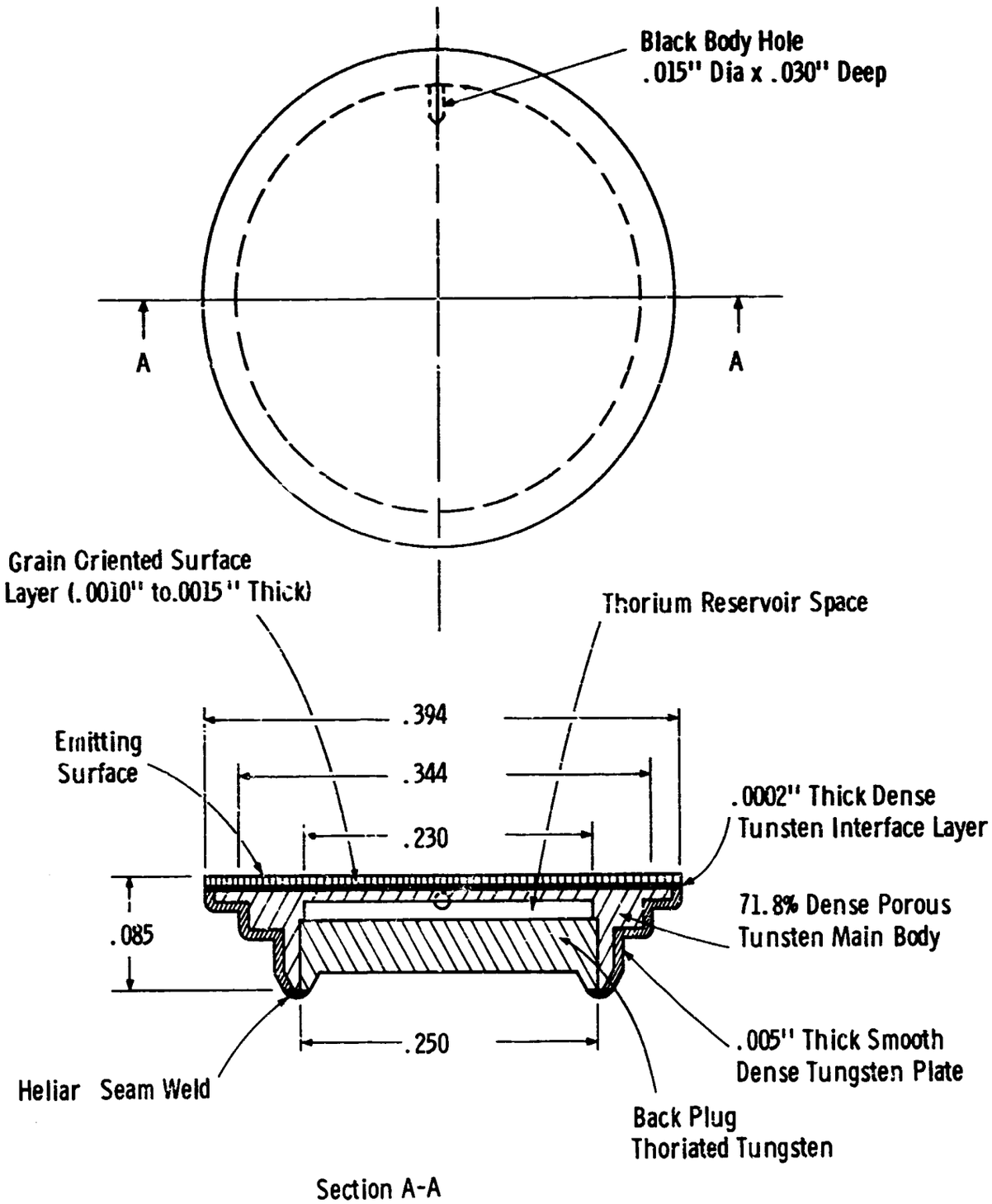

Figure 18. Type 3 Emitter

2. Place with front (i.e. emitting) face down in deposition chamber and deposit 0.005" thick smooth dense (100) oriented tungsten on sides and back.*

3. Polish or grind tungsten off back face.

4. Polish front face to 6 μ diamond finish.

5. Etch front face lightly with 25% nitric acid water solution.

6. Deposit approximately 0.001" thick smooth dense (100) oriented tungsten on front face.

7. Polish off all except 0.0002" of tungsten deposit on front face, finishing to 1 μ diamond.

8. Machine out cavity for thorium reservoir and rear plug.

9. Remove copper from remainder of main body with 25% nitric acid water solution.

10. Anneal (hydrogen fire 30 minutes at approximately 1700°C).

11. Deposit (111) grain-oriented tungsten surface layer.

12. Polish to develop the surface perpendicular to the [111] crystal direction.

13. In a dry helium environment load active material** (thorium or thorium hydride) into reservoir and heliarc back plug into place.

---

* Dense smooth (100) oriented deposits are grown easily regardless of substrate surface conditions.

** Some tungsten carbide powder is also added into the reservoir to provide carbon for gettering electronegative contaminating gases. Alternately, a small amount of carbon can be included in the main body during fabrication of the billet by powder metallurgy.

In fabricating this type emitter several factors must be considered over and above those common to the type 1 and type 2 emitters. Deposition of the grain oriented tungsten surface layer cannot be made directly onto the porous tungsten after removal of the copper because the reactants will penetrate throughout the pores and plug them. In addition, the porous surface is far too rough and will influence deposit microstructure. It is also essential that the reservoir be filled with thorium or thorium hydride after the final tungsten deposition rather than before so that fluorine present during deposition will not react with the free thorium to form a stable compound. Finally the reservoir must be filled in an inert, dry atmosphere and sealed leak tight in that environment in order to maintain the free thorium. Attempting to do the final heliarc in the presence of any moisture results in the formation of thorium hydroxide.

The 13-step procedure listed above satisfies all of these special requirements and also provides that the final deposition of the grain-oriented surface is made onto a single-phase, smooth, strain-free tungsten surface.

EMITTER EVALUATION

A. TEST FACILITY FOR PLANAR EMITTERS

Thermionic data have been obtained for each of the three types of thorium on grain-oriented tungsten emitters in an ultra high vacuum planar test diode. The diode shown in cross section in Figure 19 consists of a refractory metal emitter support ring* which holds the emitter in position facing a water-cooled copper collector, separated by a 0.005" gap from a surrounding water-cooled copper guard ring. The collector is 0.1 cm^2 in area and samples only the current from the center 0.1 cm^2 area of the emitter button. The latter is heated by electron bombardment from the rear and its temperature is determined by viewing into a black body hole in its side with a microoptical pyrometer. It is spaced from the collector-guard ring structures by three ceramic spacers. The two structures are held together under spring tension and their spacing can be changed in assembly by merely changing the thickness of the spacers. The diode is evacuated by a liquid nitrogen sorption pump and a 40 liter/sec VacIon® high vacuum pump. After inserting an emitter, pumping down, and baking out overnight at 400°C, the pressure in the diode is less than 10^{-9} Torr.

A block diagram of the entire test setup is shown in Figure 20 and a photograph is shown in Figure 21. At high emitter current density, where anode and guard-ring heating would otherwise be a problem, pulsed emission measurements are made at a very low duty cycle (10 μsec pulses at 120 cps rate). At low current density where anode heating is negligible, the pulser is disconnected and a recurrent 60-cycle signal is applied to the cathode of the test diode. Volt-ampere curves are displayed on a Tektronix 536 scope using Type G wide band plug-in units when the pulser is employed, and Type D high gain plug-in units when the 60-cycle recurrent sweep signal is used. The limited bandwidth of the high gain preamplifier makes the use of the pulser difficult at low emitter temperatures. A second dual trace oscilloscope is used to monitor the

---

* Both tantalum and molybdenum have been used for this support ring.

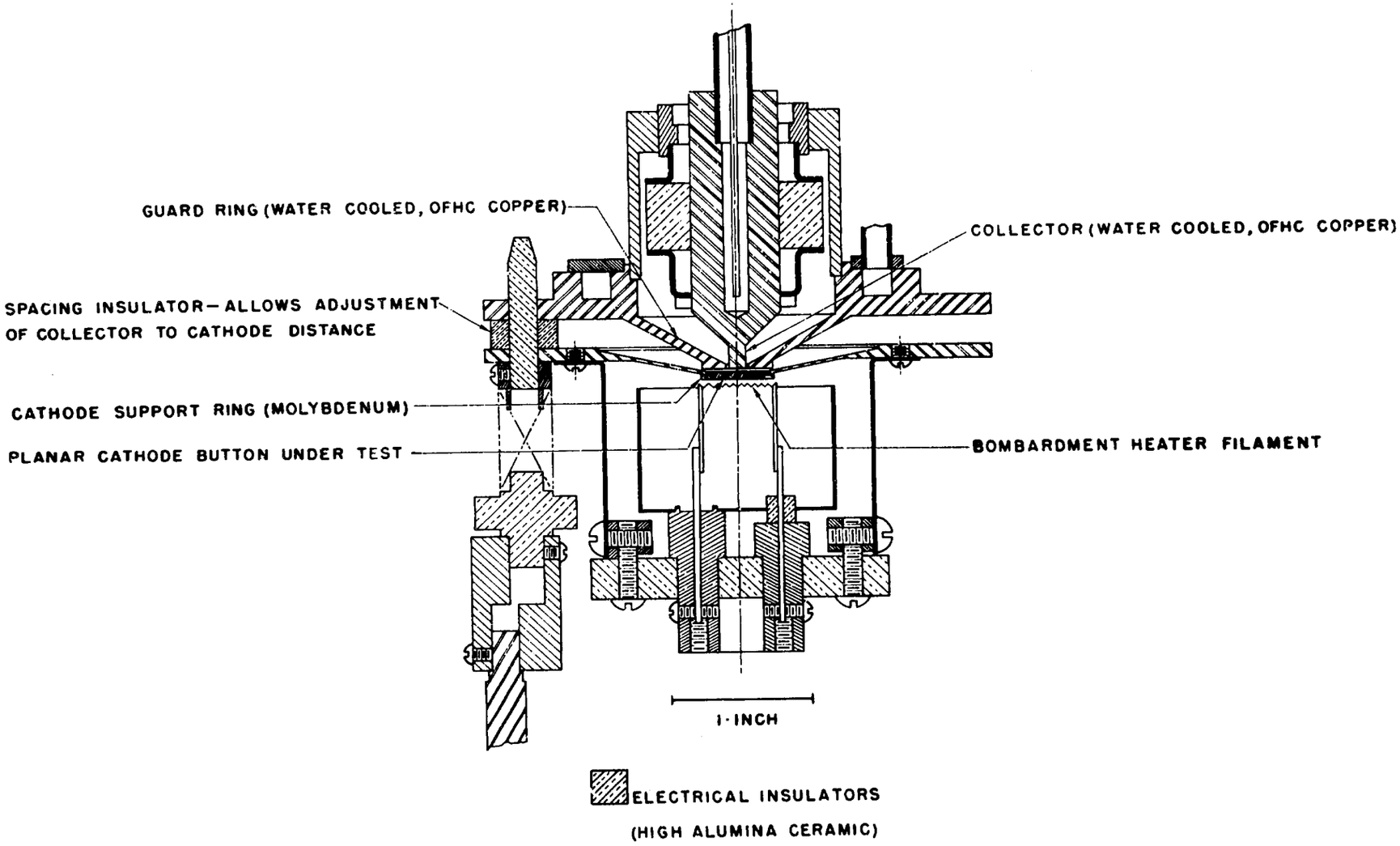

Figure 19. Cross Section of Demountable Vacuum Diode for Testing Planar Emitters

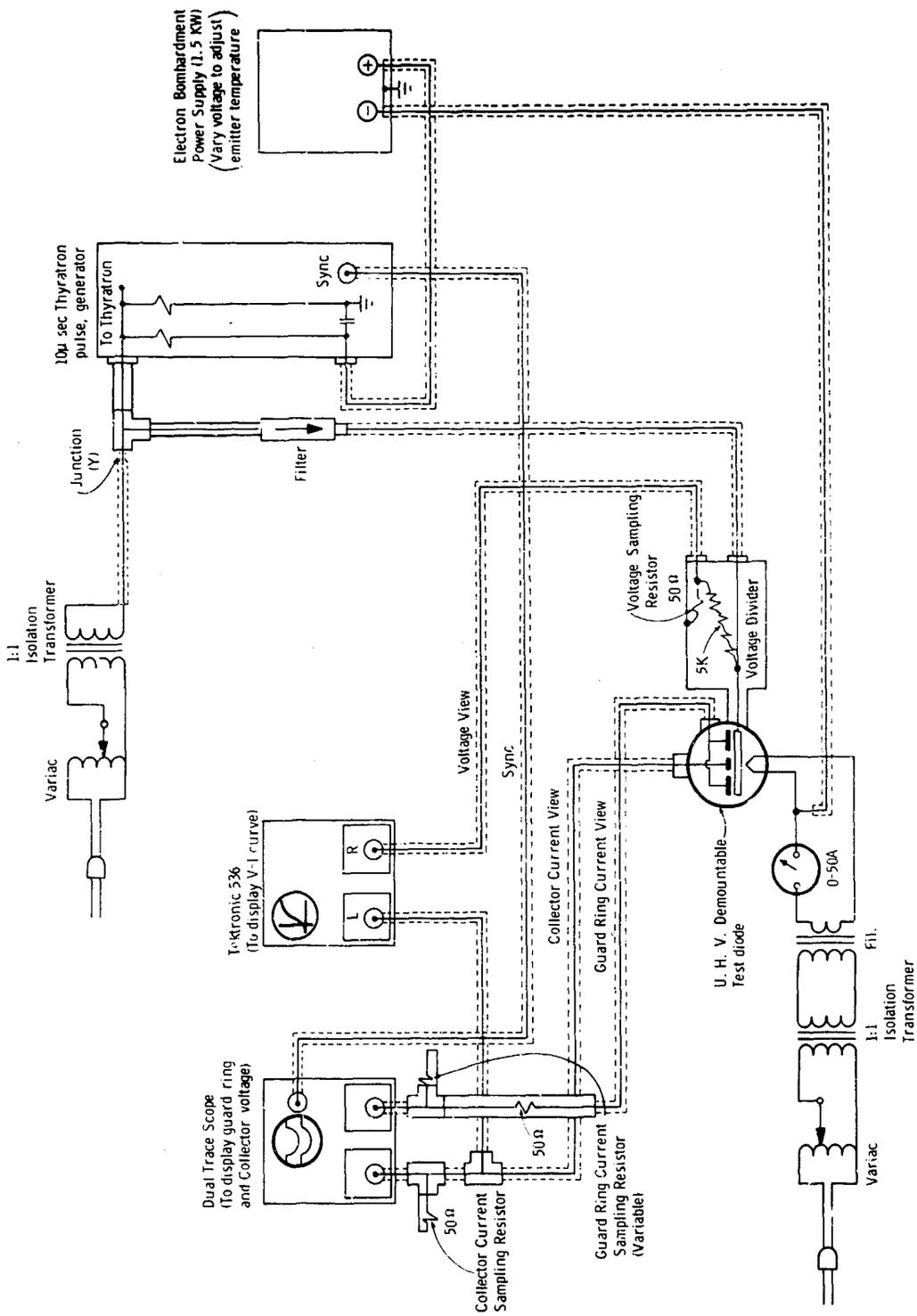

Figure 20. Block Diagram of Emitter Test Facility

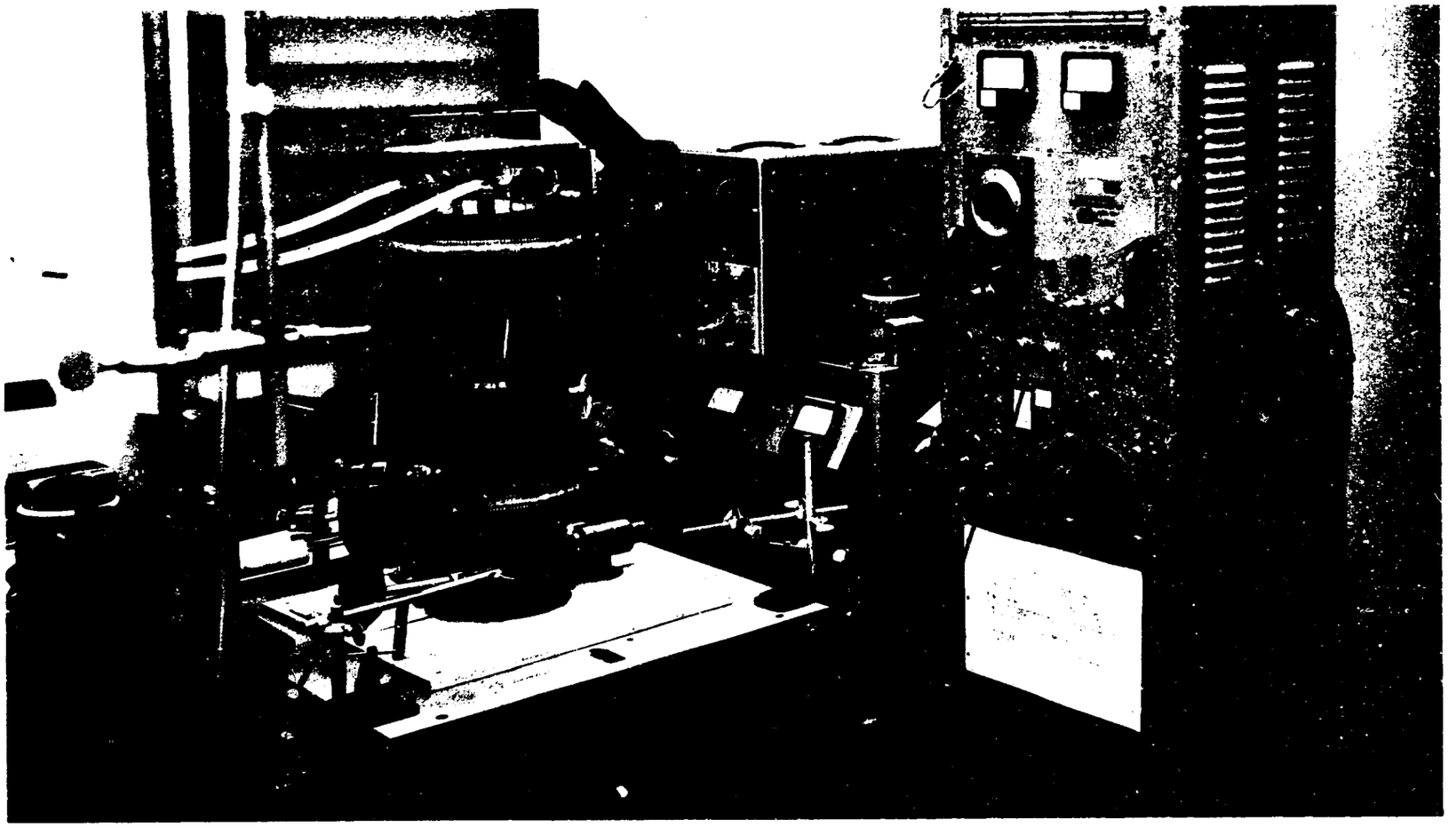

Figure 21. Photograph of Emitter Test Facility

collector and guard-ring voltages. The guard-ring sampling resistor is variable and its value is adjusted to make the collector and guard-ring voltage equal at all times during the sampling pulse. This minimizes transverse electric fields at the edge of the collector. At intermediate emitter temperatures data can be obtained using either the pulser or the 60-cycle sweep to verify that both yield identical results. Using these combined methods, data can be obtained over five orders of magnitude in current density.

B. ACTIVATION

In activating ordinary thorium thin film emitters the normal procedure following bakeout is to operate the emitter 100°C to 150°C hotter than its nominal operating temperature until the emission starts rising, and then to apply voltage to the anode and heat it by electron bombardment from the emitter to a temperature high enough to thoroughly outgas it (usually 700°C to 800°C). As the anode "cleans up" and poisoning gases are pumped away the emitter generally continues to improve until full activation is achieved. For the grain-oriented emitters of interest here it is desirable to activate at as low a temperature as possible so as to minimize any unnecessary degradation of the preferred orientation. With no a priori knowledge of the temperatures and times required for activation it was necessary to try various different schedules in an effort to arrive at a satisfactory procedure. A summary of the total time of heating for each of the emitters tested both during activation and thermionic testing is contained in Table II. In the last column in the table the rates at which each of the emitters activated are indicated.

Figure 22 is a detailed activation record for emitter P-111-SW in the form of a graph of saturation current density J_s vs time. Emitter temperature is also plotted against time in the same figure to illustrate the transient changes in current density which occur as the surface coverage returns to equilibrium after a large change in temperature.

TABLE II

PLANAR EMITTERS - TIME AT TEMPERATURE, AND ACTIVATION DATA

Emitter Number	Heating History		Activation
	Temp. Range T(°C)	Time in Range (hrs)	
P-93-ThW	1100 - 1600 1600 - 1700 1700 - 1800 >1800	17 9 3.5 1	Started activating after 7-1/2 hours at 1600°C Fully activated after 9 hours at 1600°C, 2 hours between 1600°C and 1700°C, and 2-1/2 hours at 1750°C Initial Activation - fast Full Activation - fast
P-113-ThW	1100 - 1600 1600 - 1700 1700 - 1800 >1800	42 3 58 2.5	Started activating after 3 hours below 1700°C and 3-1/2 hours between 1700°C and 1800°C Fully activated after 36 hours between 1700°C and 1800°C Initial Activation - fast Full Activation - very slow
P-109-SW	1100 - 1700 1700 - 1800 >1800	8.5 12.5 16.5	Started activating after 19 hours between 1700°C and 1800°C Fully activated after 20 hours between 1700°C and 1800°C and 13 hours between 1800°C and 1900°C Initial Activation - slow Full Activation - slow
P-111-SW	1600 1700 1800 1850	2 49 90 13	Started activating after 2 hours at 1700°C, 10-1/2 hours at 1800°C and 2-1/2 hours at 1850°C Fully activated after approx. 150 hours. (See Figure 22) Initial Activation - slow Full Activation - very slow*

* Figure 22 clearly indicates that full activation of P-111-SW might have been much faster if the temperature had been maintained at 1700°C instead of 1800°C.

TABLE II (Cont'd)

PLANAR EMITTERS - TIME AT TEMPERATURE, AND ACTIVATION DATA

Emitter Number	Heating History		Activation
	Temp. Range T(°C)	Time in Range (hrs)	
P-50-C	1100 - 1600 1600 - 1700 1700 - 1800 >1800	12 3 34 3	Started activating after 8-1/2 hours between 1700°C and 1800°C Fully activated after 10-1/2 hours between 1700°C and 1800°C Initial Activation - fast Full Activation - fast
P-102-C	Measurements not Completed	Measurements not Completed	Measurements not Completed

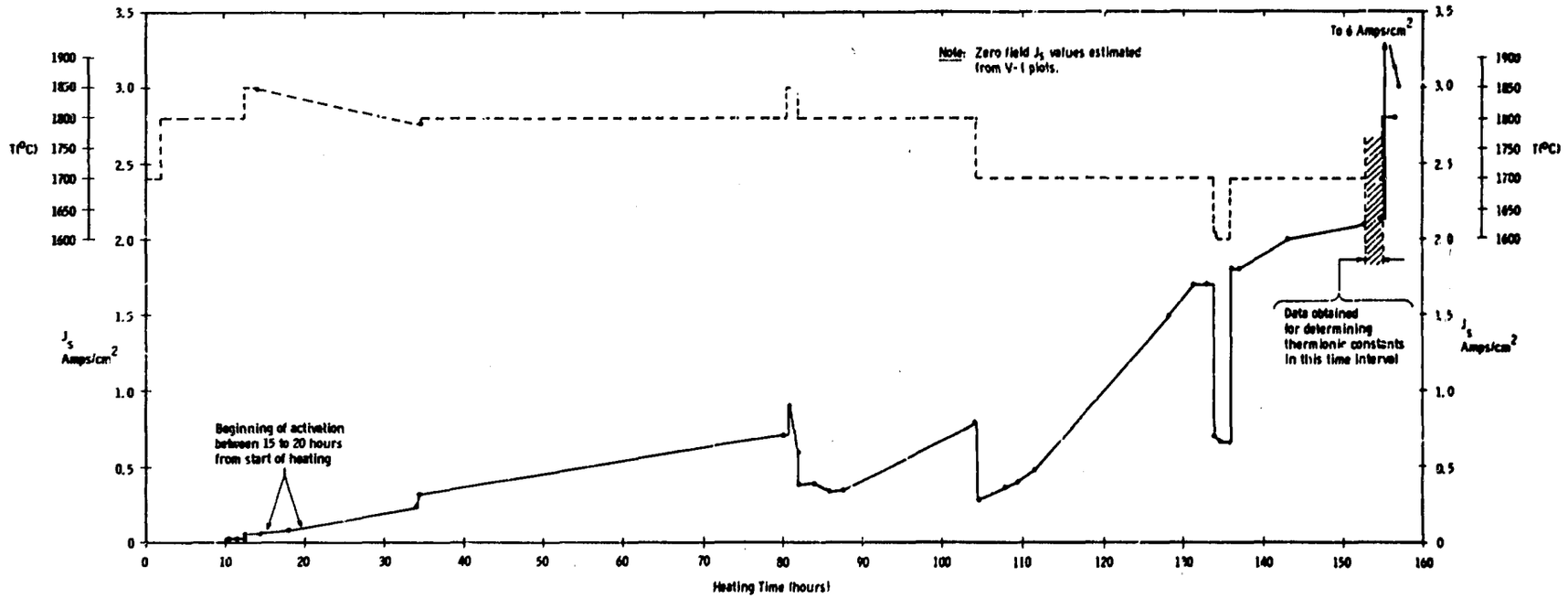

Figure 22. Saturation Current Density and Temperature vs Time for P-111-SW

C. THERMIONIC AND THERMAL STABILITY DATA - PLANAR EMITTERS

A summary of thermionic and thermal stability data for each of the three types of planar thorium on tungsten emitters is contained in Table III. In Figure 23 the zero field saturation current density for each of the emitters tested is plotted against temperature. These data were transferred to Richardson plots like the one shown in Figure 24 for emitter P-93-ThW, and values of ϕ and A were determined.

The initial preferred orientation of each of the emitters tested is shown in column 2 of Table III. Also column 2 contains the appropriate figure numbers (25 through 29) in this report where pole-figure scans, taken before and after activation and testing, are shown. From "before and after" comparisons of these pole-figure scans the thermal stability of the oriented surface layer was judged and has been indicated qualitatively in column 4 of Table III. Column 3 in the table is an estimate of the void surface area of each of the emitters which was determined by careful examination of photomicrographs of the surfaces shown in Figures 30 through 34, all of which were taken after removing the emitter from the test diode. The void surface area is a measure of the porosity of the grain-oriented surface layer.

D. SIGNIFICANCE OF THERMIONIC AND THERMAL STABILITY DATA

Several significant observations can be made concerning the data described in the preceding sections. Most conspicuously, there is a spread of over 15% in the measured values of vacuum work functions. With one exception (P-113-ThW) the thermionic constants are all high. Type 1 emitter P-93-ThW performed significantly better than any of the other emitters tested, and though its preferred orientation degraded somewhat during activation and testing it remained predominantly (111) oriented throughout. The other type 1 emitter tested, P-113-ThW, performed very poorly. Its emission was an order of magnitude lower than that of P-93-ThW and in the course of testing its surface layer lost all semblance of the initial (111) preferred orientation. The most apparent structural difference in the two type 1 emitters was

TABLE III

PLANAR EMITTERS - TEST DATA

Emitter Number	Initial Preferred Orientation	% of Void Surface Area **	Thermal Stability	Thermionic Constants		Remarks
				ϕ_R	A_R	
P-93-ThW	(111) Figure 25	15%-20%	Fair	3.1	120 ± 40	---
P-113-ThW	(111) Figure 26	0-2%	Very Poor	3.0	10	Preferred orientation completely destroyed during thermionic testing
P-109-SW	(210)(100) Mixed Figure 27	15%-20%	Good	3.55	70 ± 40	Note correlation between high ϕ and preferred orientation
P-111-SW	(111) Figure 28	0-2%	Good	3.1	70 ± 40	---
P-50-C	(111) Figure 29	15%-20%	Poor	3.3	120 ± 40	Preferred orientation badly degraded See footnote*
P-102-C	(111)	0-2%	Measurements incomplete at time of report			See footnote*

---

* Substrate for P-50-C machined from singly sintered billet. A second sintering of similar billets results in 3% increase in density (17.3 to 17.7 gms/cm^3). P-102-C substrate machined from doubly sintered billet.

** An indication of nodularity and porosity of the grain-oriented surface layer. Estimated from surface photographs - 0% void surface area would imply a 100% dense grain-oriented surface layer.

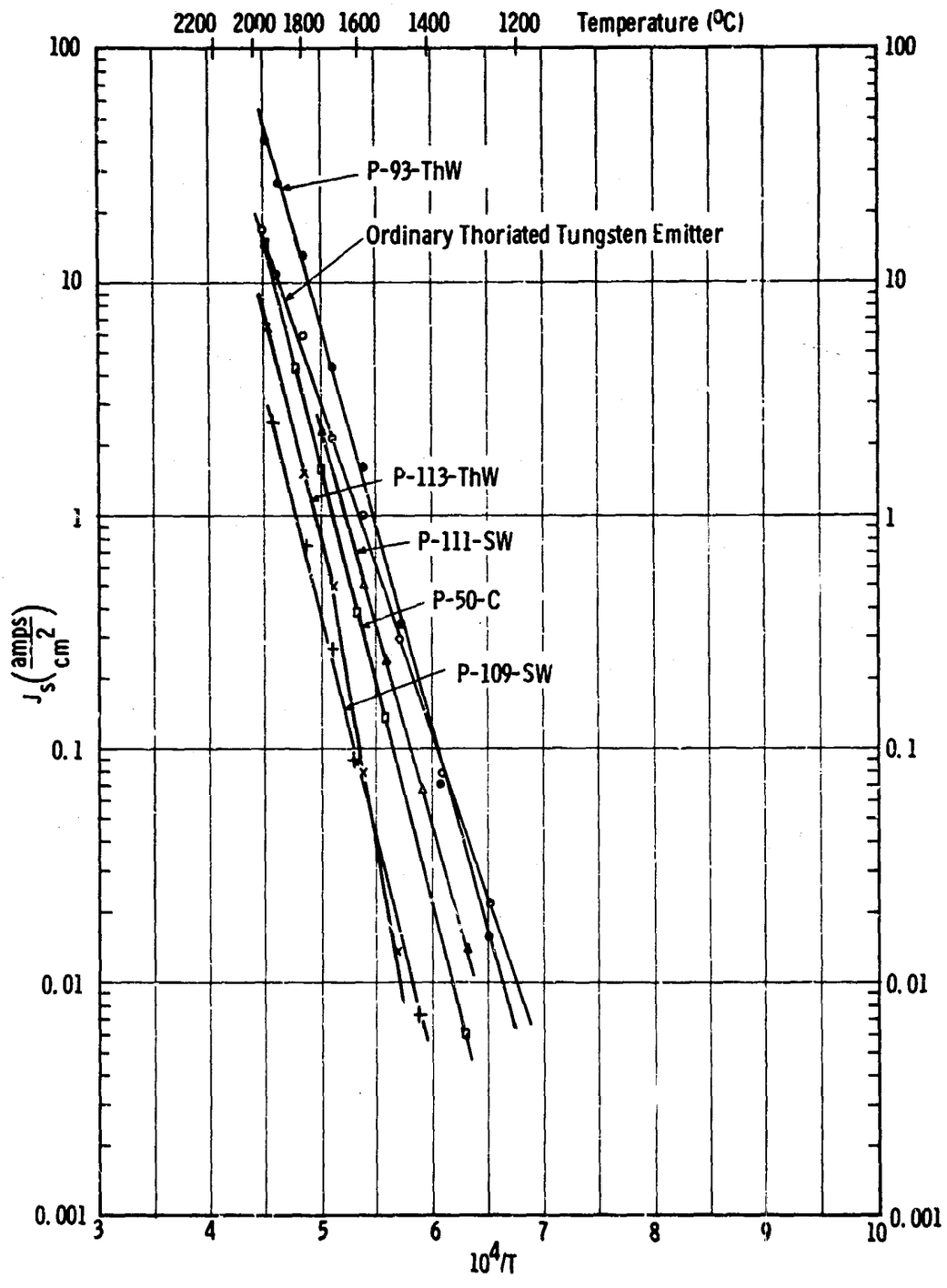

Figure 23. Current Density vs Temperature for Grain Oriented and Ordinary Thermionic Emitters

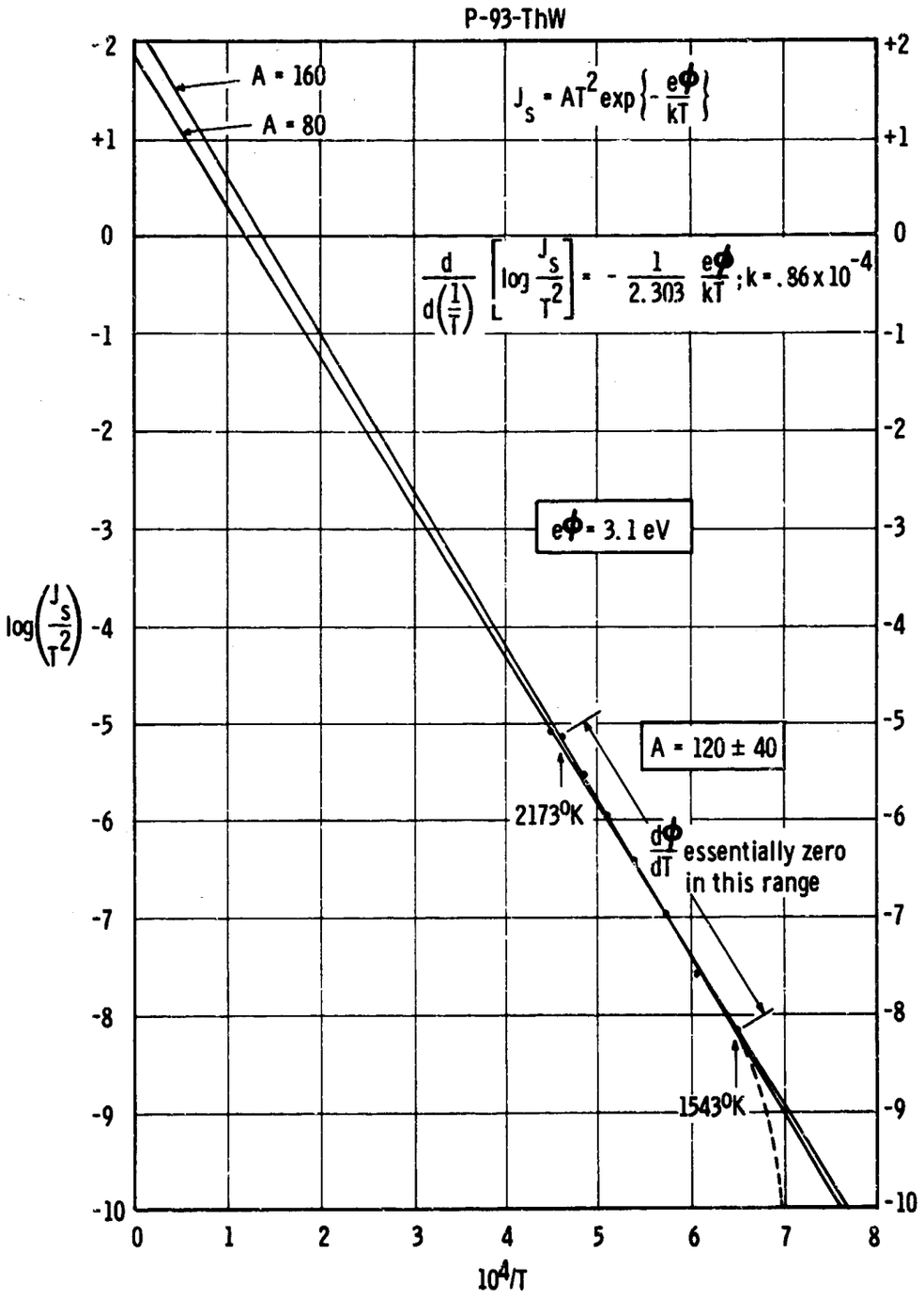

Figure 24. Richardson Plot for P-93-ThW

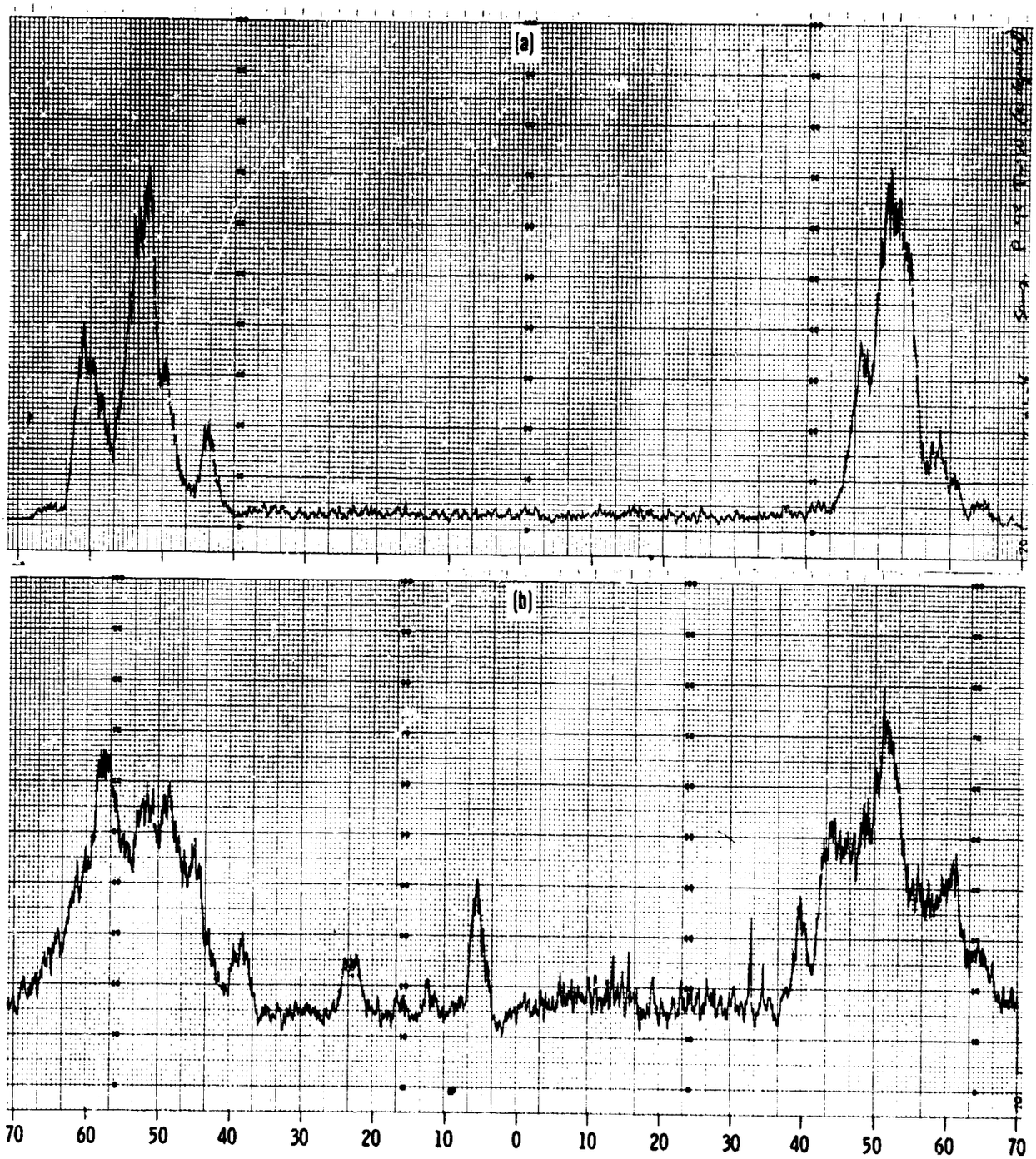

Figure 25. A Plot of the Integrated Intensity of Cu Kα X-Radiation from the [200] Planes of P-93-ThW as a Function of the Angle of Inclination of the Planes to the Surface (a) Before Activation and Testing (b) After Activation and Testing

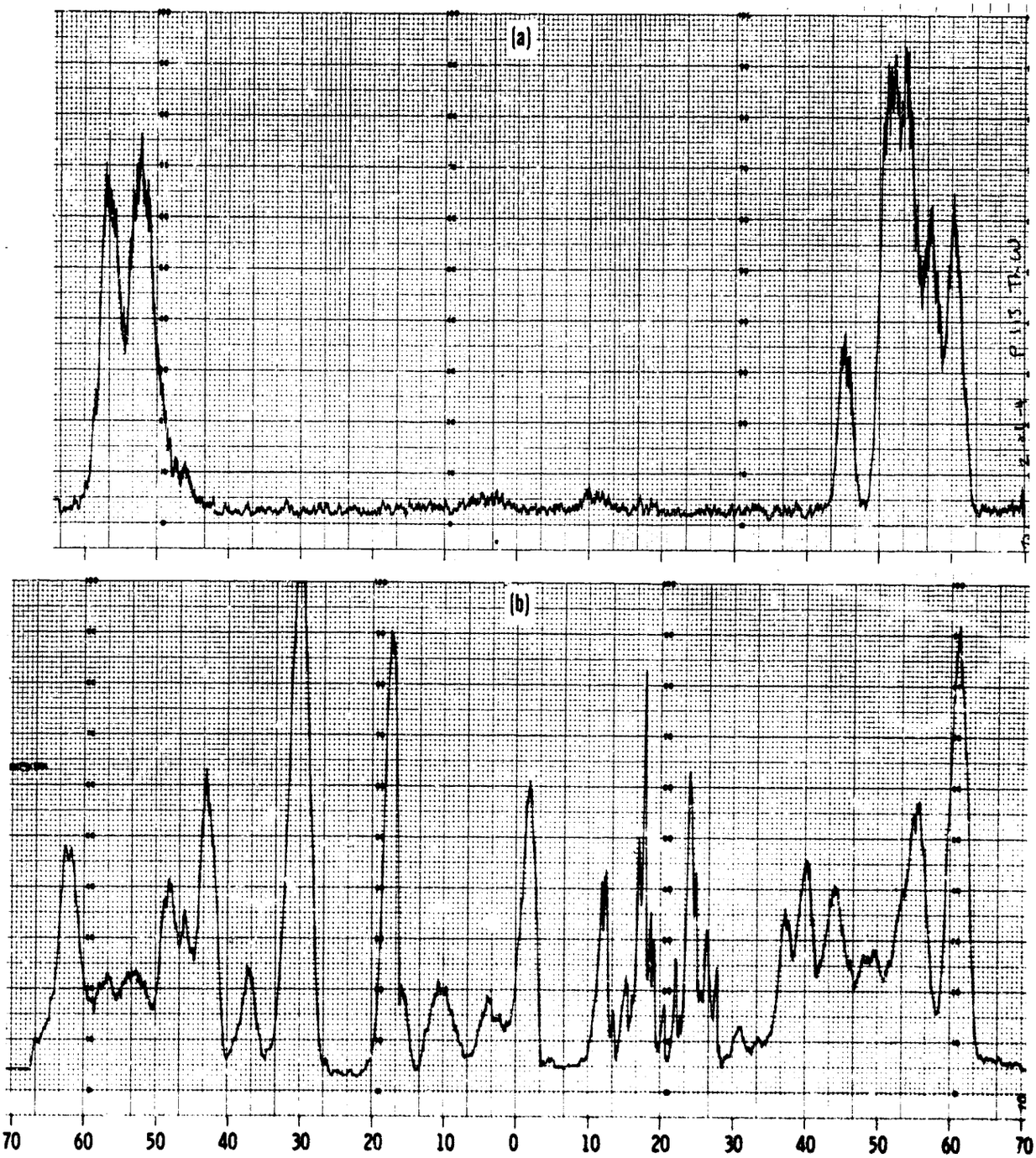

Figure 26. A Plot of the Integrated Intensity of Cu Kα X-Radiation from the [200] Planes of P-113-ThW as a Function of the Angle of Inclination of the Planes to the Surface (a) Before Activation and Testing (b) After Activation and Testing

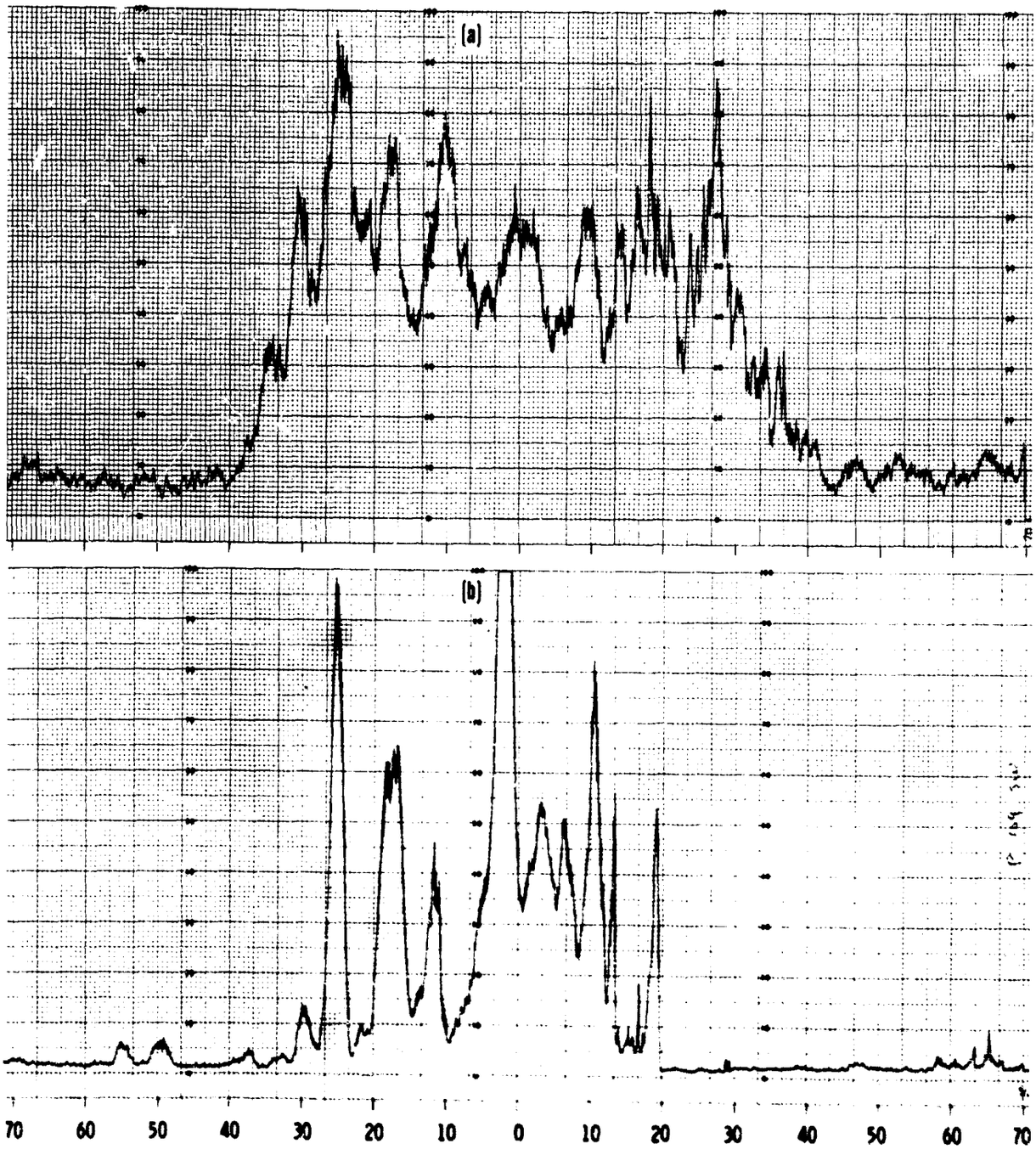

Figure 27. A Plot of the Integrated Intensity of Cu Kα X-Radiation from the [200] Planes of P-109-SW as a Function of the Angle of Inclination of the Planes to the Surface (a) Before Activation and Testing (b) After Activation and Testing

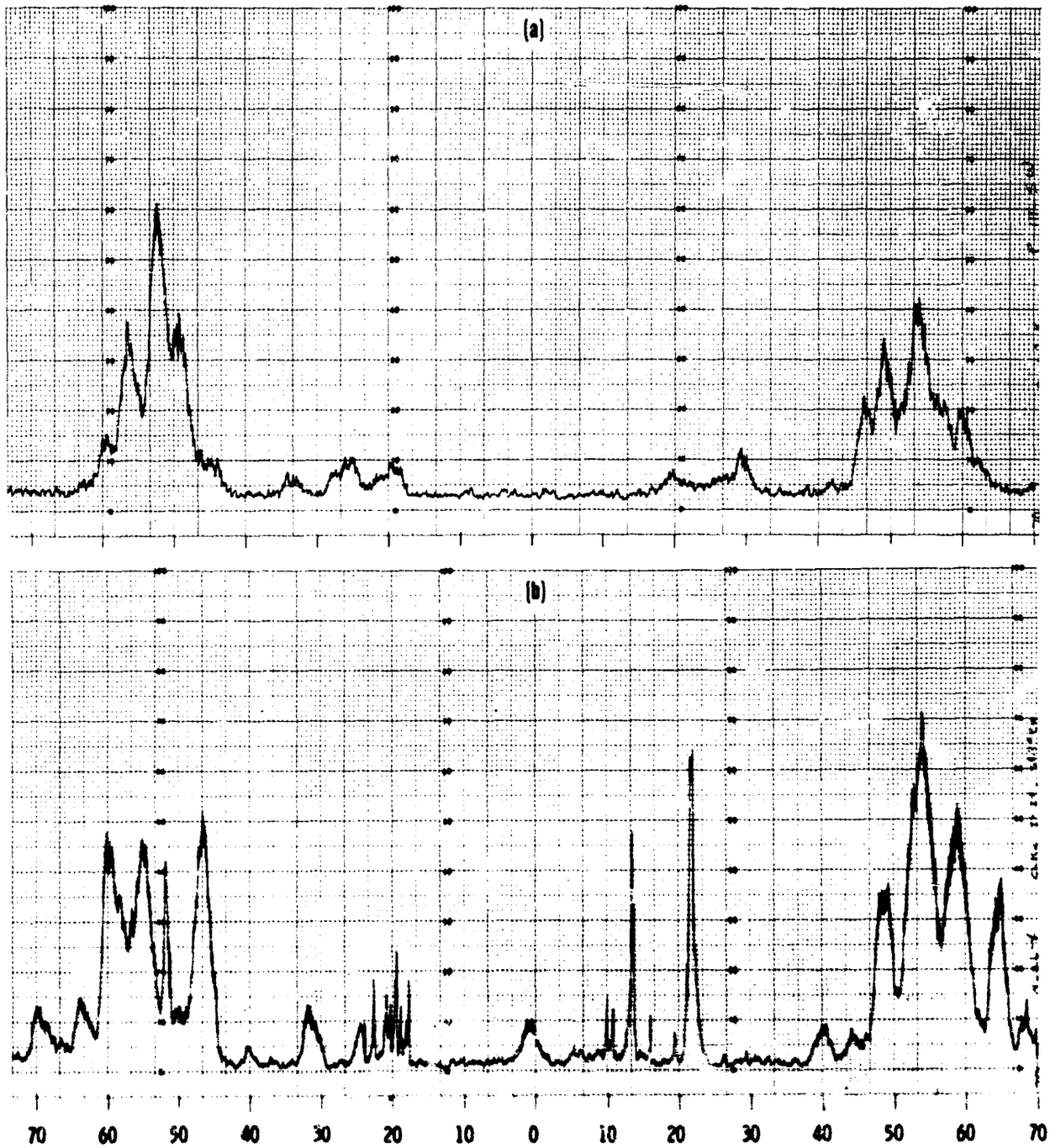

Figure 28. A Plot of the Integrated Intensity of Cu Kα X-Radiation from the [200] Planes of P-111-SW as a Function of the Angle of Inclination of the Planes to the Surface (a) Before Activation and Testing (b) After Activation and Testing

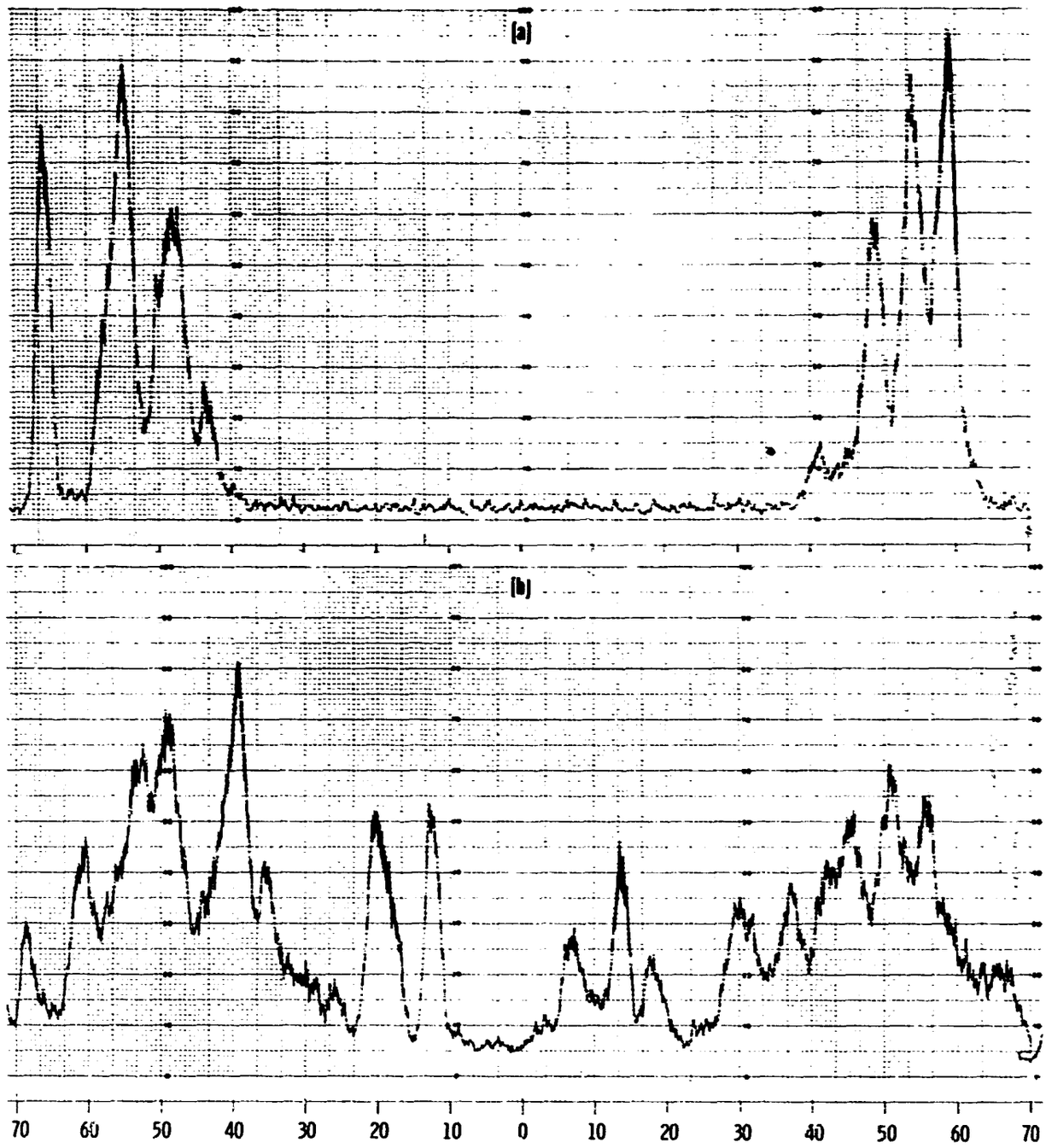

Figure 29. A Plot of the Integrated Intensity of Cu Kα X-Radiation from the [200] Planes of P-50-C as a Function of the Angle of Inclination of the Planes to the Surface (a) Before Activation and Testing (b) After Activation and Testing

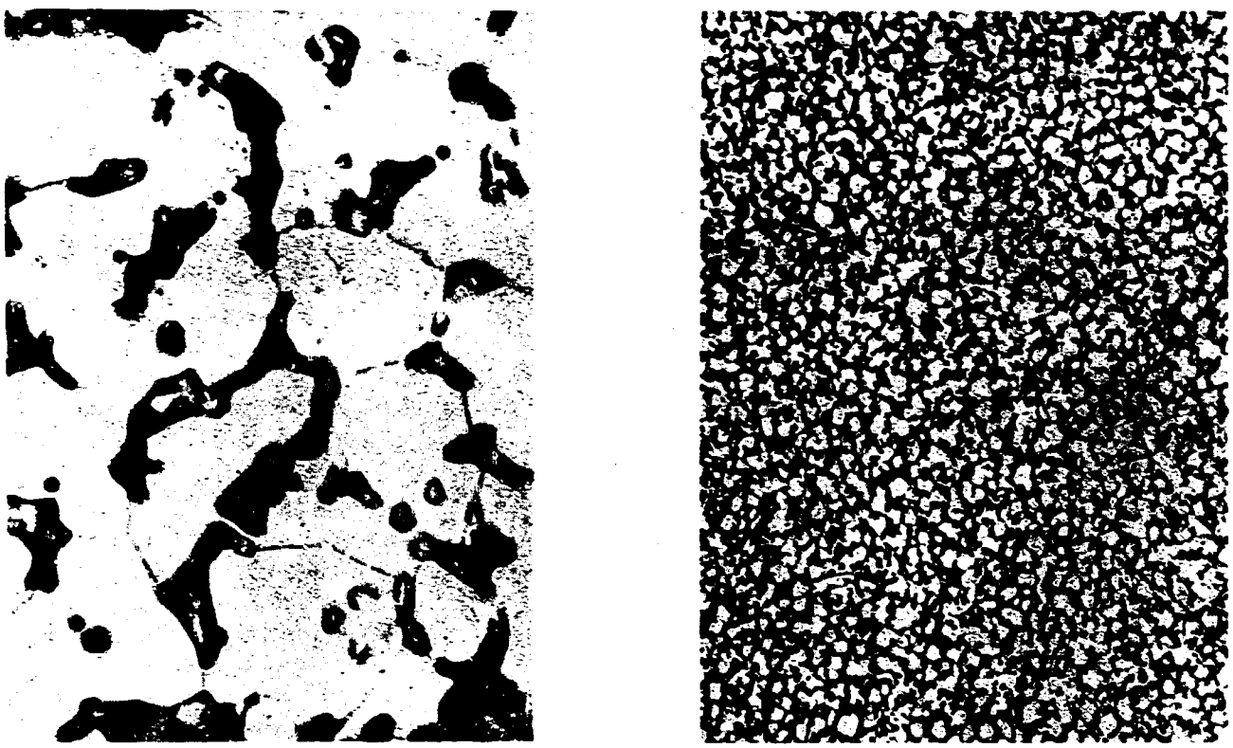

(a)
Scale X589

(b)
Scale X148

Figure 30. Surface of P-109-SW After Activation and Testing in Ultra High Vacuum Planar Diode. Note the Large Void Spaces at the Boundaries of the Crystallites

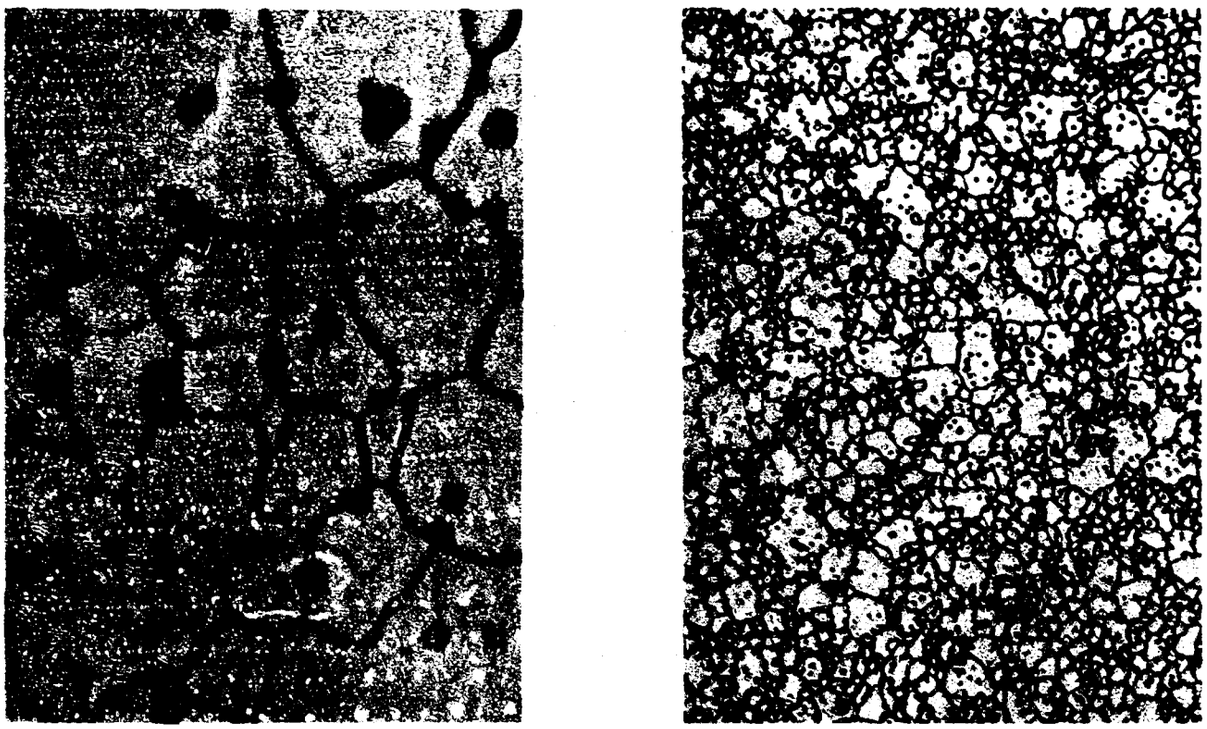

(a)
Scale X588

(b)
Scale X148

Figure 31. Surface of P-111-SW After Activation and Testing in Ultra High Vacuum Planar Diode. Note the Dense Packing of the Crystallites and the Absence of Void Spaces in the Surface Layer

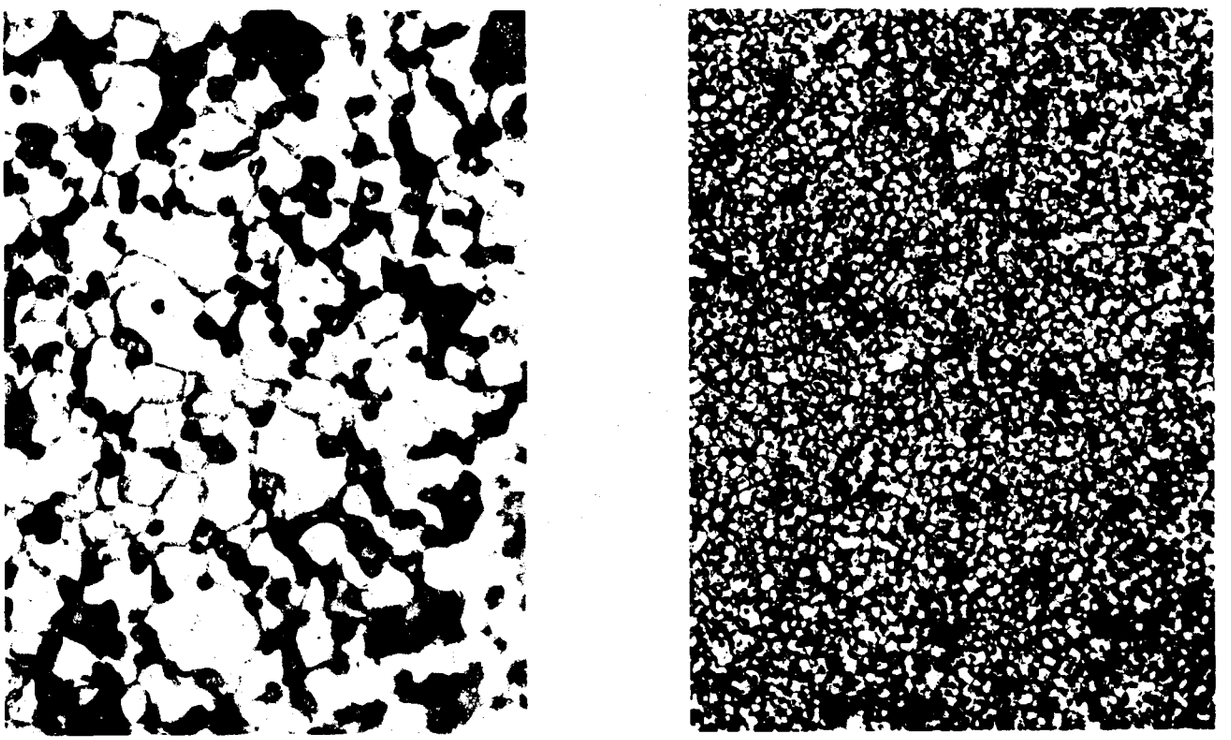

(a)
Scale X589

(b)
Scale X148

Figure 32. Surface of P-93-ThW After Activation and Testing in Ultra High Vacuum Planar Diode

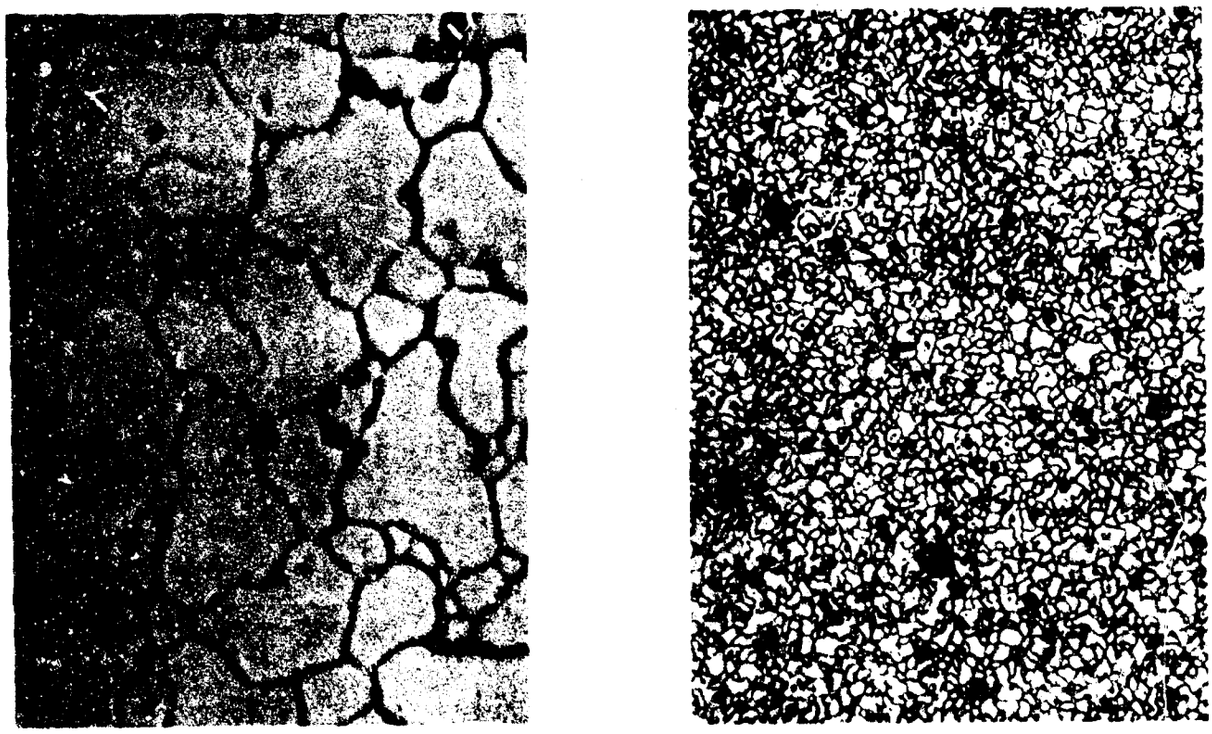

(a)
Scale X589

(b)
Scale X148

Figure 33. Surface of P-113-ThW After Activation and Testing in Ultra High Vacuum Test Diode

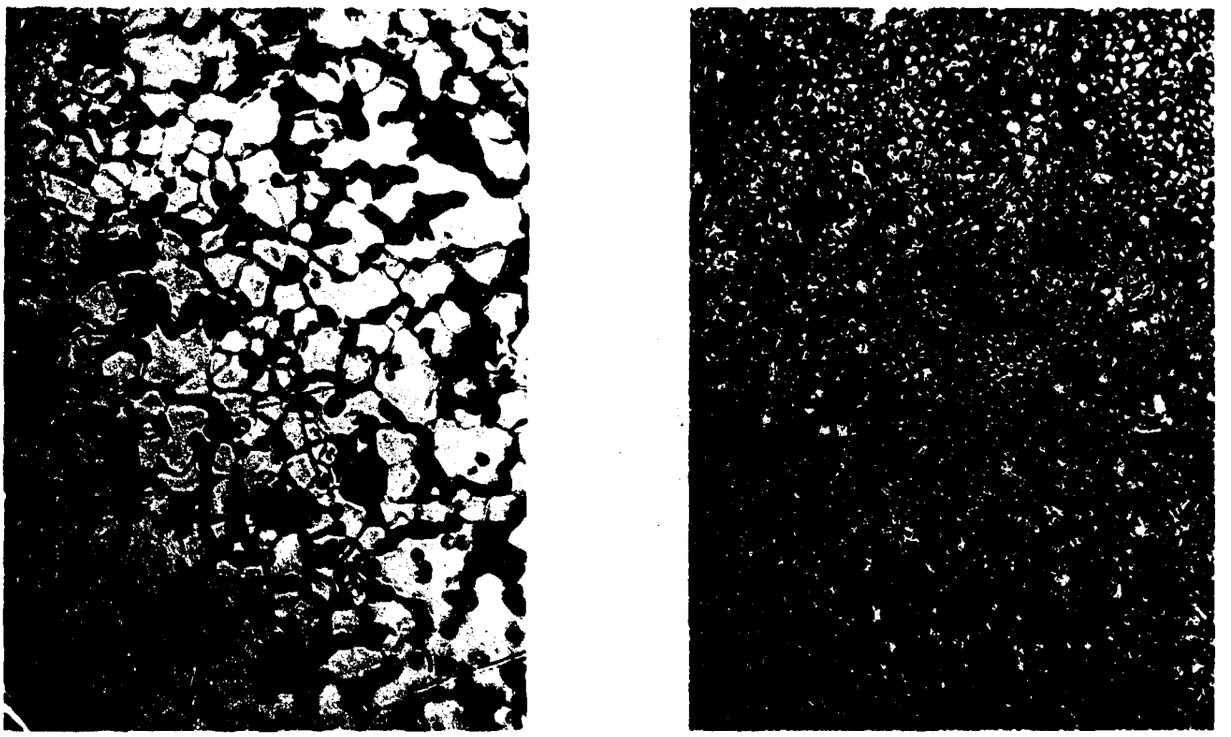

(a)
Scale X589

(b)
Scale X148

Figure 34. Surface of P-50-C After Activation and Testing in Ultra High Vacuum Test Diode

the much greater porosity of the grain-oriented surface layer of P-93-ThW. (Compare Figures 32 and 33.) As would be expected, activation of P-113-ThW took considerably longer than that of P-93-ThW despite the higher activation temperature employed for the former.

Comparison of the thermionic performance of P-111-SW and P-109-SW provides a striking example of the effect of preferred orientation on work function. The surface of the former is rich in crystallites with their (111) crystal direction essentially normal to the surface; the latter is particularly devoid of same (Figures 27 and 28). With the same value of A, their work functions differ by 0.45 eV.

The two grain-oriented emitters that delivered the highest saturation current densities at temperatures up to 1700°C were P-93-ThW and P-111-SW. These are the only two emitters of those tested that were both (111) preferentially oriented at the outset and remained so throughout activation and testing. It is significant to note, however, that P-111-SW did not maintain good emission at temperatures much above 1700°C,* whereas P-93-ThW maintained good emission up to 1955°C,** at which temperature it delivered a zero field saturation current density of 41 A/cm^2, significantly higher than is obtained from ordinary thoriated tungsten at the same temperature (Figure 23). The ability of P-93-ThW to maintain optimum surface coverage to a relatively high emitter temperature must be attributed to the greater porosity of its oriented surface layer.

The performance of the only type 2 emitter (P-50-C) fully evaluated before the time of this writing was disappointing. Its thermionic performance and thermal

---

* It is evident from Figure 22 that activation of P-111-SW proceeded very slowly at 1800°C and more rapidly at 1700°C. After fully activating at 1700°C, an attempt to increase the emitter temperature to 1800°C resulted in only a transient increase in current which quickly decayed to a relatively low value as the thorium diffusing through the dense oriented surface layer became insufficient to maintain optimum coverage in the face of an increased desorption rate at the higher temperature.

** P-93-ThW still maintained optimum surface coverage at 1955°C. No attempt was made to evaluate it at higher temperatures.

stability were both poor. Incomplete sintering of the substrate is believed to have been a contributing factor. Measurements on P-102-C (substrate machined from doubly sintered billet) were unfortunately not completed at the time of this report.

The type 3 emitters exhibited by far the best thermal stability of the three types evaluated. Both P-111-SW ((111) orientation) and P-109-SW ((210) (100) mixed orientation) maintain their initial preferred orientation throughout activation and testing (Figures 27 and 28). This stability may be a consequence of the structure, i.e. substrate plus deposit, being essentially single-phase throughout, the emitter never getting hot enough for the formation of any carbide phase by the reaction of tungsten with carbon that has been added into the reservoir.

The above observations suggest that the best overall grain-oriented thorium on tungsten emitter should consist of a (111) preferentially oriented, high porosity surface layer on a type 3 dispensing substrate.

E. TEST FACILITY FOR CYLINDRICAL EMITTERS

As indicated in the section on tungsten vapor deposition, preferentially oriented, dispenser type emitters can be made in the cylindrical as well as the planar geometry. To facilitate tests on such emitters a cylindrical diode with a guard-ring collector structure has been built. The diode is demountable and the cylindrical emitters are readily replaced, just as in the planar emitter test facility. A cross-section of the test structure is shown in Figure 35, and a picture in Figure 36. In operation the entire structure is mounted into an ultra high vacuum system of the same general type used in the planar emitter test facility. The emitter is heated by electron bombardment from a directly heated filament which runs down the cylinder axis.

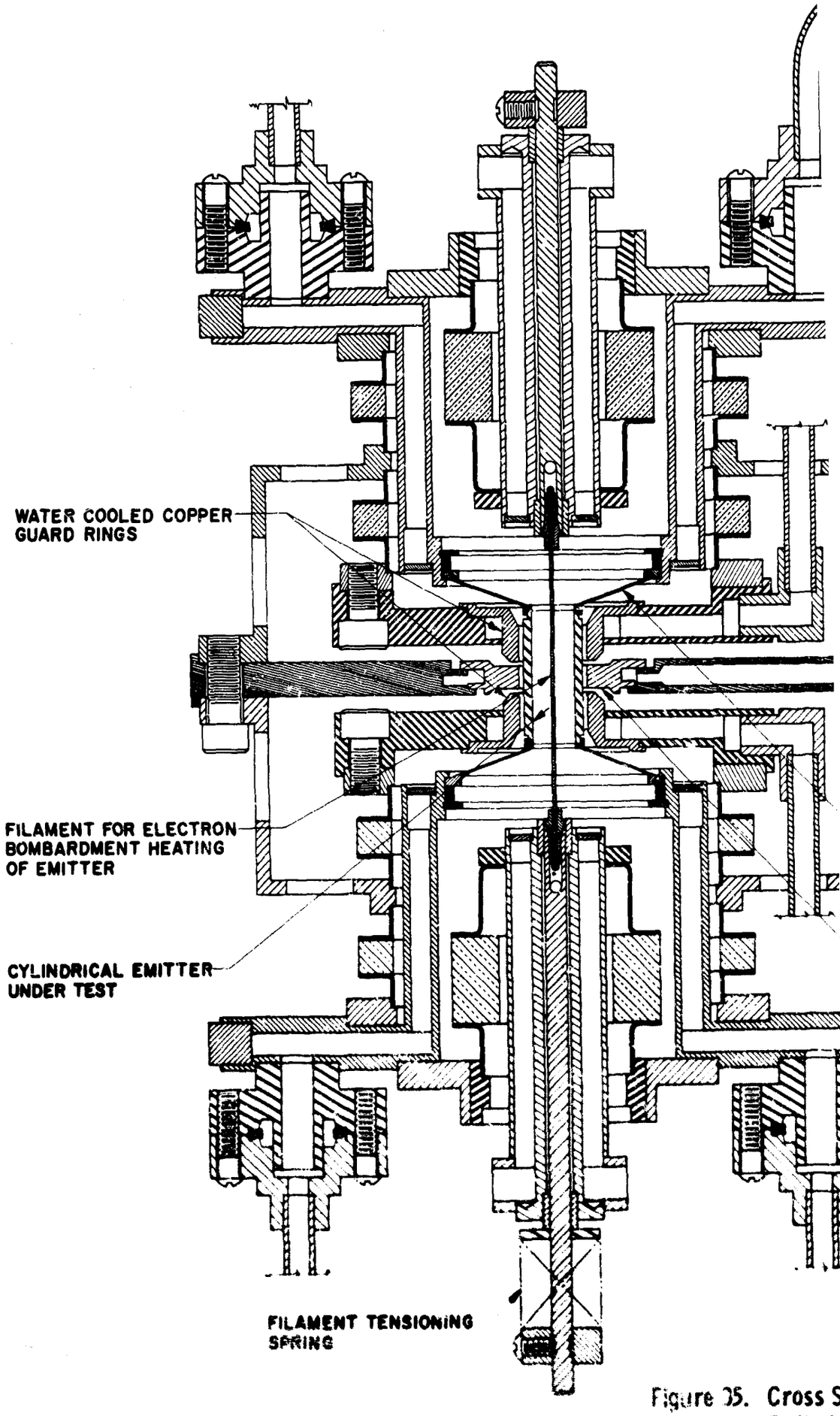

A.

Figure 35. Cross Se
Cylindri

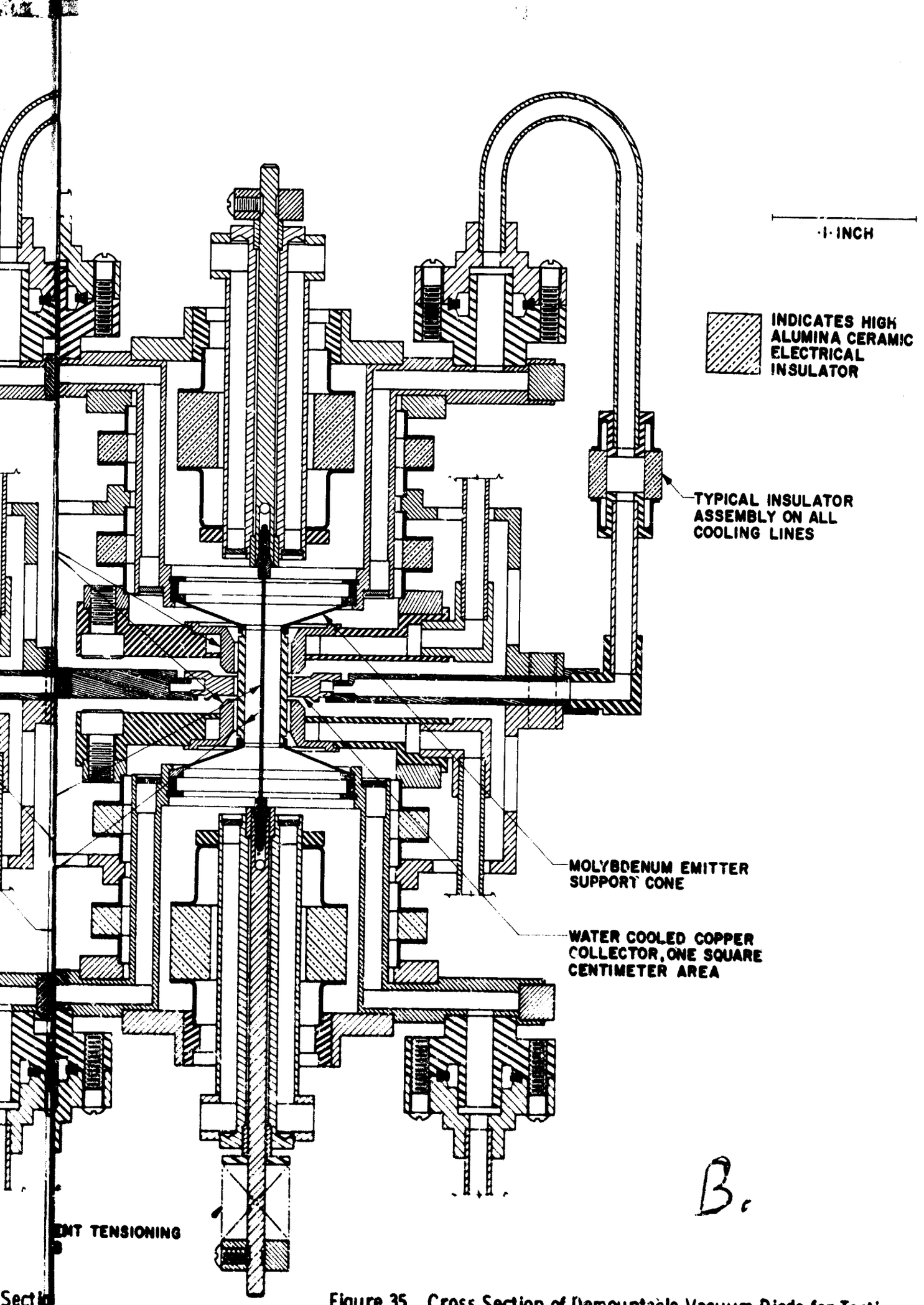

Figure 35. Cross Section of Demountable Vacuum Diode for Testing Cylindrical Emitters

Figure 36. Demountable Vacuum Diode for Testing Cylindrical Emitters

NIOBIUM VAPOR DEPOSITION

A second refractory material of considerable interest as a candidate in the role of substrate for grain-oriented thorium dispenser emitters is niobium. As shown in Reference 13, the work function of an ordinary polycrystalline thorium-niobium emitter is 2.42 eV, and its Richardson constant is approximately 12. Having a significantly lower work function than thorium on tungsten, thorium on niobium should be a better low-temperature emitter. An improvement in "A" by virtue of appropriate orientation of the emitting surface could qualify it as an ideal emitter in intermediate temperature thermionic converter applications.

An experimental system has been built for doing vapor transport and deposition of niobium onto suitable substrates. Niobium pentafluoride (NbF_5) is commercially available, and employing it as a source compound would be most analogous to the use of tungsten hexafluoride for the transport and deposition of tungsten. However, because of its relatively low vapor pressure (bp 236°C as compared to 17.5°C for WF_6), handling, monitoring, and controlling its flow is more involved. For this reason, and because NbF_5 cannot be easily prepared in situ, the decision was made to use chloride transport and to generate the source compound in situ. A flow chart and schematic diagram of the reaction tube is shown in Figure 37. Chlorine is passed over niobium metal in the 900°C zone, generating volatile chlorides, which pass down the tube into a lower temperature zone where they are mixed with hydrogen. Reduction of the chloride and thus niobium deposition occurs on a substrate located in the 1050°C zone. (This reaction zone temperature has been varied between 950°C and 1100°C during the course of experiments to establish orientation control (Table IV).) Alternately, a substrate heated to the desired deposition temperature can be inserted into the 725°C zone and held in any position relative to the baffle so as to obtain direct impingement or any other desired flow of reactants over the substrate. The reactions are:

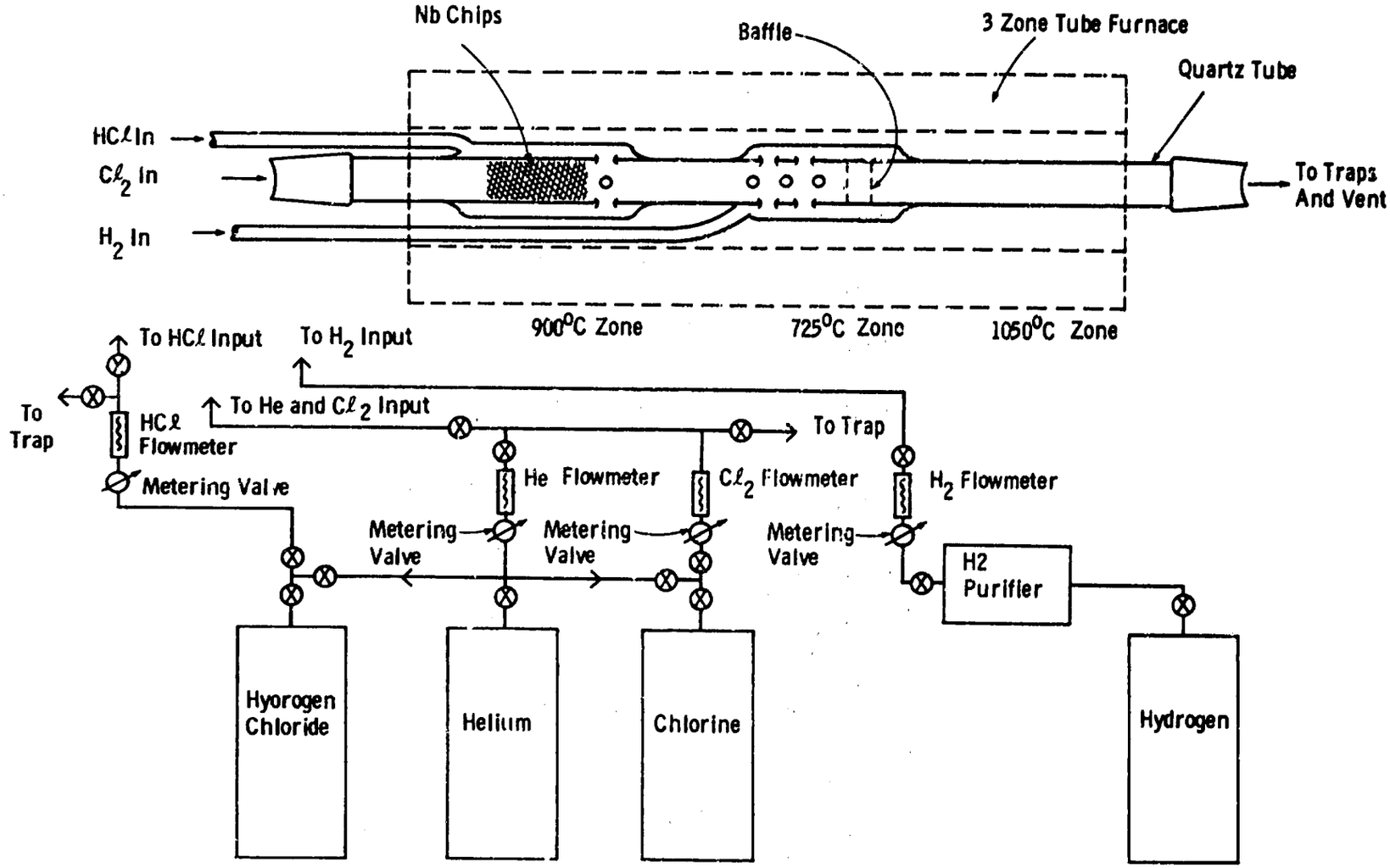

Figure 37. Flow Chart for Vapor Transport and Deposition of Niobium

TABLE IV

NIOBIUM VAPOR DEPOSITION DATA

Run No.	Flow Rate ←—cc/min—→ H_e	HCl	Cl_2	H_2	Dep. Temp. °C	Time Min	Dep. Thickness mils	Orientation of Substrate Surface to Gas Flow	Comments
13	135	100	44	1000	1050°	60	7	∥	X-Ray: Very broad (111), not distinct and probably some other orientation
14	135	36	44	250	1100°	20	1	∣	Repeat of No. 8; X-Ray: Edges: Broad (111); Center: Other plus some (111)
15	135	36	44	250	1050°	30	1.1	⊥	X-Ray: (100) 31° H.W.
16	135	36	44	250	1100°	30	3.7	⊥	Repeat of No. 8; X-Ray: (100) 15° H.W.
17	135	36	44	1000	1100°	30	→	⊥	Black powdery nonadherent deposits of Nb and $NbH_{0.89}$
18	135	36	44	1000	950°	30	1.2	⊥	X-Ray: (111) 23° H.W.
19	135	36	22	1000	950°	60	2	⊥	X-Ray: (100) 21° H.W.
20	135	36	33	1000	950°	45	2.9	⊥	X-Ray: (100) 23° H.W., Trace of (111)
21	135	36	38	1000	950°	40	3.3	⊥	X-Ray: (100) Extremely broad
22	135	36	33	1000	1000°	45	3	⊥	X-Ray: (100) 13° H.W., plus small amount of unidentified orientation

NOTES:

(1) All substrates for Run Nos. 13-22 were planar niobium disks 0.400" diameter x ~ 0.040" thick, finished to 600 grit.

(2) Run Nos. 14 and 16 same deposition conditions, only difference is the substrate orientation with respect to the gas flow in the deposition tube.

$$2\ Nb_{(s)} + 5\ Cl_{2(g)} \xrightarrow{900°C} 2\ NbCl_{5(g)} \qquad \text{Chloride Formation}$$

$$2\ NbCl_{5(g)} + 5\ H_{2(g)} \xrightarrow{1050°C} 2\ Nb_{(s)} + 10\ HCl_{(g)} \qquad \text{Deposition}$$

The results of a survey over a fairly extensive range of temperature and flow parameters is shown in Table IV. The next to last column in the table indicates the orientation of the substrate with respect to the main reactant flow direction. As indicated in the last column both (111) and (100) preferentially oriented deposits are readily obtained. Other unidentified orientations or mixtures of them have also been observed. The chloride transport system appears to provide the necessary orientation control for fabrication of grain-oriented niobium emitters.

REFERENCES

1. I. Weissman and M. L. Kinter, "Improved Thermionic Emitter Using Uniaxially Oriented Tungsten," J. Appl. Phys. 34, 3187-3194 (1963).

2. I. Weissman, "An Improved Thermionic Emitter: Thorium on Grain-Oriented Polycrystalline Tungsten," J. Appl. Phys. 36, 406-411 (1965).

3. B. D. Cullity, Elements of X-Ray Diffraction (Addison-Wesley Publishing Company, 1959), Chap. 9.

4. M. Benjamin and R. O. Jenkins, "The Distribution of Autoelectronic Emission from Single Crystal Points - Part II: The Adsorption, Migration and Evaporation of Thorium, Barium and Sodium on Tungsten and Molybdenum," Proc. of Royal Society A 180, 225 (1942).

5. J. E. Davey and E. A. Coomes, "Thermionic Properties of Thorium on Tungsten Single Crystals," Phys. Rev. 99, 1651 (1955).

6. M. N. Huberman, "Uniform Work Function Cathode Studies," Tech. Report AFAL-TR-65-155, July 1965.

7. C. E. Wicks and F. E. Block, "Thermodynamic Properties of 65 Elements - Their Oxides, Halides, Carbides and Nitrides," Bureau of Mines Bulletin 605, U. S. Government Printing Office, Washington, D. C., 1963.

8. W. L. Worrell, "A Thermodynamic Analysis of the Cr-C-O, Mo-C-O, and W-C-O Systems," Trans. of Met. Soc., of AIME, 233, 1176 (1965).

9. Kubaschewski and Evans, Metal Physics and Physical Metallurgy (Pergamon Press, 1958), p. 185.

10. D. D. Jackson, et al., "Vaporization of Thorium Dicarbide," J. Phys. Chem. 68 (1964).

REFERENCES (Cont'd)

11. R. O. Jenkins and W. G. Trodden, "The Poisoning of Thoriated Tungsten Cathodes," J. of Electronics and Control 12, 1-12 (1962).

12. J. P. Sackinger and R. J. Foreman, "Thorium-Tungsten Cermet Cathodes," Military Systems Design, Nov.-Dec. 1959, p. 310.

13. G. A. Esperson, H. E. Farnsworth, R. Levi, M. J. Lun, "Fundamental Research on Cathode Emitters," Philips Laboratory Technical Report No. 23, April 30, 1949.

APPENDIX A

INTERPRETATION OF MULTIPLE PEAKED POLE-FIGURE SCANS

A knowledge of the basic technique for determining preferred crystal orientation in polycrystalline materials by pole-figure analysis will be assumed. In any case this technique is described in detail in Elements of X-Ray Diffraction[1] and no attempt will be made to repeat that description here. The intent of this appendix is to clarify the significance of the pole-figure scans that have been used freely throughout this work to characterize the orientation of CVD surfaces.

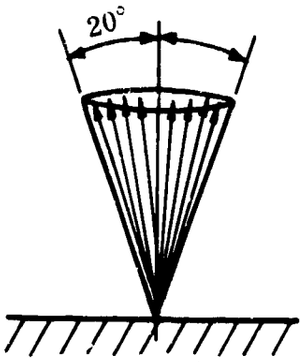

Figure A-1
Assumed (111) Distribution

For illustrative purposes, assume a uniform distribution of [111] crystal directions in a 20° cone centered about the surface normal (Figure A-1). Actually the distribution of [200] crystal directions which are distributed as in Figure A-2 is measured, and from this measurement the distribution of [111] oriented crystals is inferred from the interplanar angles.

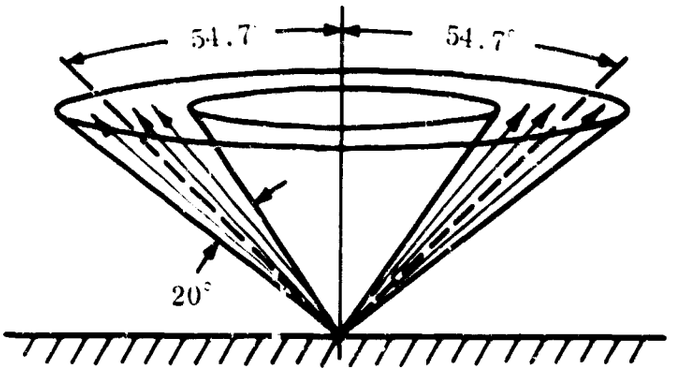

Figure A-2
(200) Distribution Corresponding to Figure A-1

---

1. Cullity, Elements of X-Ray Diffraction (Addison Wesley Press, 1956), Chap. 9, Sec. 6, p. 272.

A section through a (200) pole figure for such a distribution of [200] crystal directions, assuming no spread due to X-ray optics would be as shown in Figure A-3.

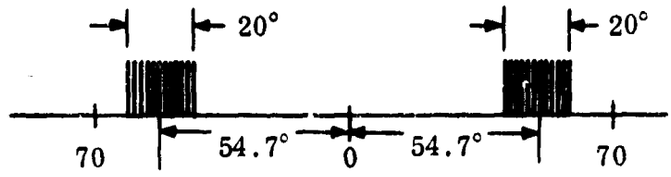

Figure A-3
(200) X-Ray Pole Figure of Assumed Distribution
Resulting from Infinite Resolution

We know by direct measurements that the response from a single crystal has a full half-width spread of 2° when the polar angle is varied and 3° when the azimuthal angle is varied which is due to the X-ray optics, i.e., the divergence of the X-ray beam, slit width, etc. Thus for a case where the crystallites in the deposit are small and the diffracted energy at any arbitrary pair of polar and azimuthal angles comes from a large number of them, a section through the pole figure will be a single smooth peak (Figure A-4).

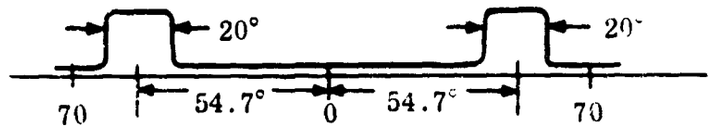

Figure A-4
(200) X-Ray Pole Figure of Assumed Distribution
Resulting from Actual Resolution

Alternatively, if the crystallites are sufficiently large, the diffracted energy at any given pair of angles can come from as few as one or two of them. At some angles within the 20° conical sector there may even be no diffracted energy measured if none of the crystallites are appropriately oriented. For this case then, the section through the pole figure will be a multiple-peaked distribution as shown in Figure A-5.

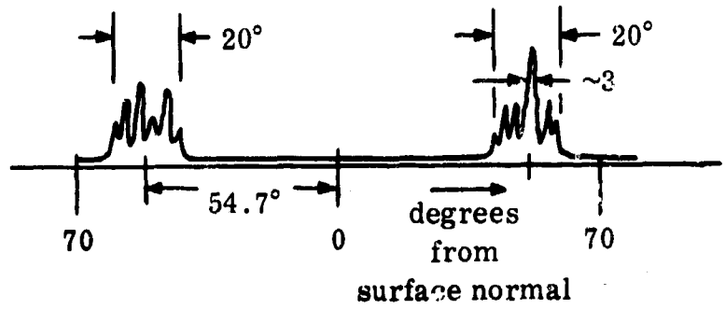

Figure A-5
(200) X-Ray Pole Figure Appearance when Crystallite Size is Large Compared to the X-Ray Resolution

It will differ in detail within the 20° sector for every different azimuthal angle θ. In fact, the section will not even be symmetric about the normal for a single azimuthal angle because each diffraction peak is produced by one or at most a few crystallites whose tilt angles with respect to the surface normal are independent of those of all of the other crystallites radiated by the X-ray source.

It remains only to establish what is meant by "small" and "large" crystallites, i.e., how large will the crystallites be when the pole-figure scan makes the transition from a smooth single peaked curve to an irregular multiple peaked one, and to correlate this with pole-figure scans and photomicrographs of (111) oriented tungsten deposits. Typically the individual (200) diffraction peaks in a multiple peaked pole-figure scan fall in a conical sector centered at 54.7° from the surface normal and within $\pm$10° of the center of the sector, i.e., between 44.7° and 64.7° from the normal (Figure A-6). Assume that all of the crystallites irradiated diffract into that sector and that it is equally probable that a given crystallite will diffract its energy into any part of the sector.

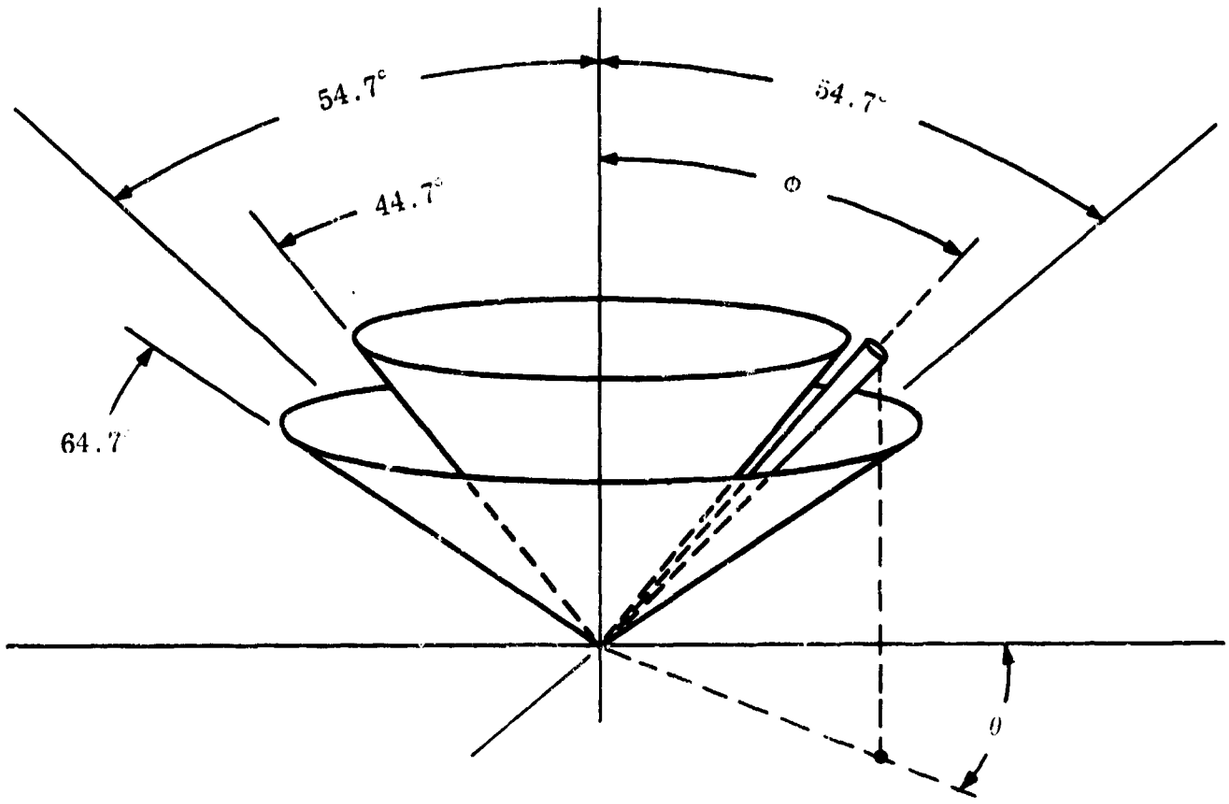

Figure A-6
Limits of (200) Distribution in Assumed (111) Distribution

Then the probability that a given crystallite will contribute appreciably to the diffracted energy detected at any arbitrary pair of angles θ_1, ϕ_1 is approximately equal to the ratio of the solid angle subtended by a 3° by 2° ellipse, to the solid angle subtended by the total sector.

$$\omega_{total} = 2\pi(\cos 44.7° - \cos 64.7°) = 0.284 \times 2\pi$$

$$\omega_{ellipse} = 0.00023 \times 2\pi$$

therefore

$$\omega_{ellipse}/\omega_{total} = \frac{0.00023}{0.284} \approx 8 \times 10^{-4}$$

and it follows that the diffraction peaks will be resolved if the total irradiated area of the sample is constituted entirely of approximately 1.25×10^3 diffracting crystallites. A group of resolved diffraction peaks (Figure A-5) is the result of a "slice" 3° thick (the azimuthal resolution) through the entire pole figure and thus represents 1/120 of the number of large crystallites present. Since a group of resolved peaks centered about 54.7° consists on the average of about six individual crystallites there must be about 720 large crystallites present in the entire irradiated area. This is in good agreement with the calculated number 1.25×10^3, remembering that the crystallites are in fact not uniformly distributed.

It is observed that when deposits are large grained and nodular in structure and exhibit a multiple peaked pole-figure scan the typical larger grains observed in 0.0025-inch thick deposits have a cross-section of approximately $10^3\ \mu^2$ at the surface (Figure 7). The total effective area of sample irradiated in our diffractometer is approximately $5 \times 10^6\ \mu^2$. Therefore, it follows that the larger more perfect crystallites that are responsible for the resolved diffraction peaks constitute approximately 25% of the irradiated surface, the remainder of the surface being made up of smaller crystals whose diffracted energy peaks are unresolved from one another. Depending on their orientation, these smaller crystallites will contribute diffracted energy either to background or to the unresolved part of the peak centered at 54.7°. It is reasonable to assume that they are oriented similarly to the larger crystallites.

APPENDIX B

CAUSE AND EFFECT OF SUBSTRATE FIBER TEXTURE

A series of operations were performed on a tungsten substrate similar to those used in optimizing deposition parameters with respect to sharpness of "as-deposited" orientation (i.e. 1" x 1" x 0.090" thick piece cut from strip stock designated P-56-W). The purpose was to determine the cause of <111> <100> double fiber texture which had been observed in these substrates and to get general information bearing on the question of the effect of substrate orientation on the thermal stability of the deposit. Following certain of the operations, pole-figure scans were made to determine the effect of that operation on preferred orientation.

The substrate was first micropolished to a one micron diamond finish, then fired in dry hydrogen at 1700°C for 40 minutes and a pole-figure scan made (Figure B-1(a)). The surface was then repolished to a one micron diamond finish and another pole-figure scan made (Figure B-1(b)). This was followed by several steps of etching using an $HF-HNO_3$ mixture, interspersed with very light polishing using 0.05 micron Alumina, finishing up finally with a light etch. A third pole-figure scan followed the final etch (Figure B-1(c)). At this point the surface was cleaned and tungsten deposited onto it using the same deposition parameters as for P-2-W, described in the first quarterly report. * A pole-figure scan was made to characterize the deposit orientation (Figure B-2(b)). The sample was then fired in dry hydrogen at 1730°C for 30 minutes and a final pole-figure scan made (Figure B-2(c)).

In interpreting these results it should be noted that the X-ray penetration depth for a (200) pole-figure scan (i.e. $2\theta = 58.3°$) is of the order of one micron which is less than the depth of plastically deformed metal resulting from polishing. Figure B-1(a) illustrates the effect of annealing after initial polishing of the substrate. The <111>

---

* Progress Report No. 1, "Research on Thermionic Electron Emitting Systems," Contract No. NObs-92494, Varian Associates, October 1965.

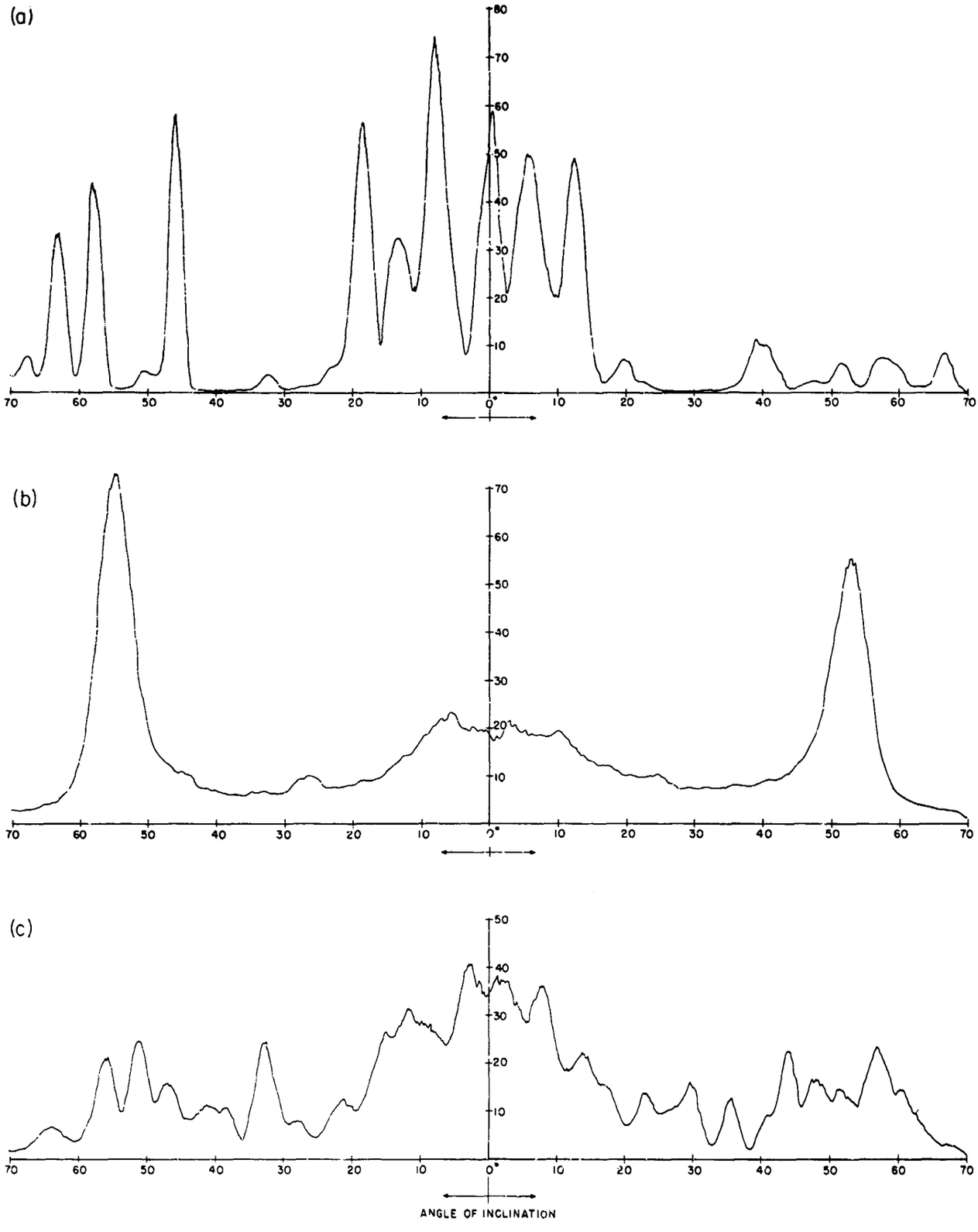

Figure B-1. Plots of the Integrated Intensity of Cu Kα X-Radiation Diffracted from the (200) Planes of P-56-W as a Function of the Angle of Inclination of the Planes to the Surface (a) Substrate, After Firing in a Dry H_2 for 30 Minutes at 1700°C (b) Substrate, After Repolishing Surface to 1-Micron Diamond Finish (c) Substrate, After Final Etching in $HF-HNO_3$

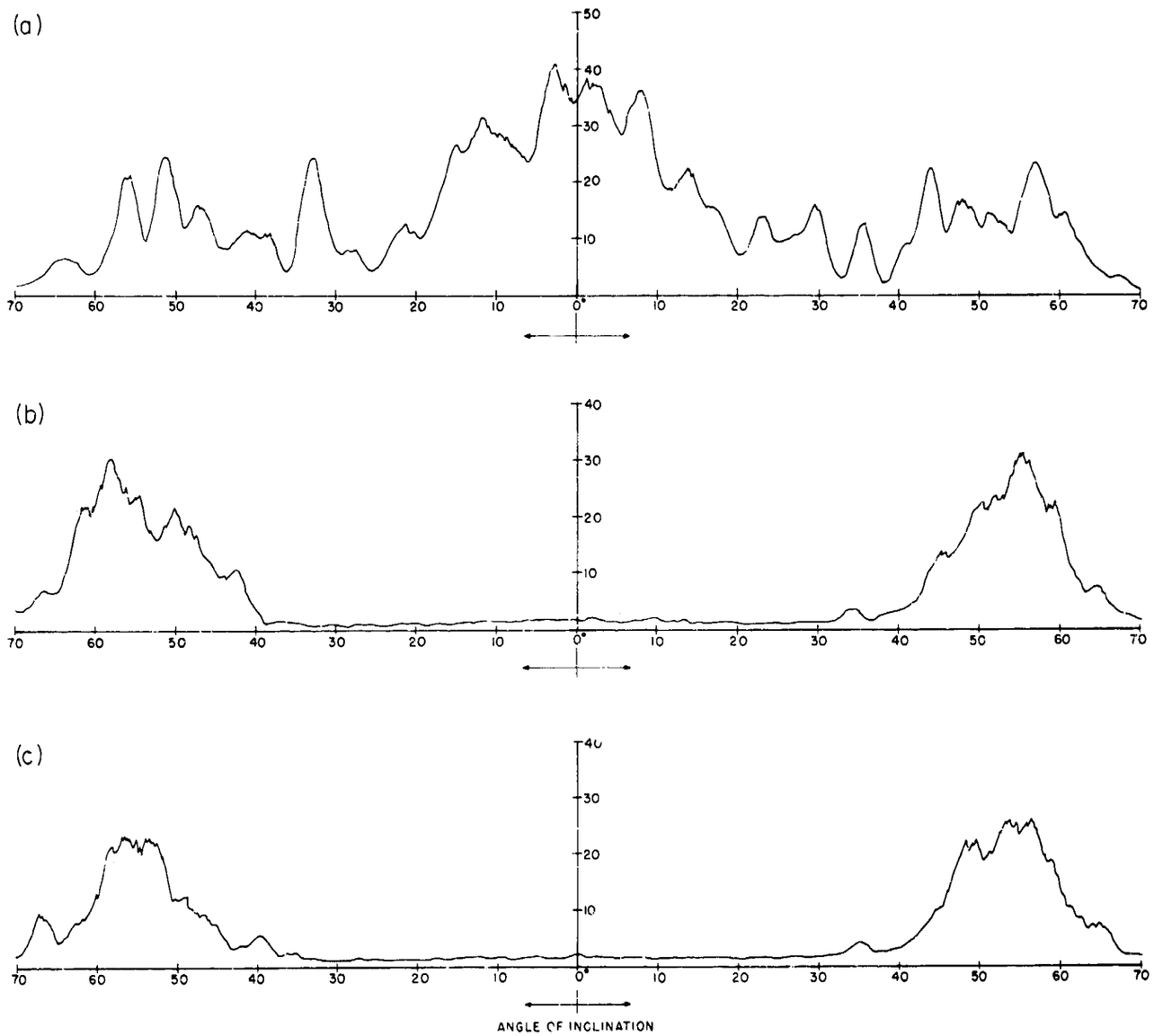

Figure B-2. Plots of the Integrated Intensity of Cu Kα X-Radiation Diffracted from the (200) Planes of P-56-W as a Function of the Angle of Inclination of the Planes to the Surface (a) Substrate, After Final Etching in HF-HNO_3 (b) Deposit, as Deposited (c) Deposit, After Firing in Dry H_2 for 30 Minutes at 1730°C

<100> double fiber texture is largely destroyed. Figure B-1(b) shows the extent to which repolishing reproduces the double fiber texture in the surface layer. In this case the density of (111) planes is greater than that of (100) planes, but this has been observed to vary considerably from sample to sample. As illustrated by Figure B-1(c), etching away the damaged surface layer again largely destroys any sign of the double fiber texture and leaves a surface which is characteristic of the microstructure of the bulk material. Figure B-1(c) has been reproduced as Figure B-2(a) to illustrate the influence of the substrate on deposit orientation. Figure B-2(b) shows the (111) preferred orientation of the chemically vapor deposited tungsten. The distribution of (100) planes about the angle 54.7° from the plane of the surface, and thus of the (111) planes about the surface plane, is much broader than it was in the case of P-2-W, which was grown under identical conditions but onto a polished substrate with <111> <100> fiber texture. Comparing Figures B-2(a) and B-2(b) it is apparent that the detailed microstructure of the substrate does significantly influence the growth. In fact, epitaxy is apparently occurring on substrate crystallites whose [111] directions correspond closely to the direction of the surface normal. Finally a comparison of Figures B-2(b) and B-2(c) illustrates that there is no significant degradation of deposit orientation due to the 30 minute hydrogen firing at 1730°C.

Several conclusions can be drawn. The <111> <100> double fiber texture observed in the substrate is a result of plastic deformation due to cold working of the surface during micropolishing. (The fiber texture resulting from cold working of metals is generally a consequence of preferred slip planes and preferred slip directions. The {100} planes have been reported in the literature[1] as preferred slip planes for rolled tungsten sheet whereas the {111} planes have not.) The deformed layer has a depth somewhat greater than one micron and it exerts a profound influence on the degree of orientation achieved. Metallographic polishing is ordinarily thought to produce disorganized surface metal extending inward to a distance of several interatomic

---

1. R. H. Atkinson, G. H. Keith and R. C. Koo, "Refractory Metals and Alloys," Proceedings of the Metallurgical Society Conferences, Detroit, 1960, Vol. II, p. 329.

distances (10 to 100 Å) and directly beneath this, a deeper layer of plastically deformed metal.[2] If such a superficial noncrystalline layer is present, it is effectively removed when the substrate is heated in hydrogen to 700°C prior to deposition and has no effect on the orientation of the subsequent deposit. Comparison of Figure B-2(a) (the etched substrate) and Figure B-2(b) (the "as-deposited" tungsten) shows that the deposit orientation is influenced in detail by the specific orientation of those substrate grains that are oriented with their <111> directions near the surface normal. The deposition parameters select the preferred direction of orientation, and the substrate has only a secondary influence as described above.

Removal of the plastically deformed substrate surface layer prior to deposition results in an apparent improvement in the resistance of the deposit to grain growth, as compared to other identical deposits subjected to similar post-deposition thermal treatment. This result is not unexpected since the higher free energy of a deformed layer at the interface provides a driving force for grain growth. Figure B-3(a) is a section of P-56-W after firing for 30 minutes at 1730°C. The boundary between the original substrate and the deposit is distinct and there has been little if any tendency for grain growth or for the deposit to recrystallize. The enlarged view shown in Figure B-3(b) illustrates a place where epitaxy occurred at the interface. Figure B-3(c) is a similar section of P-24-W, a deposit grown under conditions identical to those of P-56-W except that the plastically deformed substrate surface layer was not removed before depositing. Excessive grain growth is evident in this case. The deposit substrate interface is barely discernible. Pole-figure scans showing the degradation of the "as-deposited" orientation of P-24-W as a result of the firing are shown in Figure B-4.

---

2. G. L. Kehl, Principles of Metallographic Laboratory Practice (McGraw-Hill Book Company, Inc., New York, 1949), 3rd ed., p. 60.

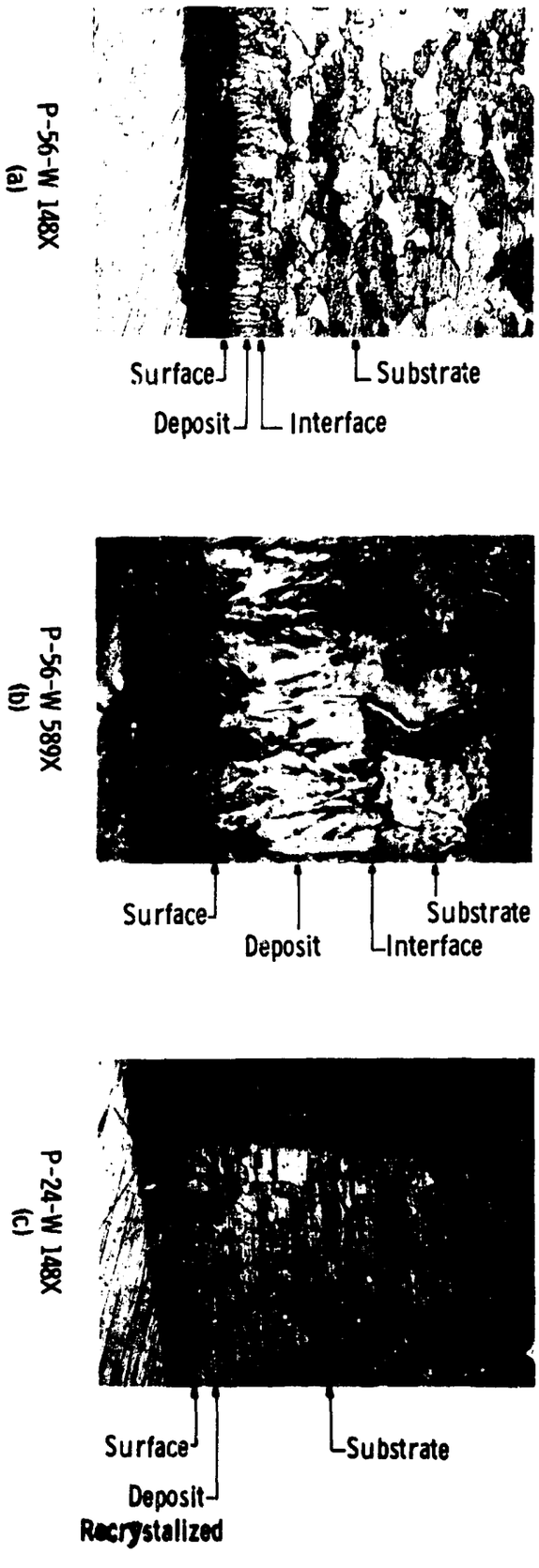

Figure B-3. Photomicrographs of Tungsten Deposits

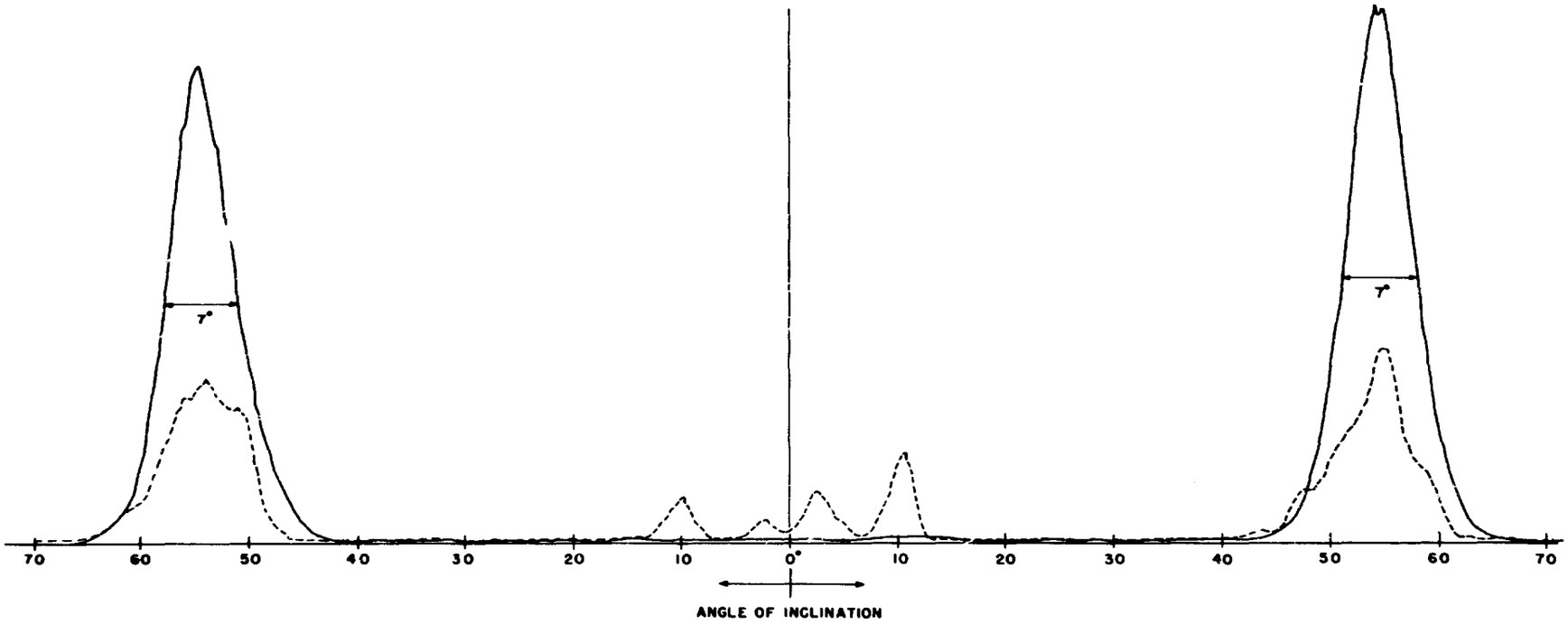

Figure B-4. A Plot of the Integrated Intensity of Cu Kα X-Radiation Diffracted from the (200) Planes of P-24-W as a Function of the Angle of Inclination of the Planes to the Surface. Solid Curve, as Deposited; Dotted Curve, After H_2 Firing at 1700°C for 30 Minutes

With thermodynamic deposition parameters adjusted to yield (111) oriented deposits (Figure 3), and with a micropolished substrate having fiber texture such as is illustrated in Figure B-1(b), the resulting deposits are very sharply oriented in the [111] crystal direction. The influence of substrate orientation on the resulting deposit orientation is illustrated by the data and curves shown in Figure B-5. The deposits P-n-W (n = 2, 24, 25, 26, 27) were all grown under identical conditions onto identically prepared tungsten substrates which had been micropolished to a one micron diamond finish. It is significant that as the deposit gets progressively thinner the f.h.w. of the distribution of (111) planes approaches an upper limit in the neighborhood of 10° to 12° rather than continuing to get larger as would be expected if substrate-independent nucleation occurred over the entire surface. * This suggests that there is continuity across the interface (i.e. epitaxy such as shown in Figure B-3(b)) at places where the surface is initially constituted of (111) oriented crystallites.

---

* For diffraction from the (200) planes of tungsten, $2\theta = 58.3°$. The depth of penetration of the X-rays at that angle is such that 99.5% of the diffracted intensity comes from a surface layer .15 mils thick. Thus for deposits > .15 mils the pole figure measures only the deposit orientation and not that of the substrate.

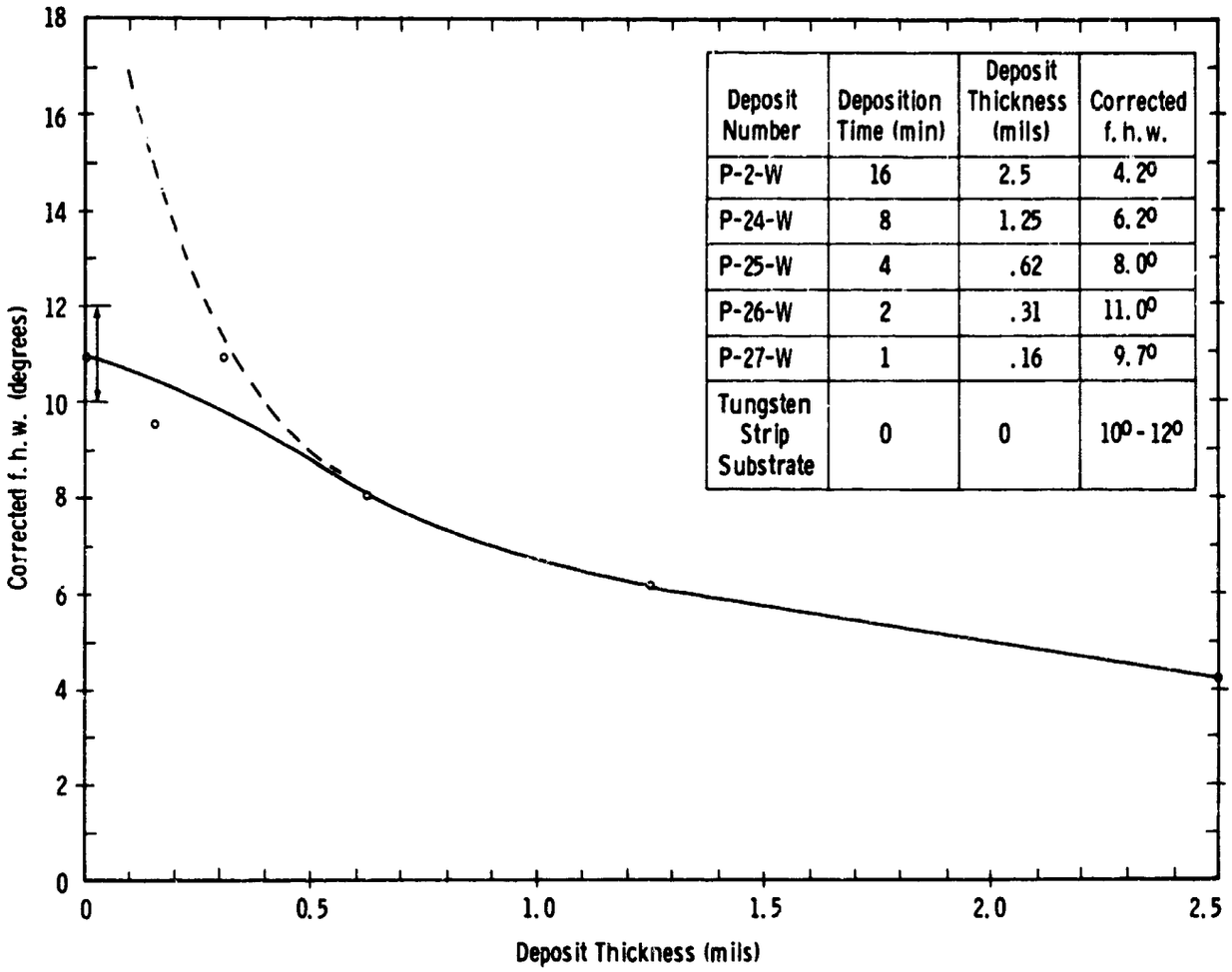

Figure B-5. Degree of (111) Preferred Orientation vs Deposit Thickness for Chemically Vapor Deposited Tungsten on Tungsten Substrate Surfaces Mechanically Polished to a 1 Micron Diamond Finish and Hydrogen Fired in-Situ at 700°C for 1 Hour Prior to Deposition. Solid Curves - Full Half-Width as Grown; Dotted Curve - Full Half-Width with Negligible Substrate Influence

APPENDIX C

SUBSTRATE-DEPOSIT BOND STRENGTH

The macroscopic structural integrity of cathodes produced by deposition of thin oriented layers, on strong ductile substrates, is dependent upon the strength of the bond at the interface between substrate and deposit. Mechanical failure of the cathode, if it occurs, is most likely to result from failure of the interface bond. A criterion of bond strength which has become a standard in the tube industry, particularly as applied to metal ceramic seals, is the peel test. This test is a more meaningful measure of interface bonding than a standard tensile test because a sheer component of force is imposed in the former which results in a relatively uniform distribution of stress throughout the volume of the interface, while in the latter test this is not generally true. For these reasons, the tab peel test has been chosen as a criterion for characterizing the macroscopic structural strength of chemically vapor deposited cathodes in this work. The testing apparatus is illustrated in Figure C-1.

Extensive data exists describing the peel strength of a large variety of metal ceramic seals tested on this apparatus under identical conditions as will be employed in testing chemically vapor deposited surface layers in this present work. That data will be used as a measure of comparison. (See Table C-1.)

As illustrated in Figure C-2(a), in this test, the CVD sample is held between guys and a linearly increasing load (i.e. pull) exerted onto a metal tab which had previously been brazed to the deposit. The magnitude of the pull is measured by a strain gauge and recorded on a strip chart. The geometry of the test piece is illustrated in Figure C-2(b), and a typical strip chart recording shown in Figure C-3. From the recording it is seen that the force on the interface increases linearly until the yield point is reached and then remains essentially constant as the deposit is stripped from the substrate. The magnitude of the pull at the yield point per inch of width of the tab is a measure of the interface peel strength. For most of the CVD samples tested to date the interface peel strength has exceeded either the braze peel strength or the

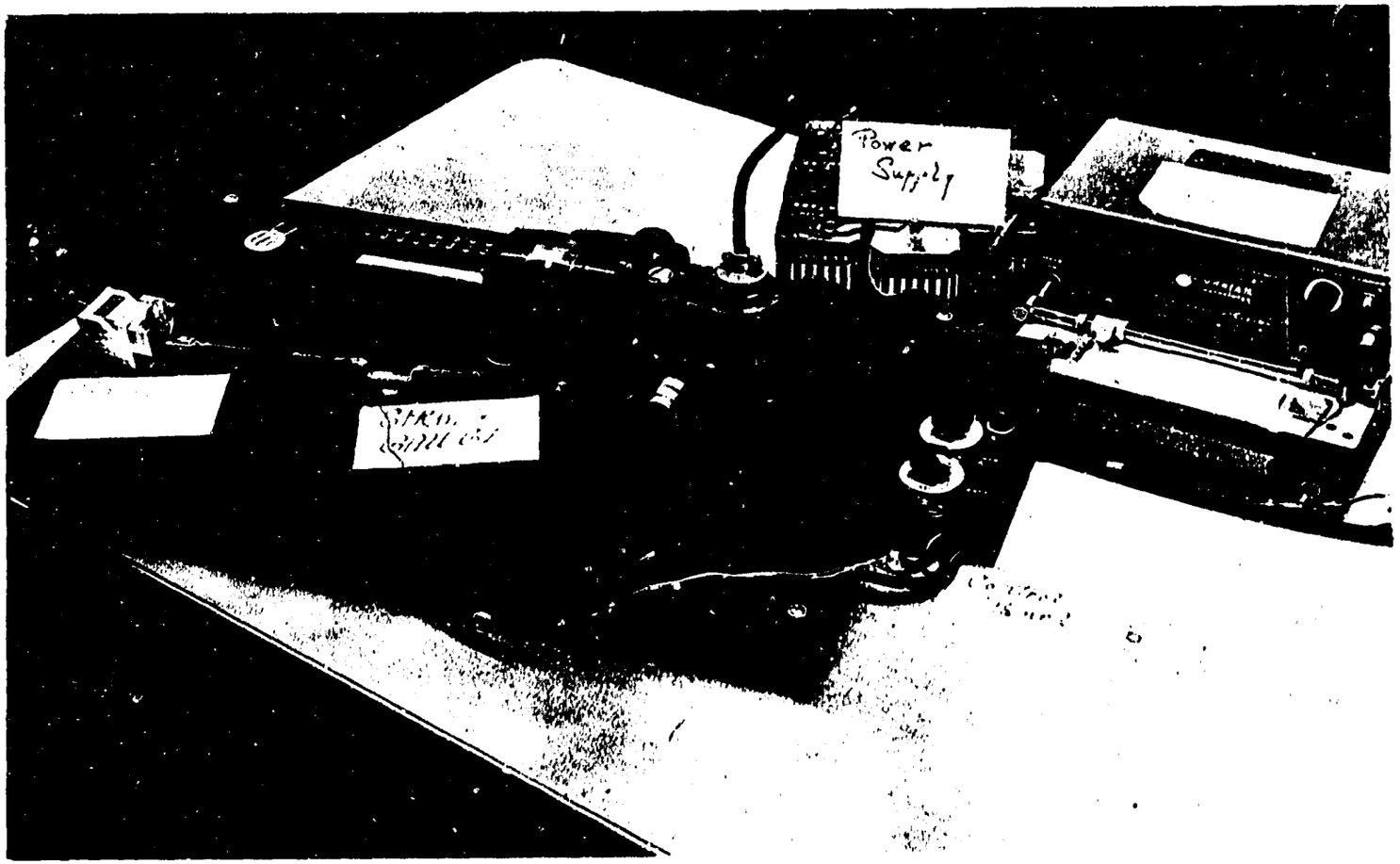

Figure C-1. Tab Peel Test Apparatus

TABLE C-1

PEEL TEST DATA ON TYPICAL METAL-CERAMIC SEALS

Type Seal	Peel Strength (ounces per inch of tab width)
Al 300 Ceramic--. 010" Kovar Cu. braze No. 33 standard metallizing paint	800
Al 300 Ceramic--. 020" Kovar Cu Braze No. 33 standard metallizing paint	380
Al 300 Ceramic--. 010" Kovar Cu. braze No. 33Fexp. metallizing paint	920
Al 300 Ceramic--. 010" Kovar Cu Ag Eutectic braze No. 33 standard metallizing paint	400
Al 300 Ceramic--. 010" Kovar Ag braze No. 33 standard metallizing paint	1200
Al 300 Ceramic--. 010" Kovar Nioro braze No. 33 standard metallizing paint	140
Al 995 Ceramic--. 010" Kovar Cu braze, 2% Tungsten metallizing paint	1400
Al 300 Ceramic--. 010" Kovar Cu braze, metallizing paint tungsten plus proprietary additive	2320

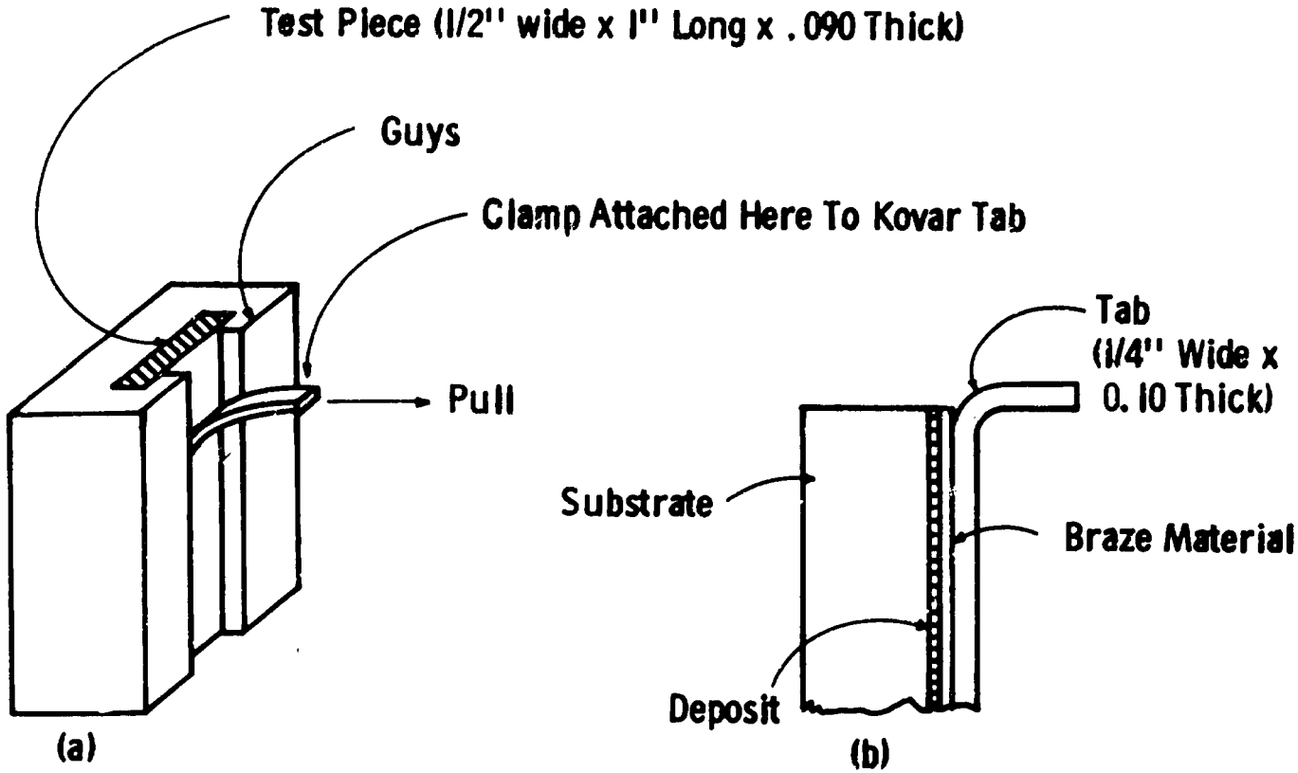
Test Piece (1/2" wide x 1" Long x .090 Thick)
Guys
Clamp Attached Here To Kovar Tab
Pull
(a)
Peel Test Geometry
Tab
(1/4" Wide x
0.10 Thick)
Substrate
Braze Material
Deposit
(b)
Typical Tab Peel Test Piece

Figure C-2.

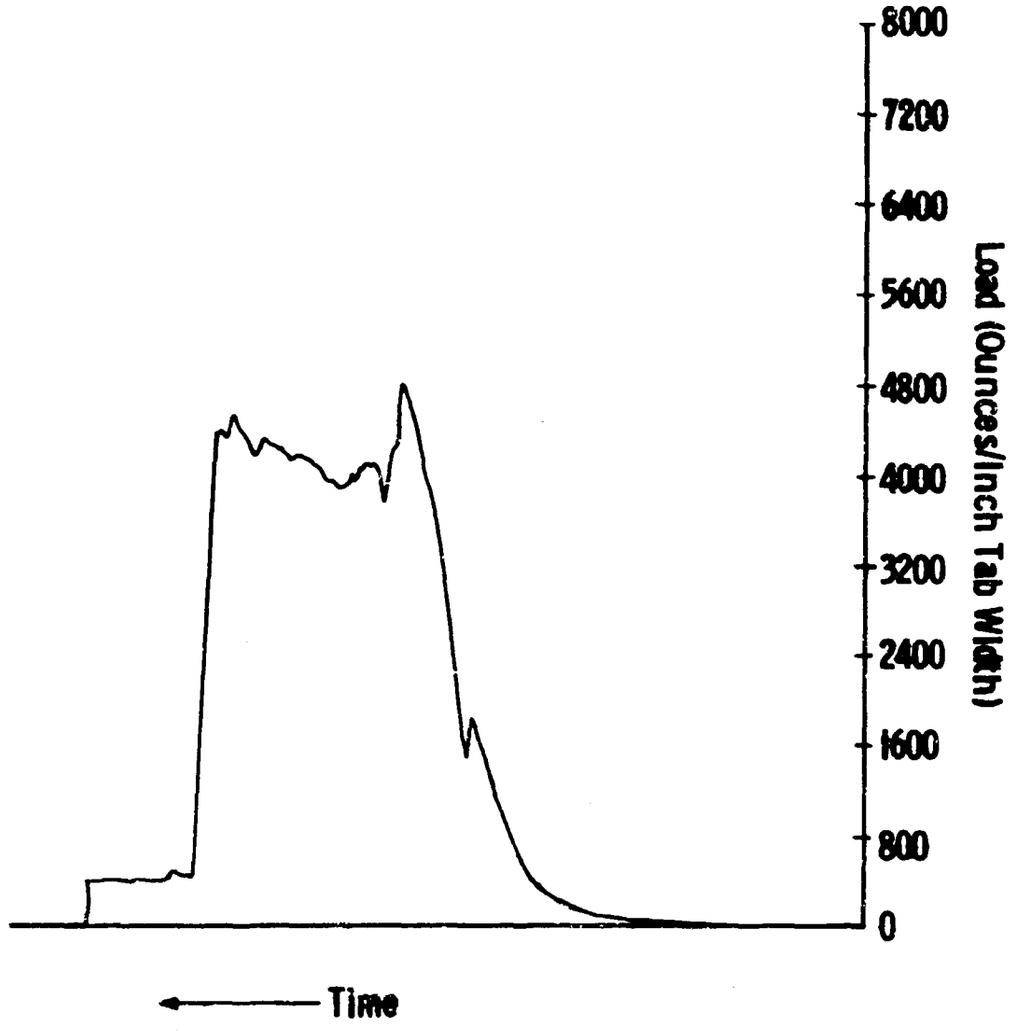

Figure C-3. Tab Peel Test for Sample P-24-W

strength of the kovar tab. In these cases a minimum value of interface peel strength is obtained since the interface remains intact and the test piece is destroyed by the other failure mechanism.

Values (or minimum limits) of peel strengths for chemically-vapor-deposited tungsten deposited on non-porous tungsten substrates are given in Table C-2. All values shown apply to as deposited samples (i.e., no heat treatment was done subsequent to deposition). However, it is likely that there are stresses present at the interfaces as a result of cooling from deposition temperature to room temperature. By comparison with the peel strengths for metal ceramic seals (Table C-1) it is evident that the tungsten deposits are very well bonded to their substrates. With the single exception of P-1-W, the minimum limits of peel strengths measured are at least one-and-one-half times greater than the best metal-ceramic seals and three to four times greater than typical metal-ceramic seals. For six of the eight samples tested, the tungsten-substrate interface peel strength exceeded even that of the copper braze bonding the tab to the deposit (see remarks in Table C-2). The following facts are also evident from the data in the table: Deposit-substrate bond strength is good for both (100) and (111) oriented deposits and also for deposits with mixed orientation. Deposit-substrate bond strength is good for both mechanically polished and electrolytically polished substrates.

In view of the above cited results and the observed partial epitaxy described in Appendix B, and because no evidence of lack of interface integrity was observed at any time during this contract period, no further deposit-substrate bond strength measurements were made.

TABLE C-2

PEEL TEST DATA:

CVD TUNGSTEN ON NON-POROUS TUNGSTEN SUBSTRATE

Deposit Number	Preferred Orientation	Substrate* Finish	Peel Strength Oz/In Tab Width	Remarks
P-1-W	(111)	1	1400	An anomolously low valve as compared to others measured. Photomicrograph reveals that the deposit-substrate separated cleanly.
P-5-W	Mixed (111) (100) (210)	1	>4800	Braze failed--Kovar tab ripped during peel. Deposit-substrate interface remained intact.
P-8-W	(100)	1	>3600	Braze failed--Kovar tab ripped during peel. Deposit substrate interface remained intact.
P-9-W	(111)	2	>3200	Braze failed--Kovar tab ripped during peel. Deposit substrate interface remained intact.
P-10-W	(100)	1	>4400	Braze failed--Kovar tab ripped during peel. Deposit substrate interface remained intact.
P-24-W	(111)	1	>4000	Braze failed at 4000 oz./in. width (see strip chart recording). Deposit-substrate interface remained intact.
P-25-W	(111)	1	>4000	Braze failed--Kovar tab ripped during peel. Deposit-substrate interface remained intact.
P-27-W	(111)	1	>8000	.020" Kovar strip used instead of .010". Braze failed over 1/3 of length of strip and then held. Deposit-substrate interface held to some value > limit of test apparatus and then failed.

*Substrate finishes designated as follows:

1. Mechanically polished to 1μ diamond
2. Electropolished.